FLOW AND STATIC ^{1}H, ^{19}F and ^{14}N NMR STUDIES IN DENSE FLUIDS

by

Lee A. Allen

Dissertation submitted to the Faculty of the
Virginia Polytechnic Institute and State University
in partial fulfillment of the requirements for the degree of

DOCTOR OF PHILOSOPHY

in

Chemistry

APPROVED:

H. C. Dorn, Chairman

L. T. Taylor

D. G. I. Kingston

H. M. McNair

J. S. Mason

April 1988

Blacksburg, Virginia

This dissertation is dedicated to

a mother and a father

whose support and encouragement

have made this endeavor possible.

ACKNOWLEDGEMENTS

Under the direction of I have been involved with applications well away from tradition for which I am indeed grateful. I envy his ability to think beyond the immediate making the experimental approaches particularly challenging. is to be thanked for his continual presence and expertise in implementing 's ideas and putting them into a practical perspective. To the colleagues with whom I have shared frustrations and triumphs, I am indebted. And to , without whom this manuscript would not have been possible, thank you.

TABLE OF CONTENTS

LIST OF FIGURES

LIST OF FIGURES (cont.)

LIST OF FIGURES (cont.)

LIST OF FIGURES (cont.)

LIST OF TABLES

FOREWORD

The direct coupling of chromatographic and spectroscopic techniques capitalizes on the information-rich spectroscopic methods. Nuclear magnetic resonance is no exception. The direct coupling of HPLC to ^{1}H NMR has proven to be a tool in the identification of eluting compounds however applications using reverse phase chromatography have been limited. Outlined in Chapter One are the developments in HPLC/^{1}H NMR and other applications of flow NMR to date. A most promising application of coupled flow NMR is the area of reverse phase chromatography, though ^{1}H detection is complicated by spectral background signals associated with the typical solvents used. Solvent signal suppression methods have been applied but with only marginal success.

One recognizes that alternative approaches can be pursued with nuclei other than ^{1}H being observed which avoid the spectral background problems associated with reverse phase HPLC/^{1}H NMR. Chapter Two describes the use of ^{19}F observation as a supplement to HPLC/^{1}H NMR. Due to the presence of J_{HF} coupling, MLEV phase cycling has been implemented and shown effective as a means of efficient decoupling in the HPLC/^{19}F $\{^{1}H\}$ NMR experiment. For cases where fluorine is present or through effective fluorine-

tagging HPLC/^{19}F $\{^{1}H\}$ NMR offers spectral simplicity without solvent background.

A chromatographic alternative is the utilization of supercritical fluid chromatography where supercritical CO_2 offers no NMR background signal. An NMR flow probe was developed for use in SFC coupled NMR and is described in Chapter Three. Chromatographic application is demonstrated, though questions associated with detection of compounds dissolved in supercritical fluids required further investigation. For example, relaxation plays an important role in the optimization of the detected NMR signal under flowing conditions.

The relaxation behavior of dilute solutions of benzene and acetonitrile in sub- and supercritical CO_2 was investigated. Chapter Four discusses these results and describes the relaxation being dominated by spin-rotation interactions, with measured T_1's covering a large range of values. Molecular motion is shown to be five fold faster than that in normal liquids. This increased molecular motion results in observed line-narrowing in quadrupolar nuclei, e.g. ^{14}N in acetonitrile, which can be related to increased S/N for the same number of accumulations,

advantageous in the observation of quadrupolar nuclei in dilute solutions.

Increased molecular motion also affects the enhancement potential of dynamic nuclear polarization. Flow NMR has been shown to be important in the optimization of signal enhancement through dynamic nuclear polarization. Solution applications are however limited under the extreme narrowing condition to relatively low magnetic fields. Use of supercritical fluids offers increased molecular motion under liquid-like densities extending the usefulness of flow DNP-NMR. The flow DNP-NMR experiment is described in Chapter Five and observed signal enhancements using supercritical fluids are presented.

The system and flow probe developed for SFC/NMR are described in detail in Appendix I. Appendix II describes the inversion recovery method of spin-lattice relation time determination. The advantage of flow DNP over static DNP results from independent optimization of the ESR and NMR processes involved. In Appendix III, typical configurations for flow and static DNP are compared. Preliminary results from the investigation of flow dynamics of supercritical CO_2 compared to normal liquids are in Appendix IV.

CHAPTER ONE

HISTORY OF COUPLED FLOW NMR

The effect of flow on the nuclear magnetic resonance (NMR) signal was first noted by Suryan (1) in 1951 and has since been studied extensively. The comprehensive mathematical treatment of Zhernovoi and Latyshev (2) outlined the theoretical expressions related to signal intensity and linewidth and suggested numerous practical applications of NMR in the analysis of flow. The review of Jones and Child (3) summarizes the many ways in which NMR has been used as a non-invasive tool in the investigation of flowing liquids.

Watanabe and Nicki (4) were the first to directly couple high performance liquid chromatography (HPLC) and ^{1}H NMR, though analysis was done in a stop-flow manner in order to compensate for the inherent insensitivity of the NMR experiment. Continuous flow HPLC/^{1}H NMR soon followed with the groups of Bayer et al. (5) and Buddrus and Herzog (6) demonstrating effective direct identification of model chromatographic eluents by ^{1}H NMR. Using this on-line approach, spectra were taken coincident with chromatographic elution, the number of scans per file dependent on the acquisition parameters and elution period. Carbon

tetrachloride was used by both groups as the solvent in order to eliminate a proton solvent background signal. Stop-flow linewidths of 2.5 and 1.5 Hz, respectively, demonstrated the ability of flow NMR to observe spin-spin coupling despite the non-spinning nature of the coupled technique. The HPLC/^{1}H NMR approach was applied by Dorn and coworkers to model and actual jet fuel samples (7) using Freon 113 (trichlorotrifluoroethane) as the non-protonated solvent with static observed linewidths of 5 Hz. Chromatographic reconstruction using the ^{1}H NMR data was demonstrated as a complement to refraction index detection. Use of deuterated solvents in the on-line HPLC/^{1}H NMR analysis of steroids was shown though through stopped flow (8). The exclusive use of deuterated solvents is however, prohibitively expensive in analytical scale or higher applications of HPLC. Analysis using the protonated solvent $CHCl_3$ was demonstrated by Buddrus and Herzog (9). The strong NMR solvent signal was reduced through the methods of expanded ADC dynamic range and selective presaturation. Resolution remained at <2 Hz. High field superconducting NMR (4.7 Tesla) was applied by Dorn et al. in the 200 MHz ^{1}H NMR analysis of aviation fuels (10) and coal conversion recycle solvents (11). The analytical power of the NMR technique is utilized in the direct identification of

constituents of these complex mixtures. The use of high superconducting fields improved both the observed signal to noise (S/N) and the achievable field homogeneity under unlocked conditions.

Reverse phase HPLC/^{1}H NMR was addressed by Bayer et al. (12) and the problem of gradient elution in NMR detection was noted. Under gradient conditions, the solvent background signals vary continually with concentration making solvent signal suppression very difficult. Superconducting fields of 5.9 T and 9.4 T (250 MHz and 400 MHz ^{1}H NMR, respectively) were used. Deuterated solvents were used in the adsorption separations noted. Despite the lack of chromatographic separation, NMR detection allowed compound identification. Solvent signal suppression using acetonitrile as the reverse-phase solvent using ^{1}H NMR at 250 MHz was accomplished through increased ADC dynamic range. Co-solvent signal suppression of acetonitrile and water at 400 MHz ^{1}H was accomplished using homo decoupling and homo-gated decoupling when 100% acetonitrile and isocratic acetonitrile/water mixtures (30:70) were used, respectively. In order to implement efficiently the latter approach, long cycle periods were necessary requiring stopped flow operation. The conditions for quantitative

flow ^{1}H NMR were addressed in detail by Haw (13). Average structure approaches were applied by Haw to class separation and analysis of aviation fuels using the on-line approach (14). Through separation prior to NMR detection, the evaluated average structure of the chromatographic fraction best represents that fraction.

On-line and off-line LC/^{1}H NMR were compared by Buddrus using steroids with protonated chloroform as the solvent (15). Contamination in off-line fraction handling was offset by more concentrated samples and unrestricted accumulation periods. Resolution loss was insignificant with 1.95 Hz versus 1.46 Hz for the on-line and off-line approaches, respectively. On-line analysis obviously requires additional equipment with advantages in cases of mixtures sensitive to light or water. Both techniques suffer from solvent background suppression required when protonated solvents are used.

Continuous flow ^{13}C NMR was shown by Bayer and Ernst as a method to avoid the long relaxation times typical of ^{13}C nuclei in the absence of relaxation agents (16). A continuous supply of fresh sample allows more rapid analysis through increases in the scan repetition rate. Proton

resolution was <1 Hz with ^{13}C observed linewidths of 0.37 Hz under flowing conditions using continuous wave decoupling. A review by Dorn concerning directly coupled HPLC/^{1}H NMR (17) illustrated the advances and importance of this developing technique.

Analytical scale HPLC/^{1}H NMR was described by Laude and Wilkins using a 20 μL observation volume resulting in observed linewidths of 0.54 Hz under flowing conditions (18). The effect of flow rate on resolution was studied with stop-flow linewidths of 0.18 Hz using the capillary flow cell. Premagnetization was ensured through placement of the analytical column within the magnet bore. Previous investigations utilized either oversized flow cells or pre-equilibrium coils prior to detection. The elimination of the latter two reduces post-column band broadening which can degrade chromatographic resolution. Detection limits for on-column injection of heptane and naphthalene were found to be ≈50 μg each for spectra of 8 coadded scans at a flow rate of 0.5 mL/min. Chromatographic reconstruction is demonstrated at the analytical scale using the ^{1}H NMR spectra with injections below 200 μg being sufficient for application in reconstruction, a clear advantage when weak or non-UV absorbing species were investigated.

Recycled flow ^{13}C NMR was described in more detail by Laude et al. where the effective reduced spin-lattice relaxation as a result of flow allowed more optimum acquisition when long ^{13}C T_1's are present (19). A premagnetization coil prior to detection insured a fresh supply of spin-polarized sample. Quantitative analysis is aided by the lack of large variation in T_1's. Applicability to other nuclei having inefficient relaxation mechanisms was suggested.

Reverse phase HPLC/^1H NMR separations of biomolecules were shown by Laude et al. (20). Low grade D_2O (1-2% H_2O) and CH_3CN were the solvents used with CH_3CN kept at <3%. The residual solvent background signal was suppressed using the 1-1 hard pulse technique of Clore (21). As has been previously noted, gradient elution results in changes in the solvent signal chemical shift with respect to concentration. It was noted that the 1-1 hard pulse provides a sufficient window for D_2O/CH_3CN gradients of 100-75%. Separations shown, however, were analyzed under isocratic elution with applied 1-1 hard pulse solvent suppression. Albert et al. have studied cell optimization in continuous flow HPLC/^1H NMR for analytical and semi-preparative columns (22). Using

modified fluorescence detection, detector volumes of up to 200 μL were allowable under certain conditions. Using the 1-3-3-1 hard pulse sequence of Hore (23), very effective solvent suppression of a 1% solution diethylether in CH_3CN/H_2O (50:50) was shown. A suppression ratio of 200:1 was obtained.

Continuous flow ^{13}C NMR has proven advantageous over static approaches (16,19). The distortionless enhancement polarization transfer (DEPT) sequence of Doddrell et al. (24,25) has been applied by Albert et al. to continuous flow ^{13}C NMR in order to generate carbon-proton multiplicities in flowing liquids (22).

Application of the 1-1 hard pulse was then applied by Laude and Wilkins to fully protonated reverse-phase solvents (26). Isocratic elution examples are supplemented by an example of a minor gradient of 90:10 ratio D_2O/CH_3CN to an 80:20 ratio. The problems of gradients with respect to NMR detection was again addressed with the added note that eluent chemical shifts can also change with respect to co-solvent composition.

Allen and Dorn have developed and used directly coupled

supercritical fluid chromatography ^{1}H NMR (SFC/^{1}H NMR) as an alternative to LC/^{1}H NMR for the direct identification of eluting compounds. The supercritical solvent, CO_2, offered no background signal and deuterated modifiers were effectively used at low concentrations (27). This work is described in Chapter Three.

Allen, Dorn et al. have used ^{19}F detection in conjunction with MLEV-16 phase cycled ^{1}H decoupling in the LC/^{19}F (^{1}H) NMR analysis of derivatized alcohols. Observation of ^{19}F serves as a complement to normal phase LC/^{1}H NMR and offers spectral simplicity and selectivity (28). This work is described in Chapter Two.

The direct coupling of gas chromatography (GC) and ^{1}H NMR has seen limited investigation by Herzog and Buddrus. Operating at <50°C, eluting volatile samples were analyzed using on-line ^{1}H NMR (29). Through an added heated interface, GC fractions up to 200°C were analyzed (30), however larger injected quantities were required in order to compensate for temperature effects on the observed signal to noise. Resolution remained at a respectable 2 Hz. The inherent insensitivity of NMR makes off-line NMR analysis of GC fractions in a solvent advantageous over the on-line

approach.

It is important to realize that application of solvent suppression techniques, both selective presaturation (9,12,15) and the binomial suppression methods (20,23,26) reduce or eliminate solvent signals and those signals coincident or immediately adjacent to them. Nearby observed signals are often distorted due to non-linear excitation. Minimization of this distortion through increased cycles (12) is not appropriate in continuous flow HPLC/^{1}H NMR. Signal intensity distortions make quantization difficult. Alternatives therefore should be sought which avoid the solvent background problem. Other chromatographic approaches and observation of alternative nuclei offer many advantages in directly coupled flow NMR.

CHAPTER TWO

DIRECTLY COUPLED LC/^{19}F {^{1}H} NMR FOR THE ANALYSIS OF FLUORINE CONTAINING MIXTURES

Introduction

While the direct coupling of ^{1}H NMR to liquid chromatography has proven successful in the characterization of chromatographically eluting compounds, the extension to ^{19}F NMR observation selectively identifies species containing the ^{19}F nuclide where ^{1}H NMR spectra might not allow unequivocal identification (28). With NMR sensitivity comparable to that of ^{1}H, ^{19}F is an ideal alternative NMR nuclide to monitor. The characterization of active hydrogen functional groups using p-fluorobenzoate derivatization and ^{19}F NMR has been previously reported (31,32). P-fluorobenzoyl chloride has been similarly used in the derivatization of amino acids and steroids which were then characterized using static ^{19}F NMR (33). The large chemical shift range of ^{19}F (≈375 ppm) relative to that of ^{1}H supports high sensitivity to chemical structure changes. The observed modest ^{19}F chemical shift differences of para-substituted fluorobenzenes can be useful probes of electronic changes (34). The p-fluorobenzoate derivatized primary, secondary and tertiary alcohols exhibit an ≈2 ppm fluorine chemical shift range. Mixtures of derivatized

alcohols are generally difficult to characterize based solely on ^{1}H NMR spectra due to relatively minor spectral differences while the use of ^{19}F NMR observation allows characterization of mixtures using a different chemical shift dimension (δ_F). Preliminary results using on line HPLC/^{19}F NMR support alternative nuclide observation, but the multiplets resulting from J_{HF} coupling to the aryl protons reduce the usefulness of fluorine tagging unless broadband ^{1}H decoupling is used (17).

Phase-alternated decoupling sequences have proven to be useful for reducing ^{1}H decoupler power levels for broadband decoupled ^{13}C nuclear magnetic resonance spectroscopy. Numerous sequences have been developed including the MLEV, WALTZ and PAR sequences (35-37). Average Hamiltonian methods have been effectively used to evaluate and compare the increased efficiencies of these newer methods with the more traditional techniques (e.g. noise modulation) (38). The reduced ^{1}H decoupler power needed using these sequences minimizes the sample heating and line-broadening typical of conventional broadband noise decoupling techniques.

The application of MLEV-16 to broadband ^{1}H decouple ^{19}F NMR using a cross-coil configuration is described. The

ability to efficiently decouple protons over the entire ^{1}H chemical shift range as well as large J_{HF} couplings is illustrated. Mixtures of derivatized alcohols are then analyzed using both LC/^{1}H NMR and LC/^{19}F (^{1}H) NMR, illustrating the usefulness of the dual approach.

Experimental Section

The ^{19}F signal was observed at 187.7 MHz using a JEOL FX-200 NMR spectrometer and a home-built probe. While the probe used was designed for measurement of flowing samples, the decoupling technique described is applicable to both static and flow modes. This probe has an observed limited linewidth of 1.5 Hz and was built for flow NMR experiments under nonspinning conditions. The observation volume is 20 μL based on coil geometry. A single coil double-tuned circuit was tried and found ineffective apparently due to the close proximity of the resonance and decoupling frequencies, 187.7 and 199.5 MHz, respectively. A cross-coil configuration was adopted and despite the expected isolation of orthogonal coils, additional filtering was necessary in order to suppress decoupler noise (Figure 2.1). The decoupling field achieved using MLEV-16 was optimized through ^{19}F observation of fluorobenzene at a proton decoupler frequency setting 1.5 kHz off-resonance. The base

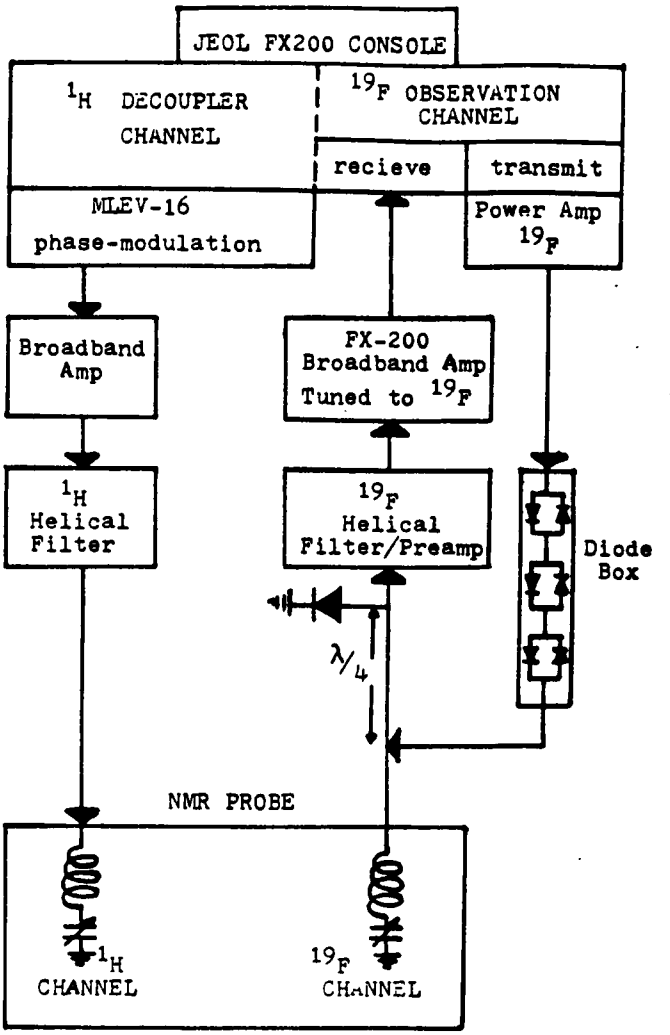

Figure 2.1 Block diagram of the NMR spectrometer for ^{19}F observation with MLEV-16 broadband ^{1}H decoupling. The MLEV-16 was assembled as described elsewhere (33). A Hamtronics HRF-220 helical resonator filter was retuned to 187.7 MHz. The ^{19}F filter/preamp was a GLB Electronics model P-18770C.

frequency f_o of 2 kHz was predetermined by an 8 kHz internal clock satisfying $f_o = \gamma B_2/2\pi$, where γ is the magnetogyric ratio (35). The proton decoupling field (B_2) was then varied for optimum decoupling. In operation, about 0.1 watts (6V peak to peak) of decoupler power was delivered to the probe. This can be compared to much higher power needed using more classic noise modulation techniques.

A JEOL FX-200 nuclear magnetic resonance spectrometer was used to obtain LC/^{1}H and LC/^{19}F {^{1}H} spectra at 199.5 and 187.7 MHz, respectively. Typical ^{1}H and ^{19}F acquisition parameters are found in Table 2.1. The incorporation of the MLEV-16 decoupling sequence has made efficient broadband ^{1}H decoupling of the LC/^{19}F NMR spectra now possible. The p-fluorobenzoate derivatized alcohols were prepared using p-fluorobenzoyl chloride as previously described (32,33). The m- and o-fluorobenzoate derivatives were similarly prepared.

A Whatman Magnum 9x250 mm Propyl Amino Cyano (PAC) column having 10 μm packing was used for both LC/^{1}H and LC/^{19}F NMR. The solvent system consisted of a 50:50 mixture of d-chloroform and Freon-113 (trichlorotrifluoroethane) delivered using a Waters M-45 solvent pump at a flow rate of

TABLE 2.1

TYPICAL ACQUISITION PARAMETERS

	LC/NMR	
	^{1}H	^{19}F $\{^{1}H\}$
Observation Frequency	199.50 MHz	187.70 MHz
Pulse type	90°-Aqu	90°-Aqu
90° Pulse Width	20 μsec	23 μsec
Spectral Width	2000 Hz	2000 Hz
Number Points	2048	4096
Number Sample Points	2048	4096
Acquisition Times	0.512 sec	1.024 sec
Number of Scans	varied	varied

1.0 mL/min. Hexamethyldisiloxane (HMDS) was added to the solvent (0.01% v/v) as the chemical shift reference in the LC/^{1}H NMR separations. Fluorobenzene was added (0.01% v/v) as the chemical shift reference in the LC/^{19}F NMR separations. Injected quantities ranged from 5-10 mg. Either ^{1}H or ^{19}F NMR spectral files were taken periodically during a given chromatographic elution with conditions indicated in the figure captions.

Results and Discussion

A mixture of trifluoroethanol and fluorobenzene (2% v/v) in carbon tetrachloride was used for the evaluation of the MLEV-16 decoupling sequence (Figure 2.2). All NMR spectra were recorded with 10 scans coadded under non-flowing conditions. Complete ^{1}H decoupling with observed linewidths of 1.5 Hz was clearly evident with the decoupler frequency at the ^{1}H spectral midpoint (4.2 ppm) as well as at +/-2 kHz off-center decoupler offsets. Even at a +4 kHz offset in decoupler frequency, partial decoupling of trifluoroethanol was still observed with a reduced coupling of 3.4 Hz ($^{3}J_{HF}$ = 8 Hz). The fluorobenzene ^{1}H coupled spectrum consists of a complex multiplet pattern covering 40 Hz. However, even at a -4 kHz offset in ^{1}H decoupler frequency, the fluorobenzene signal remained nearly

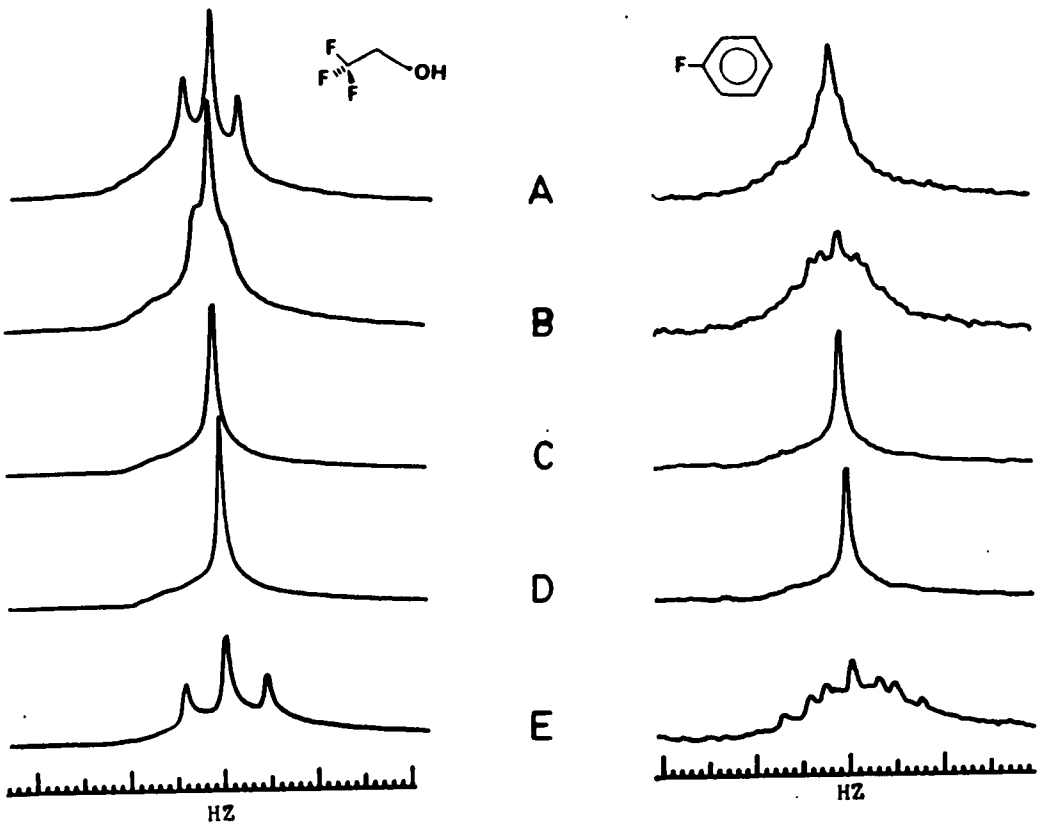

Figure 2.2 The 187.7 MHz ^{19}F NMR spectra of trifluoroethanol and fluorobenzene with various $\{^1H\}$ decoupler frequencies.

(A) -4 kHz offcenter offset
(B) +4 kHz offcenter offset
(C) +2 kHz offcenter offset (-2 kHz offcenter offset yielded the same result)
(D) $\{^1H\}$ decoupler frequency at the midpoint of the ^1H spectrum
(E) completely coupled

decoupled with an observed linewidth of only 7 Hz. No degradation of decoupling efficiency was observed at decoupler frequency settings of +/-2 kHz offset from the ^{1}H spectral midpoint corresponding to an effective $\geq$30 ppm ^{1}H decoupling spectral width.

The ability to decouple large J_{HF} couplings is illustrated using the sample 1,2-dichlorodifluoroethane (Figure 2.3). A geminal J_{HF} coupling of 40 Hz and a vicinal J_{HF} coupling of 15 Hz are apparent. The two major resonance signals are due to the meso and d,l enantiomeric pair, (confirmed through ^{13}C NMR with and without decoupling). Complete ^{1}H decoupling was observed with residual 3 Hz ^{19}F linewidths using on-resonance ^{1}H decoupling and at ^{1}H decoupler frequency offsets of +/-1.5 kHz. Even at +/-3 kHz decoupler offsets, only partial coupling exists with observed linewidths of 10 Hz.

The decoupler field (B_2) can be determined (33,34) using the relationship:

$$J_{HF}(B_2) = (J_{HF} * \Delta B)/B_2 \qquad [1]$$

where $J_{HF}(B_2)$ is the residual coupling as a function of decoupler power and ΔB is the decoupling frequency offset

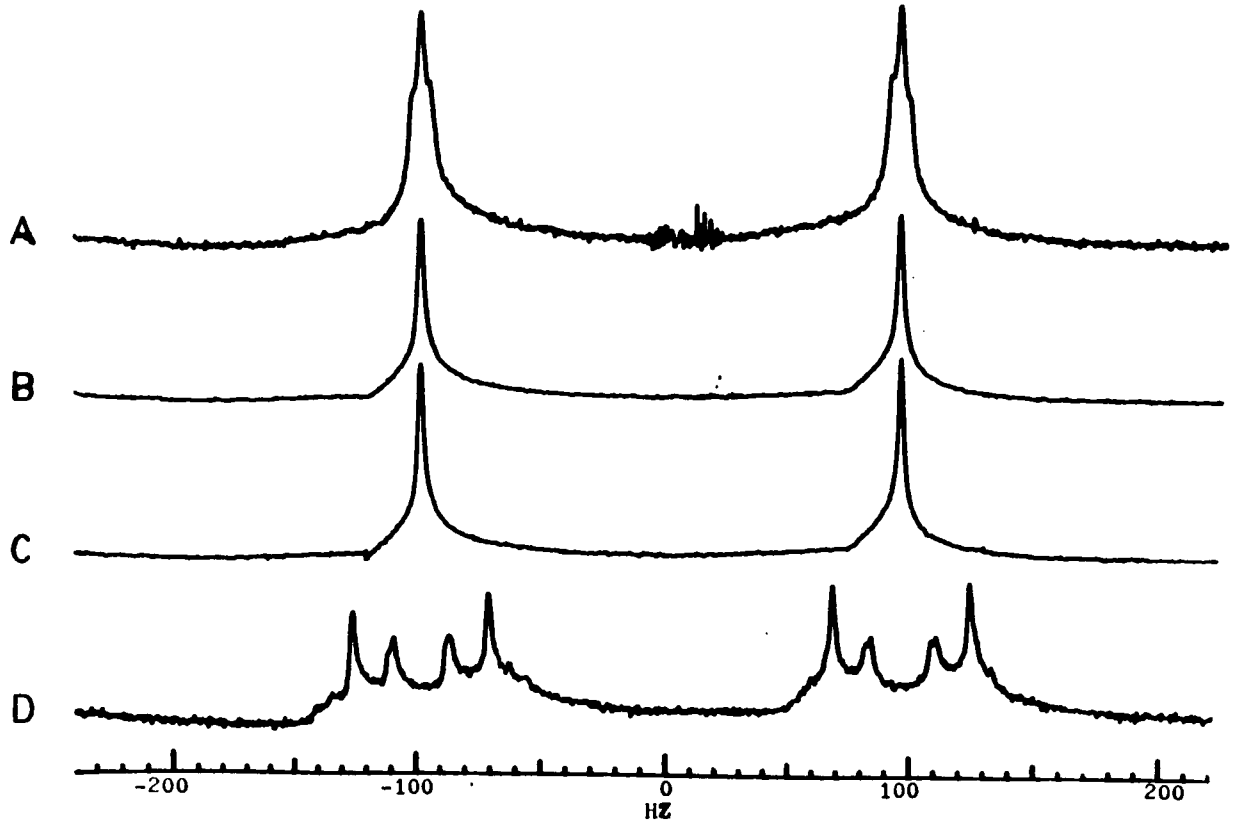

Figure 2.3 The 187.7 MHz ^{19}F NMR spectra of 1,2-dichlorodifluoroethane with various (^{1}H) decoupler frequencies.
(A) +3 kHz offset from on-resonance (or -3 kHz offset from on-resonance)
(B) +1.5 kHz offset from on-resonance (or -1.5 kHz offset from on-resonance)
(C) on-resonance
(D) completely coupled

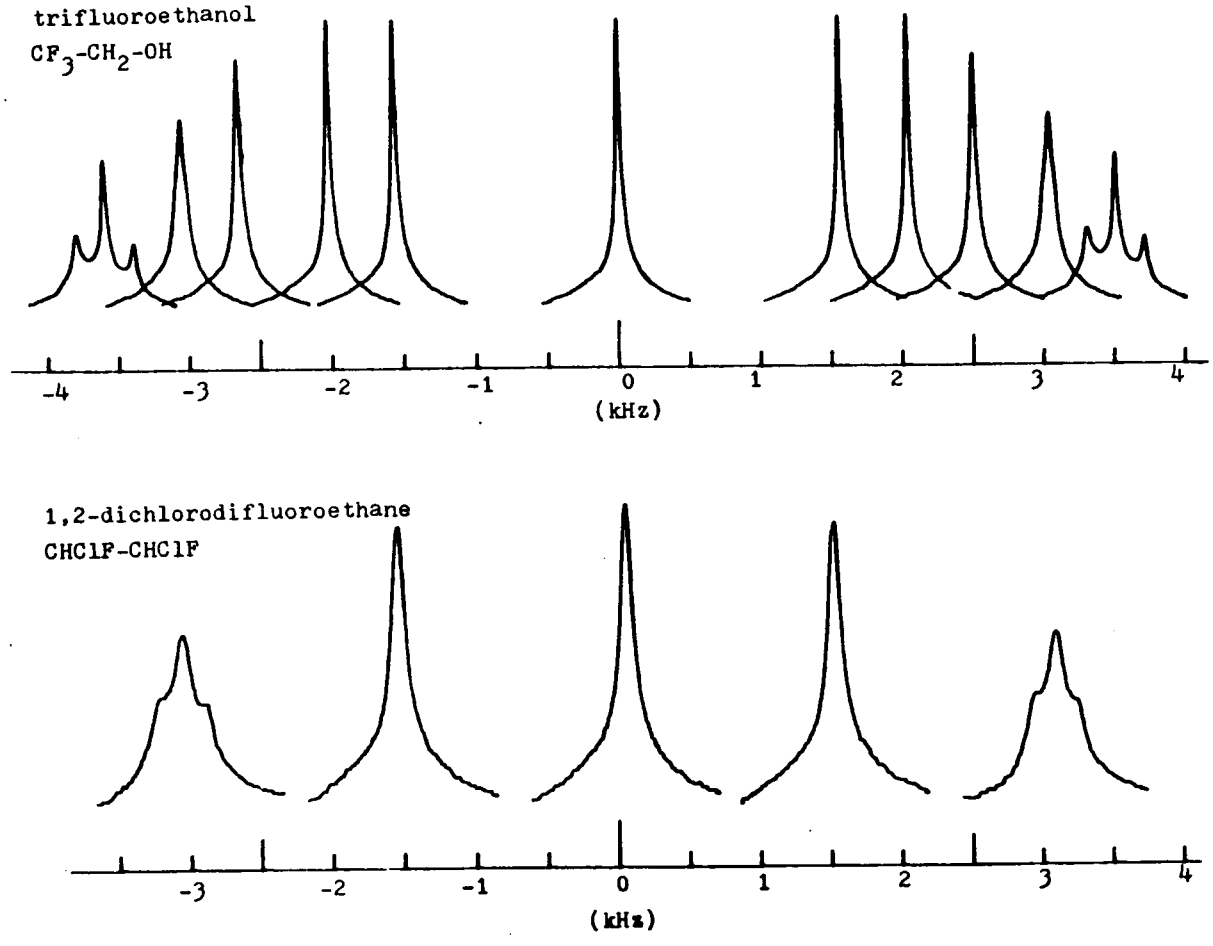

Figure 2.4 The ^{19}F decoupled spectra of trifluoroethanol and 1,2-dichlorodifluoroethane as functions of ^{1}H decoupler frequency.

in gauss. Trifluoroethanol and 1,2-dichlorodifluoroethane are shown in Figure 2.4 as functions of decoupler offset. At a ΔB = 3.5 kHz, trifluoroethanol has a $J_{HF}(B_2)$ = 5.0 Hz yielding B_2 = 1.3 gauss by Equation 1. Similarly, at a ΔB = 3 kHz, 1,2-dichlorodifluoroethane has a $J_{HF}(B_2)$ = 5 Hz yielding B_2 = 5.6 gauss. Thus, even in the presence of large J_{HF} couplings, efficient ^1H broadband decoupling using the MLEV-16 sequence was observed over a 20 ppm ^1H spectral width (+/-2 kHz).

Mixtures of alcohol derivatives were examined to illustrate how LC/^{19}F NMR can complement the LC/^1H NMR approach. The LC/^{19}F NMR elution profile of phenol derivatives shows broad fluorine resonances resulting from J_{HF} coupling to adjacent aryl protons (Figure 2.5). Despite a simplified spectrum through fluorine detection, multiplet overlap results in minimal information concerning elution and identification. The LC/^1H NMR approach, however, yields even less information due to the expected extensive spectral overlap.

The utility of broadband ^1H decoupling for LC/^{19}F NMR is illustrated in the chromatographic profiles of the p-fluorobenzoate derivatives of model alcohol mixtures. A

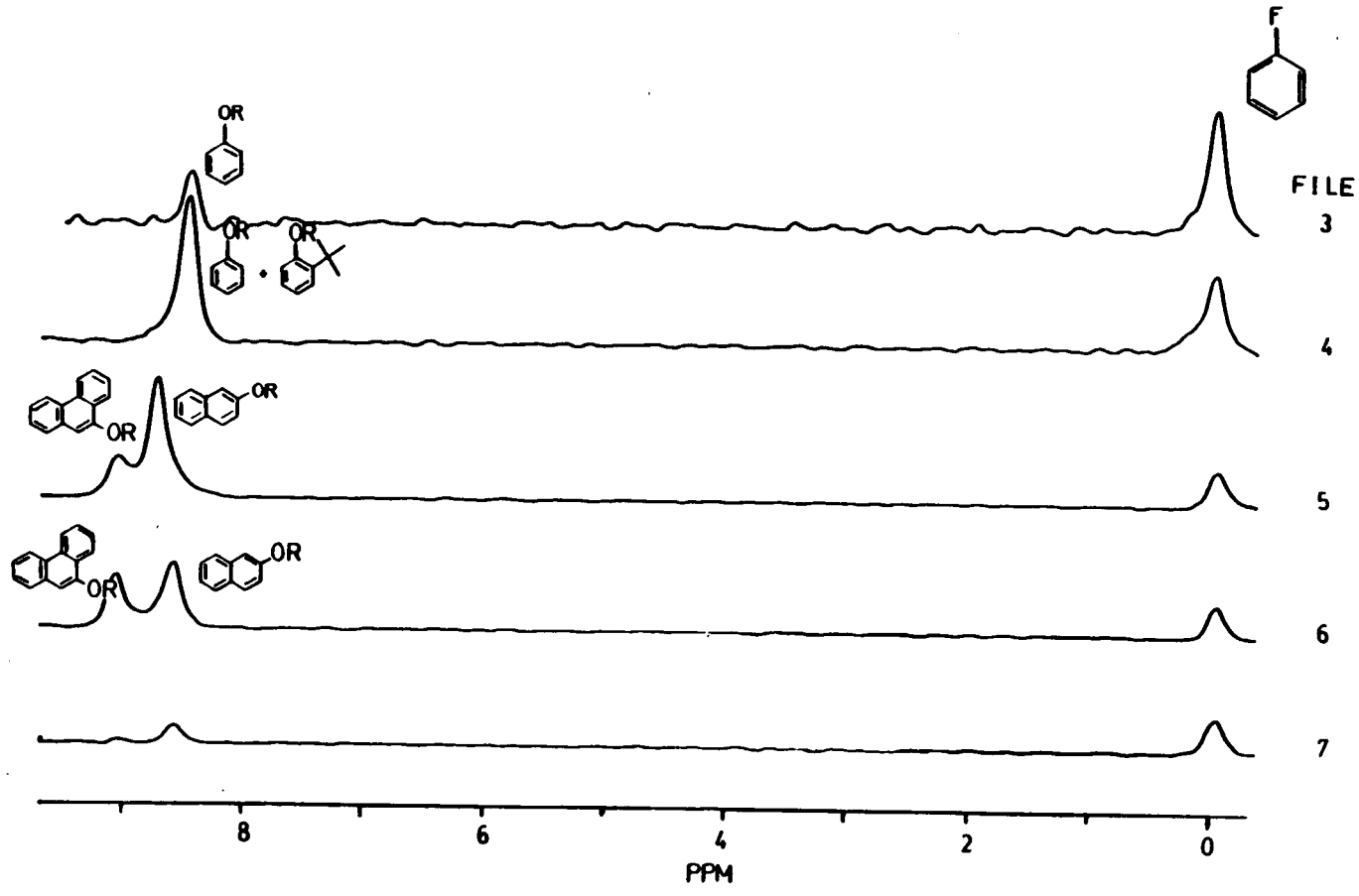

Figure 2.5 LC/^{19}F NMR profile of a mixture of aryl p-fluorobenzoates without decoupling.

simple binary mixture of 4-octanol and 1-hexanol p-fluorobenzoate derivatives can be characterized using both LC/^{1}H NMR and LC/^{19}F NMR approaches (Table 2.2). With the inclusion of 3-pentyl-p-fluorobenzoate in the mixture, LC/^{1}H NMR fails to totally characterize the mixture (Figure 2.6). A methine ^{1}H resonance (5.0 ppm) in file 3 followed by the methylene resonance (4.2 ppm) in files 4-6 suggests derivative elution orders as before with coelution of 3-pentyl-p-fluorobenzoate over files 4-6 resulting in the reappearance of a methine resonance at 5.0 ppm. The dominant ^{1}H resonances present, both alkyl and aryl, offer minimal information making minor spectral features critical for compound identification. The use of ^{19}F NMR detection (Figure 2.7) of the same mixture offers a much simpler and direct means of compound identification. The ^{19}F resonance at 6.58 ppm (files 3-4) identifies the initial elution of 4-octyl-p-fluorobenzoate. The characteristic fluorine resonance of 1-hexyl-p-fluorobenzoate is found in files 5-6. Coelution of 3-pentyl-p-fluorobenzoate clearly occurs over files 5-6 having its fluorine resonance of 6.59 ppm relative to fluorobenzene. The use of Freon-113 (trichlorotrifluoroethane) as the chromatographic solvent generates the unfortunate fold-over peak at 2.7 ppm which could be eliminated by a more appropriate choice of

TABLE 2.2

^{19}F NMR CHEMICAL SHIFTS FOR STEROL AND ALCOHOL P-FLUOROBENZOATE DERIVATIVES RELATIVE TO FLUOROBENZENE

p-Fluorobenzoate Derivative	δ_F Relative to Fluorobenzene
4-octanol	6.57
1-hexanol	6.84
3-pentanol	6.59
cholesterol	6.70
phenol	8.39
β-napthol	8.55
1-Adamantol*	5.98

* The chemical shifts (δ_F) of 1-adamantyl di-o-fluorobenzoate and 1-adamantyl m-fluorobenzoate relative to fluorobenzene are 1.20 and 0.10 ppm, respectively.

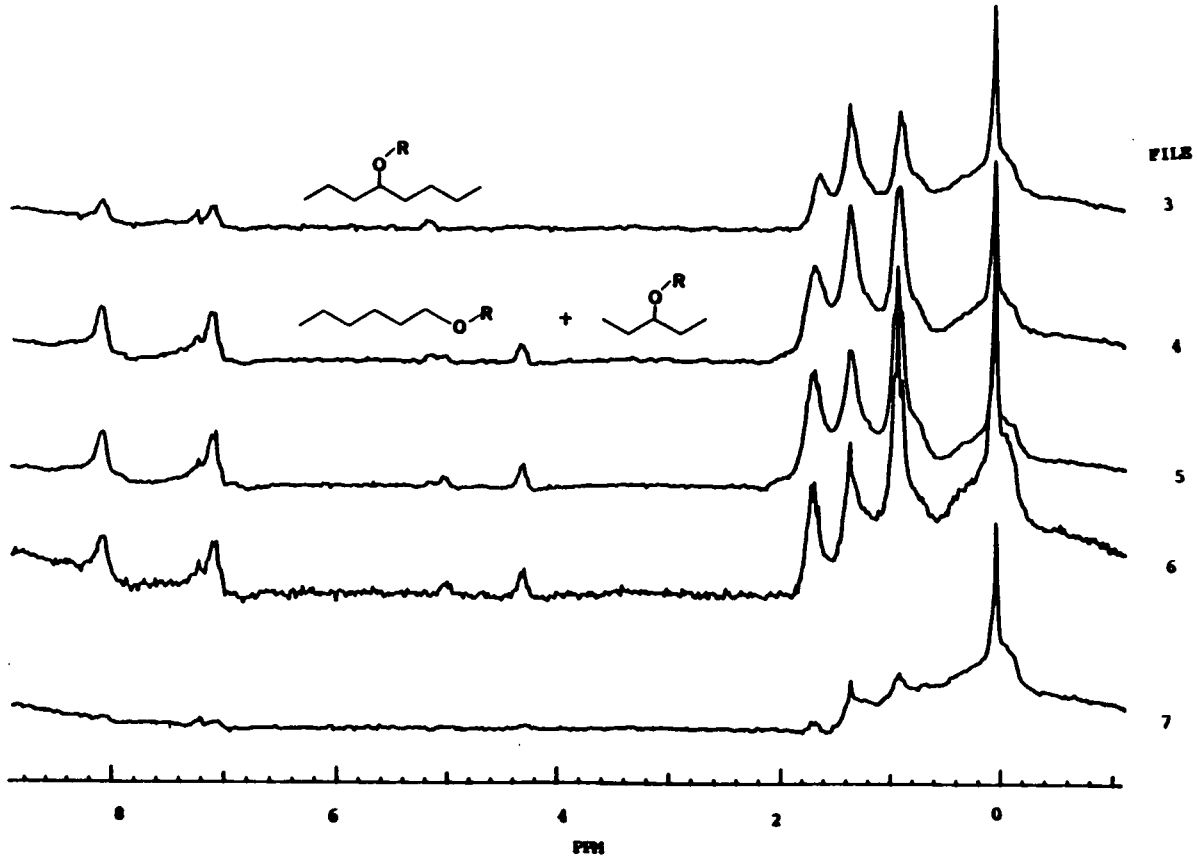

Figure 2.6 LC/^{1}H NMR profile of a ternary mixture of alkyl p-fluorobenzoates. Each file consists of 20 scans (3.5 sec/scan) for a total elution period of 70 sec.

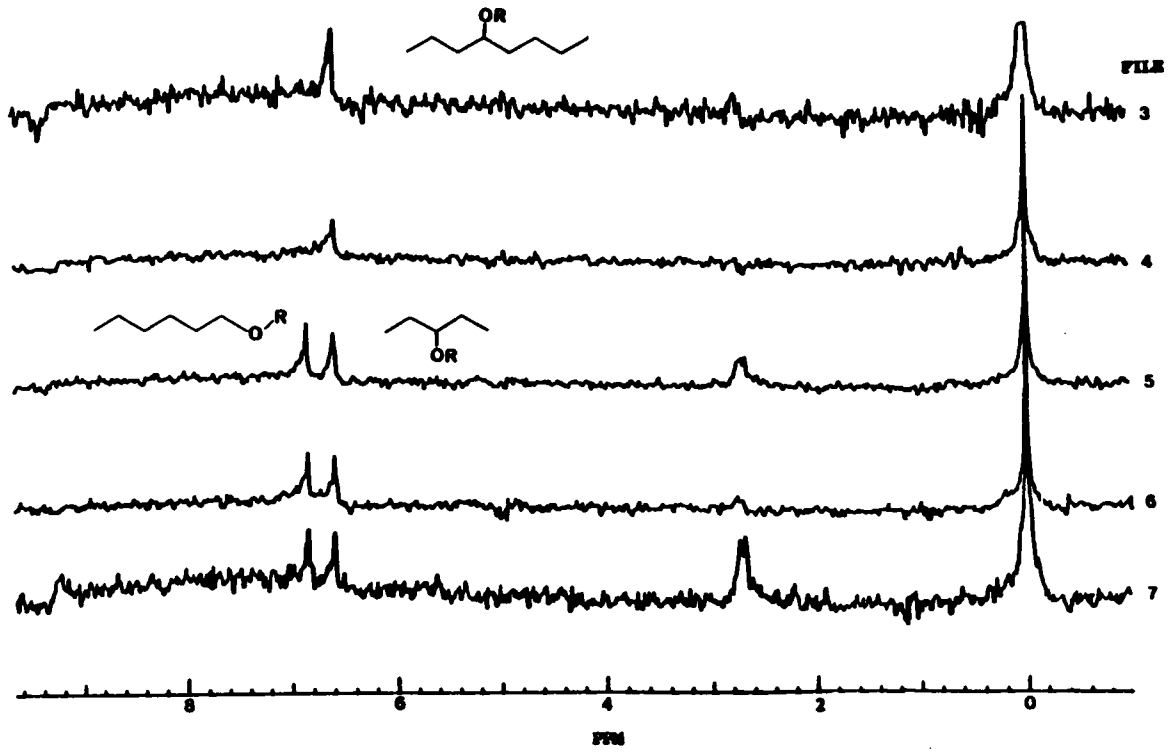

Figure 2.7 LC/^{19}F (^{1}H) NMR profile of a ternary mixture of alkyl p-fluorobenzoates. Decoupling is accomplished through MLEV-16 phase cycling. Each file consists of 20 scans (3.0 sec/scan) for a total elution period of 1 min.

solvents. Freon-113 was used in both LC/^{1}H and LC/^{19}F (^{1}H) NMR approaches in order to preserve the chromatography and allow a more direct comparison of the two methods.

Introduction of aryl alcohol p-fluorobenzoate derivatives further illustrates the utility of ^{1}H decoupling in LC/^{19}F NMR. The LC/^{1}H NMR elution profiles (Figure 2.8) support alkyl followed by aryl derivative elution. Initial elution of the cholesterol derivative followed by the 3-pentanol derivative is suggested by the dominant alkyl resonances at 0.5-2.0 ppm over files 3-4 followed in files 5-6 by the simpler resonance pattern of 3-pentyl-p-fluorobenzoate. Coelution of benzyl and β-naphthyl derivatives is supported by the prominent aryl ^{1}H resonance at 7.0-8.2 ppm occurring over files 7-8 though specific features for compound identification are absent. The reduced spectral complexity through ^{19}F NMR detection makes specific compound identification possible (Figure 2.9). The ^{19}F resonance of the cholesterol derivative at 6.70 ppm (files 3-5) is clearly unique from that of the 3-pentanol derivative occurring at 6.59 ppm (files 5-7). The nominal observed flow NMR linewidths of $\approx$5 Hz with ^{1}H decoupling allow differences in chemical shift of 0.03 ppm to be observed in the ^{19}F chemical shifts. Coelution of the β-

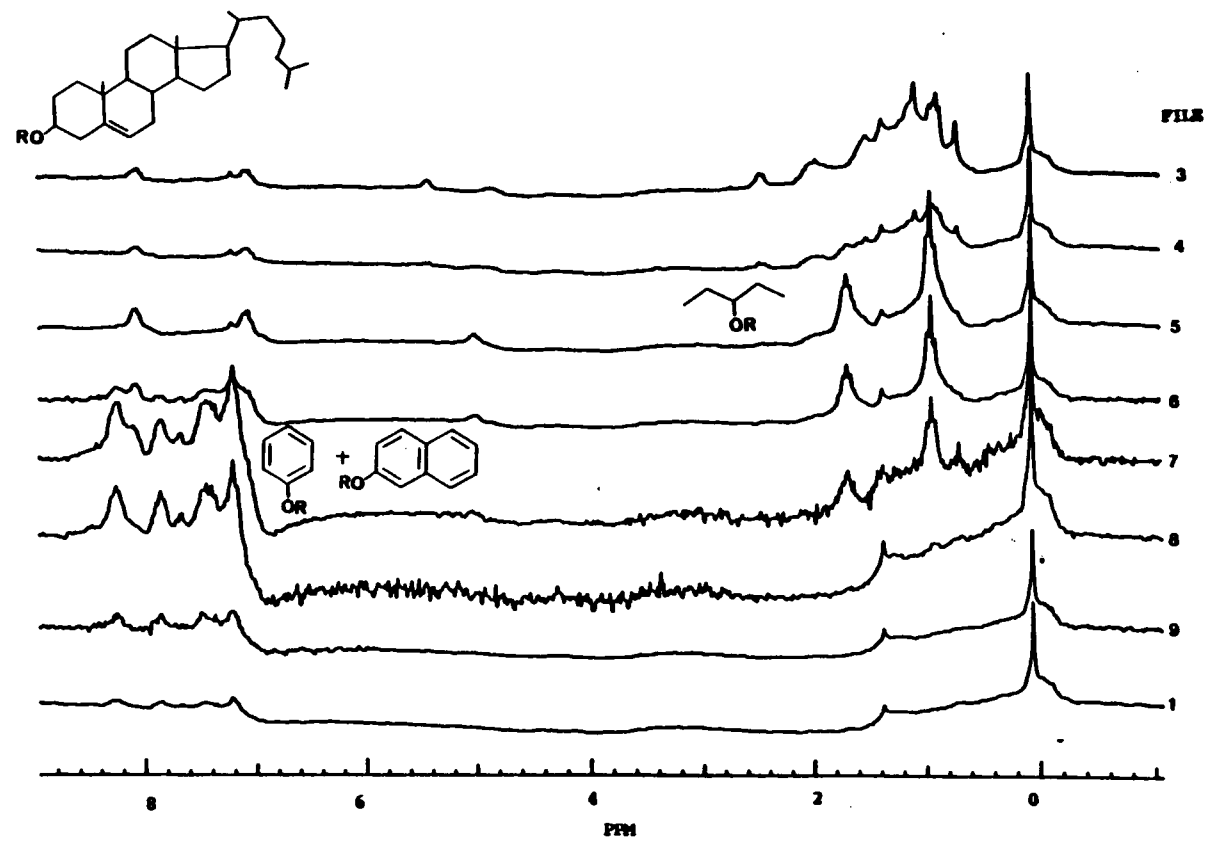

Figure 2.8 LC/^{1}H NMR profile of a mixture of alkyl and aryl p-fluorobenzoates. Each file consists of 20 scans (3.0 sec/scan) for a total elution period of 1 min.

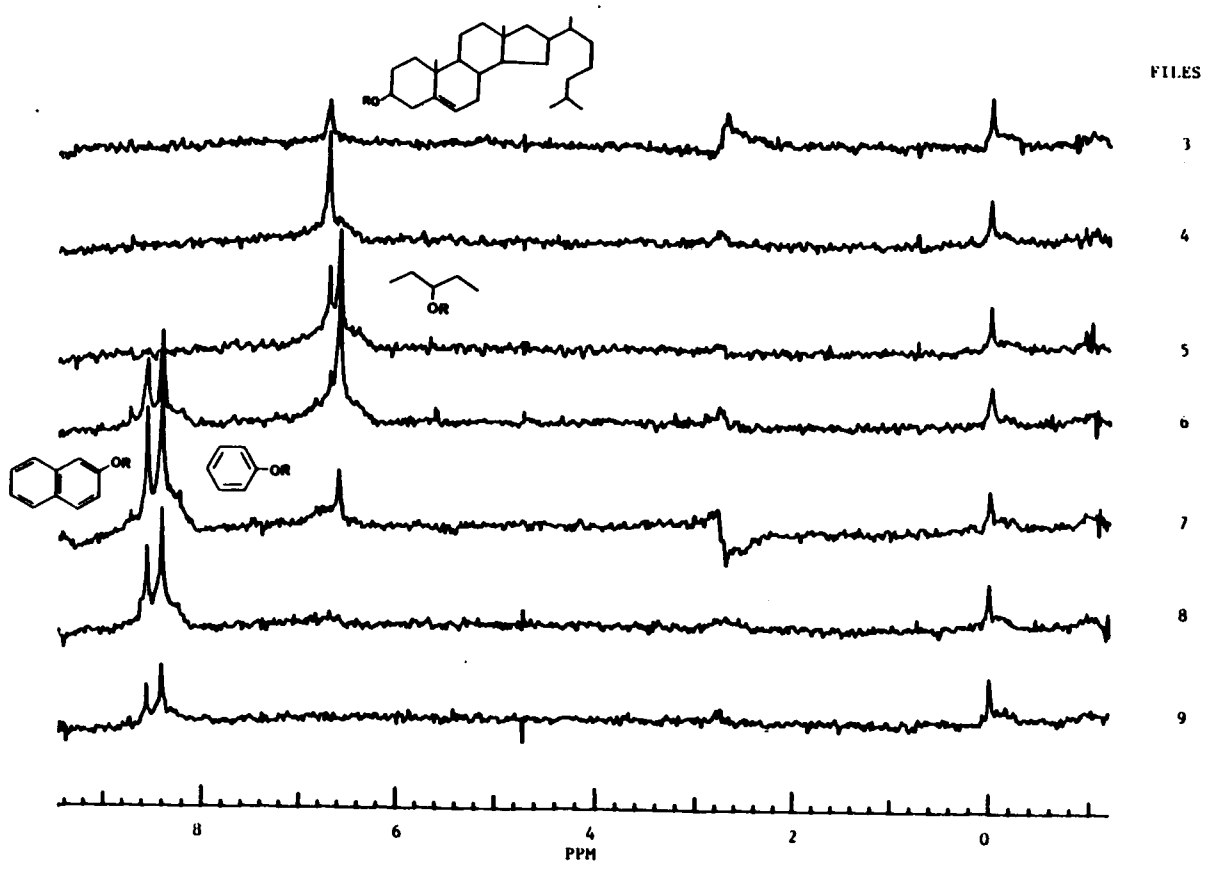

Figure 2.9 LC/^{19}F (^{1}H) NMR profile of a mixture of alkyl and aryl p-fluorobenzoates. Decoupling is accomplished through MLEV-16 phase cycling. Each file consists of 20 scans (3.0 sec/scan) for a total elution period of 1 min.

naphthyl and benzyl derivatives occurs over files 6-9 as evidenced by their unique ^{19}F resonances at 8.55 and 8.39 ppm respectively. Specific identification of these two compounds is possible only through the reduced spectral complexity of ^{1}H decoupling.

The sensitivity of fluorobenzene to the electronic environment is demonstrated in a mixture of ^{19}F substituted benzoates of 1-adamantanol. Ortho, meta, and para substitutions are compared. Separation by LC is poor and, as expected, the LC/^{1}H profile (Figure 2.10) provides no information concerning elution behavior. Examination, however, of the LC/^{19}F {^{1}H} NMR profile clearly describes the elution behavior of this very similar mixture (Figure 2.11). 1-Adamantyl-m-fluorobenzoate elutes first (file 3), with a chemical shift δ_F of 0.1 ppm relative to fluorobenzene. The p-fluorobenzoate derivative coelutes (files 3-5) having a ^{19}F resonance at 6.0 ppm and the di-o-fluorobenzoate of 1-adamantanol quickly follows (files 4-7) with a δ_F of 1.2 ppm. The chemical shift range shown of 6 ppm through fluorine ortho, meta and para aryl substitutions illustrates the high sensitivity of ^{19}F to its local electronic environment.

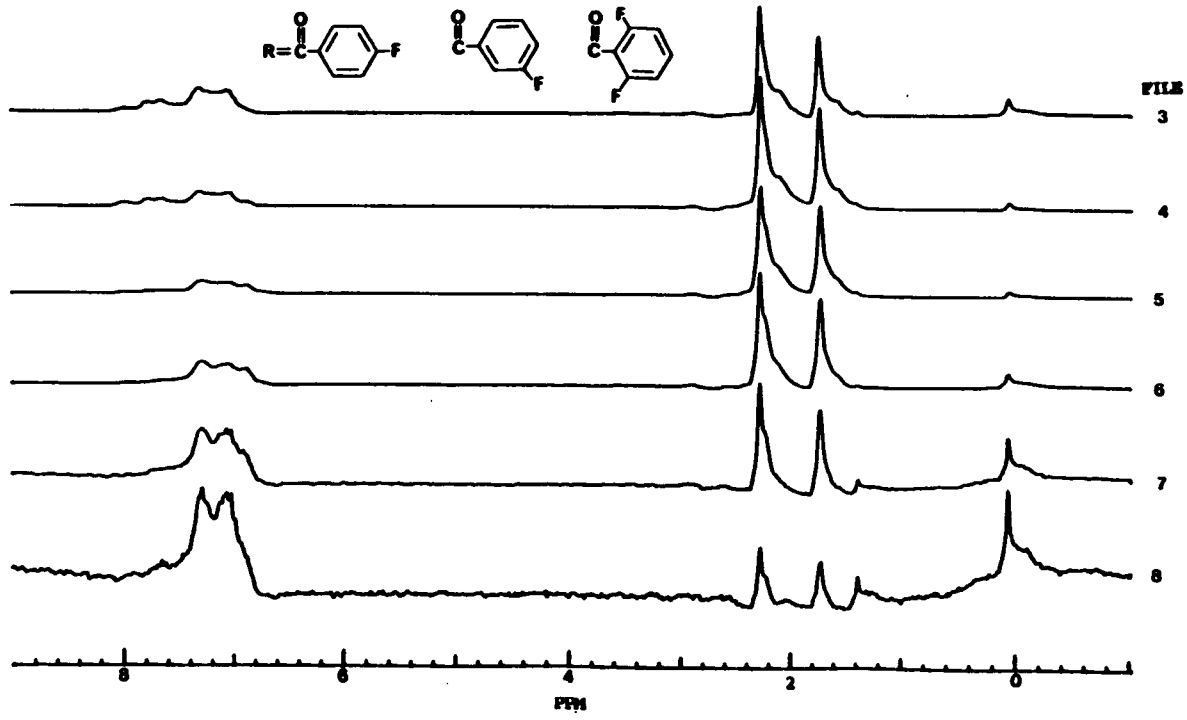

Figure 2.10 LC/^{1}H NMR profile of a mixture of ^{19}F substituted benzoates of 1-adamantanol (Di-ortho, meta, para). Each file consists of 20 scans (3.0 sec/scan) for a total elution period of 1 min.

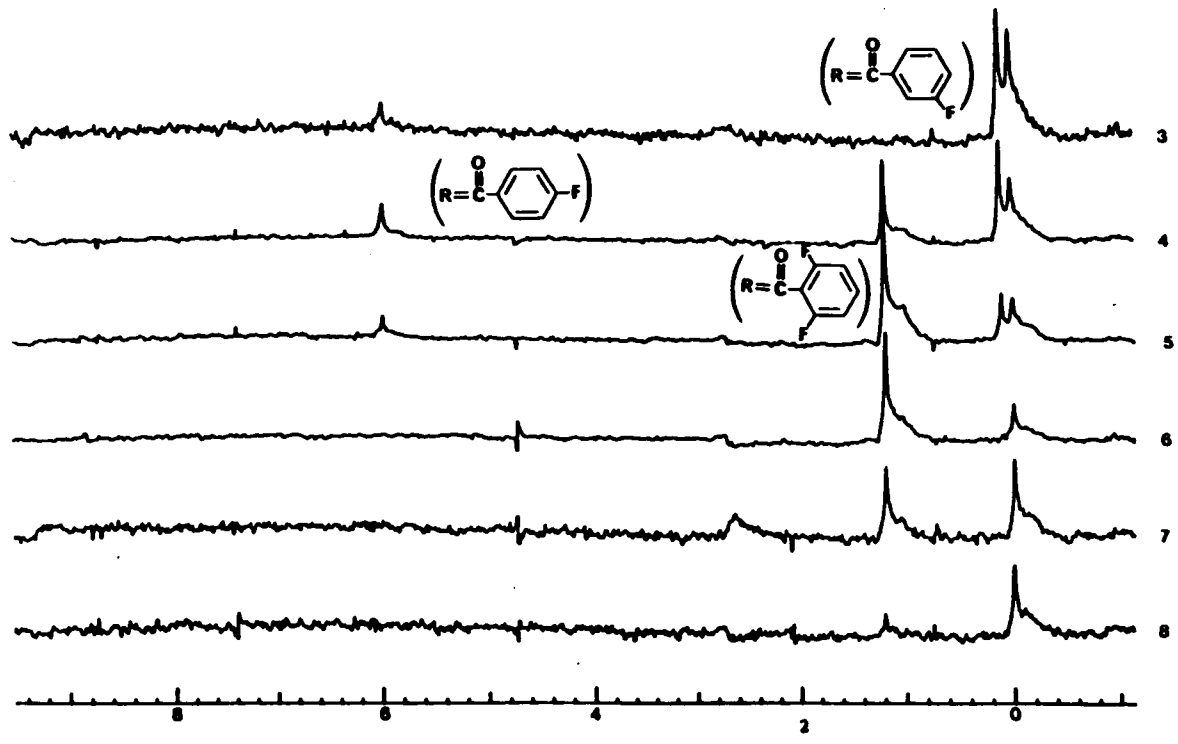

Figure 2.11 LC/^{19}F (^{1}H) NMR profile of a mixture of ^{19}F substituted benzoates of 1-adamantanol (Di-ortho, meta, para). Decoupling is accomplished through MLEV-16 phase cycling. Each file consists of 20 scans (3.0 sec/scan) for a total elution period of 1 min.

Conclusions

Just as phase-alternated ^{1}H decoupling sequences have proven useful in ^{13}C NMR spectroscopy, the MLEV-16 sequence was successfully applied to ^{19}F $\{^{1}H\}$ NMR over an effective ^{1}H spectral decoupling range of 20 ppm. This method clearly encompasses the normal ^{1}H spectral region and provides effective and efficient (0.1 watts) broadband decoupling.

The large range of ^{19}F chemical shifts and the high sensitivity of the ^{19}F nuclide to changes in the electronic environment make ^{19}F NMR a promising method for mixture analysis. The usefulness of ^{1}H decoupled ^{19}F NMR is also demonstrated in the comparison of LC/^{1}H and LC/^{19}F NMR in the analysis of mixtures of p-fluorobenzoate derivatives of alcohols. Structural similarities made ^{1}H NMR detection of the elution profiles often inconclusive while ^{19}F observation provided a simple and distinctive method of identification of the eluting compounds. The use of ^{19}F NMR detection avoids the spectral background problems normally encountered in reverse phase chromatography applications of LC/^{1}H NMR. Through effective fluorine tagging reverse phase separation and direct, selective identification by ^{19}F NMR is now feasible.

CHAPTER THREE

DEVELOPMENT AND APPLICATION OF DIRECTLY COUPLED SFC/^{1}H NMR

Introduction

Supercritical fluids are becoming increasingly important in a number of different applications because of their unique properties. High molecular weight and/or thermally labile species can be separated, and the coupling of extraction with separation has become an important application of supercritical fluid chromatography (SFC) (39). The solvating ability of supercritical fluids is related to the density of the fluid, which is readily varied by changes in either temperature or pressure. This increased flexibility can be an advantage of SFC over normal liquid and gas chromatography. To operate in the supercritical region, temperatures and pressures above the critical point (T_C,P_C) must be used. A common SFC solvent, CO_2, has the advantage of relatively low critical point parameters, T_C = 31°C and P_C = 1072 psi.

Proton nuclear magnetic resonance has been shown to be an effective detector for liquid chromatography (LC/^{1}H NMR). Solvent systems such as halocarbons (e.g. CCl_4 and Freon 113) and deuterated solvents have been used in normal phase

chromatography to help eliminate ^1H NMR background signals. For the case of reverse phase chromatography, large residual ^1H NMR background signals are usually present for the solvents typically used (e.g. D_2O, CH_3CN, etc.). Multipulse techniques have been used to suppress this residual ^1H signal, however, certain spectral regions of interest are normally not observable. An alternative chromatographic approach is the use of supercritical fluids (e.g. CO_2) which have no ^1H NMR background signal. The use of supercritical fluids requires a flow system capable of operation at elevated temperatures and pressures.

An apparatus has been developed enabling the direct coupling of supercritical fluids to a high field superconducting NMR instrument. Of particular interest is the home built NMR flow probe possessing variable temperature and pressure capabilities. The custom built NMR flow probe described is capable of operating at temperatures as high as 100°C and pressures of ≈3500 psi. An important application of this apparatus is the direct coupling of supercritical fluid chromatography to ^1H NMR (SFC/^1H NMR) (27).

Experimental

A diagram of the complete SFC/^{1}H NMR apparatus is presented in Figure 3.1. An important component in this apparatus is the pump for delivering the supercritical fluid. Reciprocating piston pumps have been modified and used effectively as solvent delivery systems for supercritical fluids (40). Pulsing, while present, can be minimized using appropriate techniques. While syringe pumps are typically used in SFC studies, the associated high expense and the need for larger flow rates made them less amenable. For our work, a single piston reciprocating pump has been effectively modified to deliver the larger flow rates needed in analytical and semi-preparative scale packed column SFC. Together with a gas chromatography oven, an effective SFC system has been assembled (Discussed in detail in Appendix I). In cases where separations were not required, the supercritical fluids were monitored with the chromatographic columns excluded from the apparatus.

The spectrometer employed was a JEOL FX-200 with a ^{1}H resonance frequency of 199.5 MHz. In order to directly couple SFC to a ^{1}H NMR spectrometer, a custom flow probe was developed capable of withstanding high pressures and maintaining stable elevated temperatures. A diagram of the

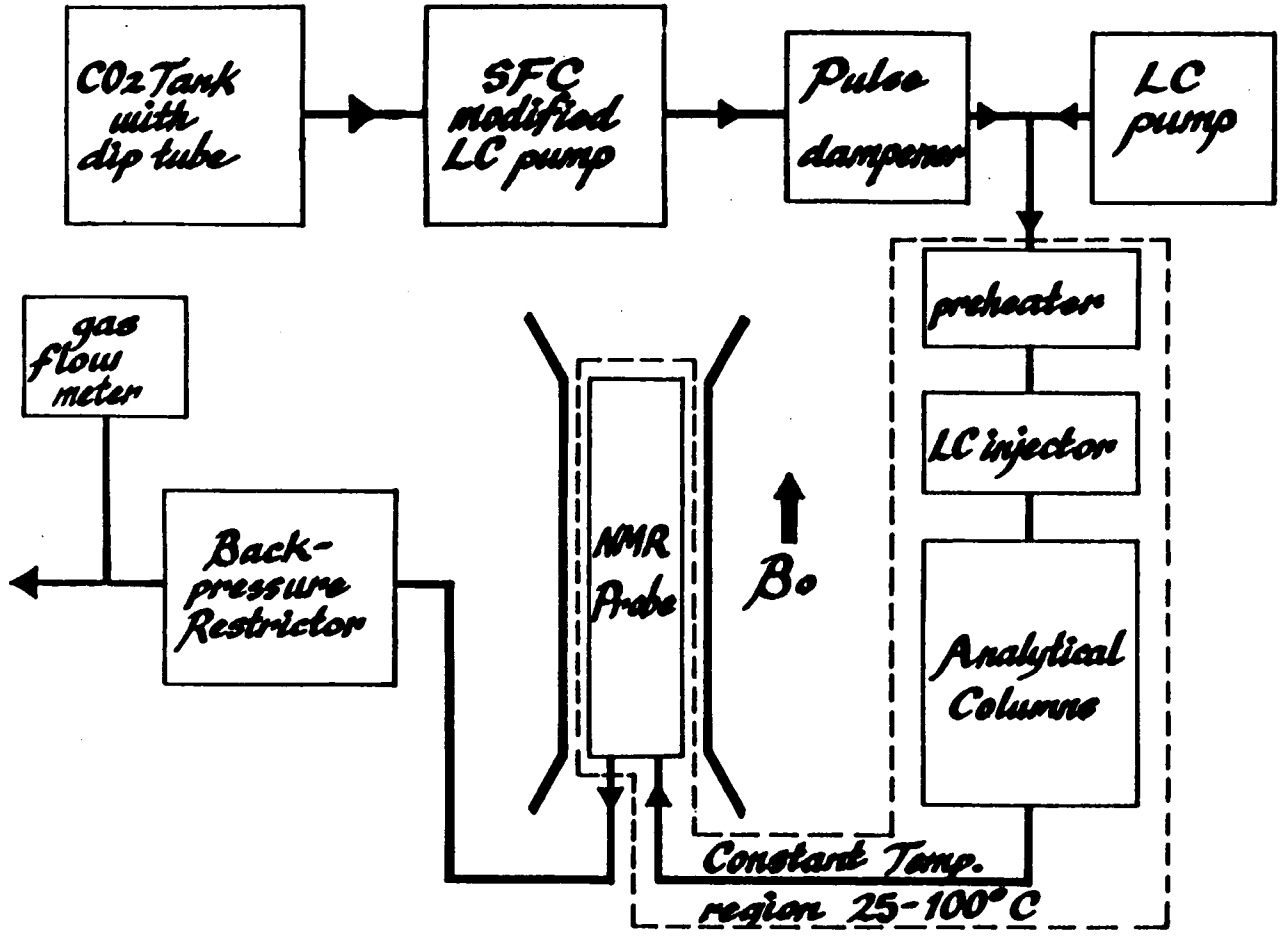

Figure 3.1 Block diagram of the SFC/^{1}H NMR system.

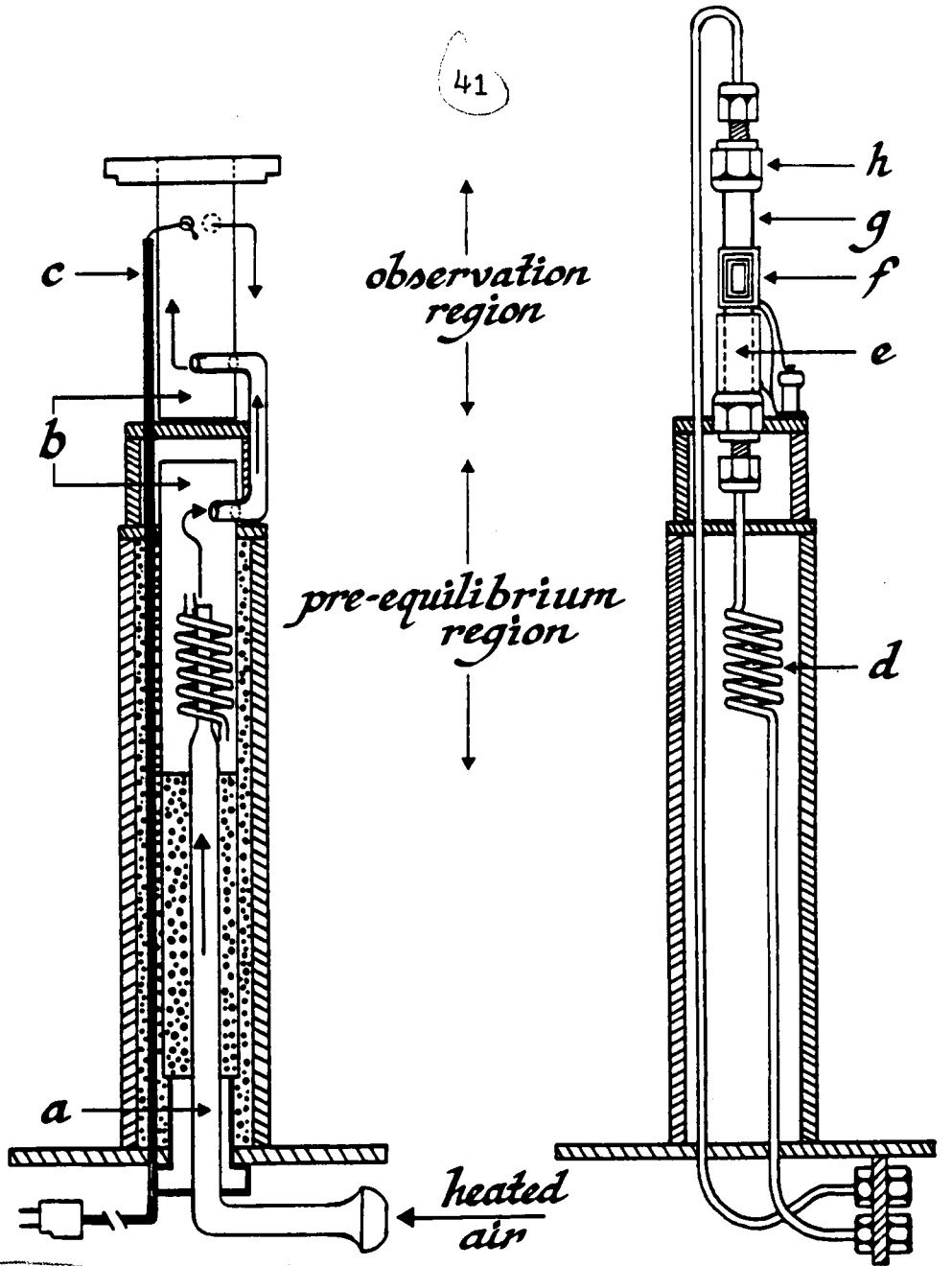

Figure 3.2 The custom flow probe for use in directly coupled SFC/NMR. Variable temperature with elevated pressure is featured.

(a) Insulated glass transfer line
(b) Glass insert
(c) Cu/Constantan thermocouple
(d) SS pre-equilibrium coil
(e) Brass shield
(f) Helmholtz coil
(g) Ceramic flow cell
(h) Brass Swagelok fitting

probe is shown in Figure 3.2. Non-magnetic materials were used exclusively in the probe construction. Equilibration of the Boltzmann magnetization at the magnetic field employed was required prior to NMR measurement; therefore, a pre-equilibrium coil precedes the observation cell. A 0.25" OD alumina ceramic tube (Omegatite 450) was used for the observation cell. This provided no NMR background with high pressure capability. Different internal diameter tubes allow a range of observation volumes (20-80 μL). Orthogonal Helmholtz coils, tuned to the respective frequency of interest (e.g. ^{1}H, 199.5 MHz and ^{14}N, 14.4 MHz) were employed. Variable temperature was achieved using forced air and blast-tube monitored by a thermocouple adjacent to the observation cell and controlled using a JEOL VT unit. Measures were taken to insure temperature stability and minimize thermal gradients. The eluent sample then passed out of the spectrometer to the back-pressure restrictor. (Further discussion of the flow probe is in Appendix I.)

Results and Discussion

A ceramic flow cell of internal diameter 1/16" was used for most experiments. A static ^{1}H NMR linewidth ($\Delta\nu$) of 1.4 Hz was obtained for this configuration. This linewidth is slightly higher than that usually obtained in HPLC/^{1}H NMR

(<1 Hz) and is presumably due to the increased possibility of ferromagnetic materials adjacent to the observation region which make optimized resolution more difficult. Based on the height of the NMR Helmholtz coil (15 mm), a detection volume of 30 μL is estimated based on geometric considerations.

A more accurate way of measuring the internal NMR observation volume (V_c) can be obtained from a [90°(HS)-τ-90°-T] sequence (41) where the observed magnetization $M_{xy}(2)$ after the second 90° pulse obeys the equations below (42):

$$M_{xy}(2)=f(1)M_o + [1-e^{-(\tau/T_1)}]\ M_o[1-f(1)] \qquad [2]$$

$$M_{xy}(2)=f(1)M_o \quad \text{for} \quad \tau<<T_1 \qquad [3]$$

where M_o is the equilibrium magnetization and f(1) is the fraction of "new" spins which flow into the NMR detector during the time period (τ). Thus, the first and second terms in Equation [2] are due to "new" and "old" spins, respectively, in the NMR detector after the time (τ). Assuming either plug or laminar flow for f(1) < 0.5, the appropriate equation for f(1) is:

$$f(1)=F\tau/V_c \qquad [4]$$

where F is the flow rate.

Data was obtained for the [90°(HS)-τ-90°-T] sequence using benzene 3.3% (v/v) dissolved in Freon 113 (undegassed) at room temperature and atmospheric pressure. Since the measured spin-lattice relaxation time (T_1) for this sample was 2.6 sec. (undegassed), Equation [3] is appropriate for these conditions ($\tau<T_1$) with τ less than 0.2 sec. A plot of $M_{xy}(2)/M_o$ versus τ provides a limiting slope of F/V_c. Since the flow rate (F) is known and M_o can be readily measured, the NMR observation volume (V_c) can be determined. Shown in Figure 3.3 is data obtained for the [90°(HS)-τ-90°-T] sequence at flow rates of 4 and 8 mL/min. From the slopes in Figure 3.3, values of 19.5 μL and 22.5 μL were obtained for V_c. Thus, a measured observation volume V_c of $\approx$20 μL appears reasonable, with this value 67% of the value obtained from geometric measurements of the Helmholtz coil.

The effect of flow on the observed NMR linewidth has been described as a relaxation mechanism as a result of the influx of "new spins" into the observation region (2,43):

$$(\Delta\omega)_{flow} = (\Delta\omega)_{static} + 1/\tau \qquad [5]$$

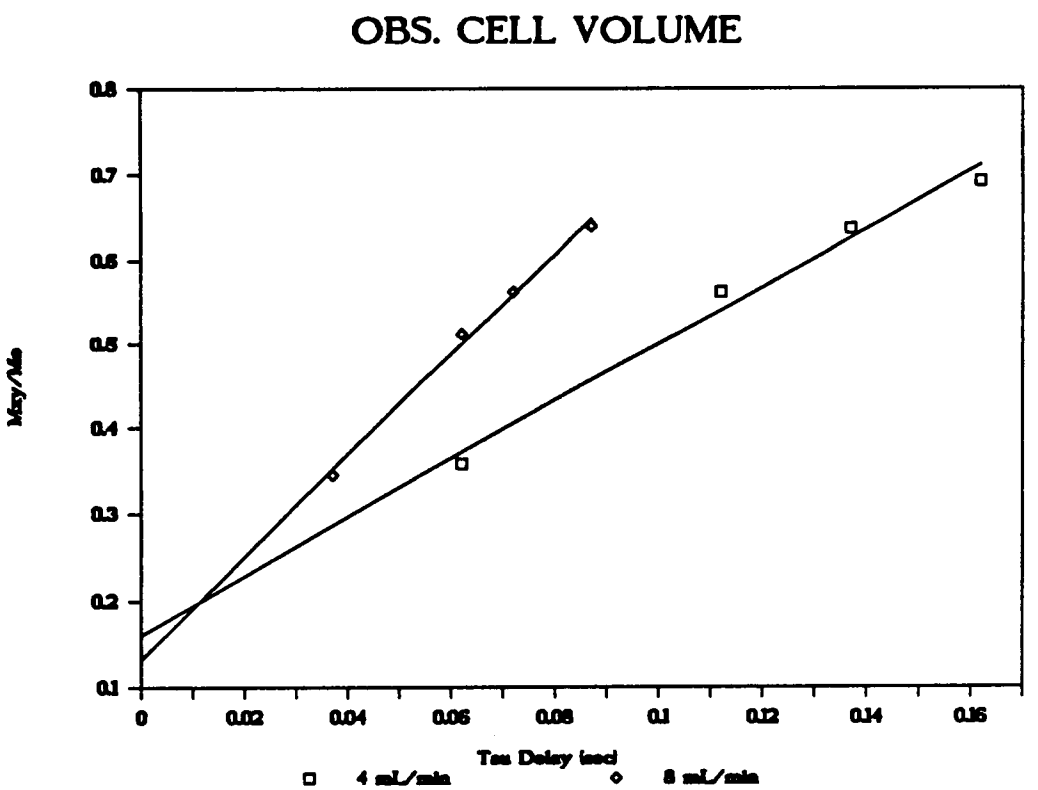

Figure 3.3 Relative magnetization ($M_{xy}(2)/M_o$) versus delay period (τ) for two flow rates.

where τ is the average residence time of a bolus in the observation region ($\tau = V_c/F$). Figure 3.4 is a plot of observed ^1H NMR linewidths versus flow rate for the present apparatus. Good agreement of observed and predicted linewidths $(\Delta\omega)_{flow}$ are obtained if a V_c ≈20 μL is used to obtain τ at a given flow rate. Additional broadening was observed at a given flow rate when temperatures above ambient temperature were employed. For example, at a flow rate of 2 mL/min., the ambient temperature linewidth of 2.9 Hz increased to 3.4 Hz at 49°C and 69°C. The additional line broadening is believed due to thermal gradients present in the SFC/NMR probe. High sensitivity to temperature fluctuations results from the strong dependence of supercritical solvent density on temperature in contrast to normal liquids. This sensitivity is particularly evident at or near the critical temperature.

Although the relatively small volume (V_c ≈20 μL) of the present NMR detector and relatively broad lines (≈4-5 Hz) at modest flow rates (≈2 mL/min.) limit the S/N of our present instrumentation, one application is the direct coupling of supercritical fluid chromatography to ^1H NMR. In cases of unlimited sample, SFC/^1H NMR is a viable approach with our present SFC/^1H NMR apparatus. As an example, a continuing

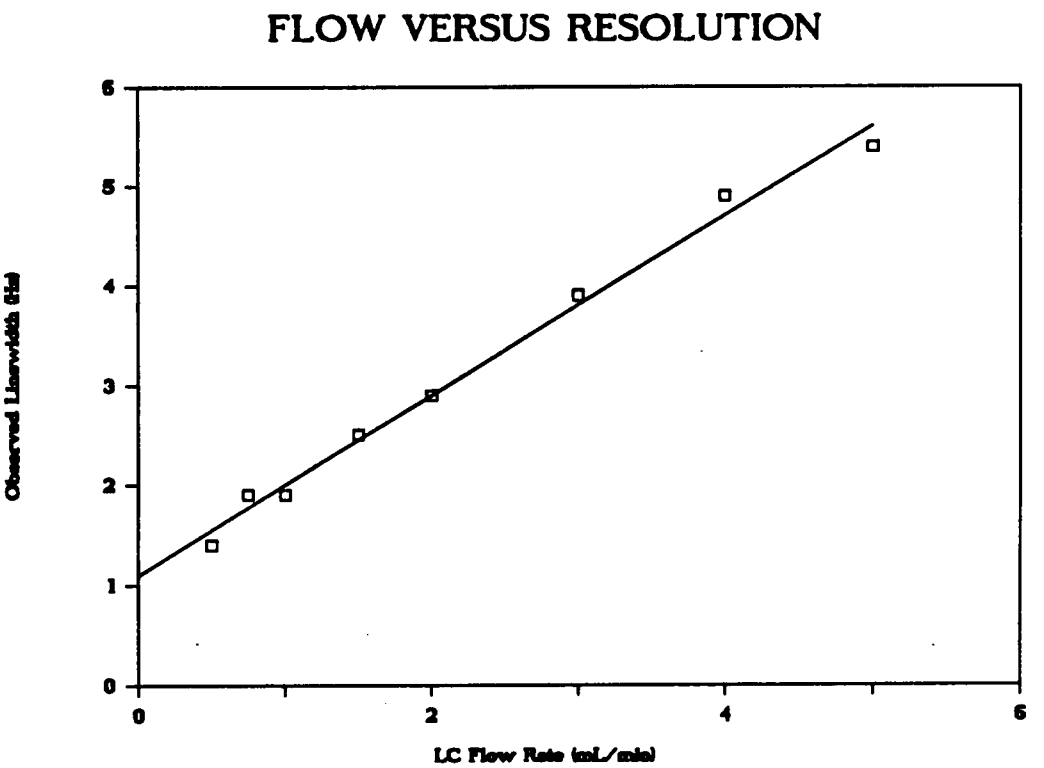

Figure 3.4 Observed changes in linewidth versus flow rate.

research interest of ours is the group analysis of petroleum distillates and fuels (7,10,11,14). Since up to 90% of a given fuel can be aliphatic, further analysis of this fraction is desirable. However, under the normal phase liquid chromatography conditions currently used, separation of this fraction is not obtained (Figure 3.5). The fuel model shown in Figure 3.5 is a mixture of components (e.g. aliphatics, monocyclic aromatics, etc.) which represent a typical fuel. The aliphatic components were isooctane (2,2,4-trimethylpentane), n-hexane, n-nonane, n-dodecane and n-hexadecane. During chromatographic elution, NMR spectra were collected. Shown in Figure 3.5 is that portion of time during which elution of the aliphatic components occurred. Due to normal phase chromatographic conditions, separation and identification of specific compounds was not possible. Separation of alkanes using reverse phase liquid chromatography is well-known and, similarly, these compounds have been extensively investigated using SFC (44). While reverse phase HPLC/^{1}H NMR using solvent suppression techniques has been described (12,20,26), elimination or distortion of alkyl resonances as a result of solvent suppression would prevent compound identification.

Using SFC/^{1}H NMR, the aliphatic components of the fuel

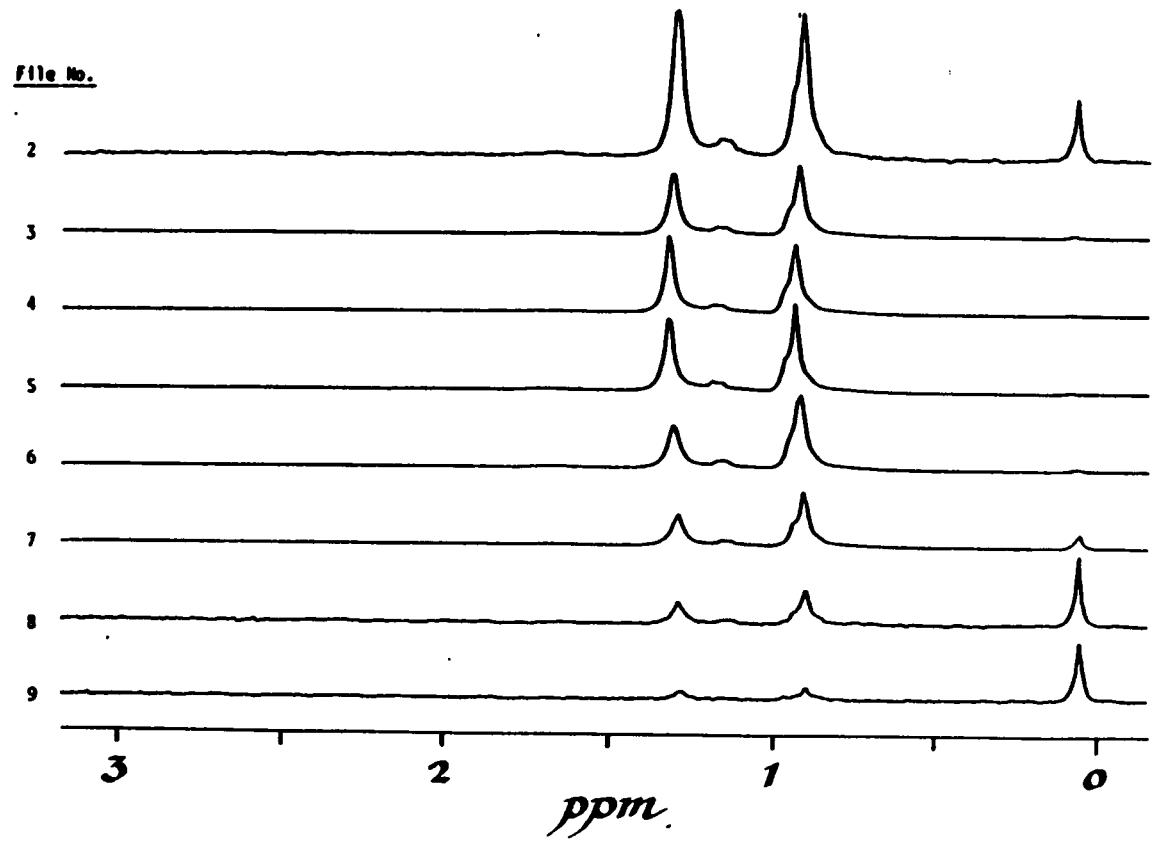

Figure 3.5 LC/^{1}H NMR elution profile of a fuel model mixture. Only those files with aliphatic components are shown. The solvent was Freon 113/$CDCl_3$ (97.5/2.5 % v/v) at a flow rate of 1.0 mL/min. A Whatman M9 10/50 PAC column was used. Each NMR file (2K points taken over a 2K bandwidth) consists of 10 scans at 3 sec/scan for an elution period of 30 sec.

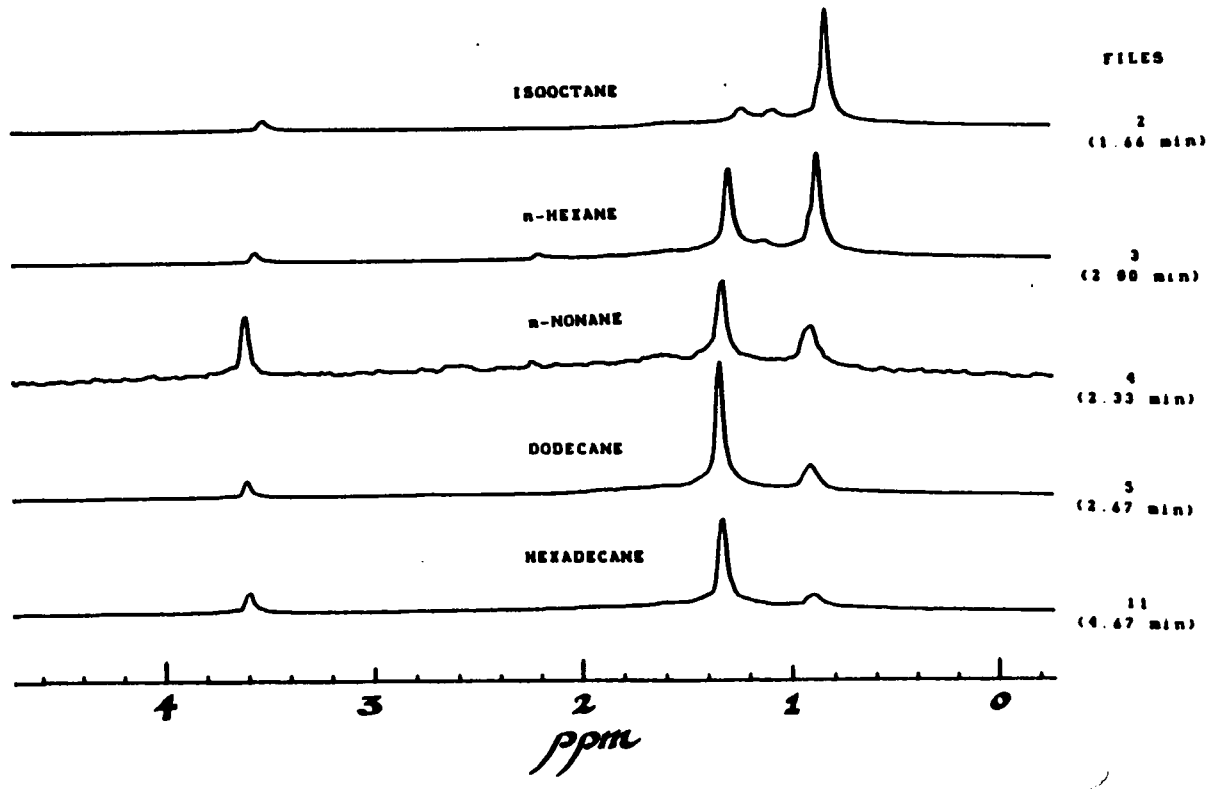

Figure 3.6 SFC/^{1}H NMR elution profile of a fuel model mixture. Only those files with aliphatic components are shown. The solvent was CO_2 with 1% (w/w) CD_3CN added as a polar modifier at a flow rate of 2.0 mL/min. Dioxane at 0.1% (w/w) serves as an internal reference (3.5 ppm). Seperation was accomplished using an Econosphere C18 250*4.6 column at an isobaric pressure of 1500 psi and 50°C. Each NMR file (2K points taken over a 2K bandwidth) consists of 20 scans at 1 sec/scan for an elution period of 20 sec per file.

model were readily separated and identified (Figure 3.6). Shown are those files during which aliphatic elution occurred, corresponding approximately to the elution periods of Figure 3.6. Individual species were identified through integration of the methyl and methylene regions of the NMR spectrum (i.e. 0.5-1.0 ppm and 1.0-1.5 ppm), respectively. Isooctane is easily identified by the disproportionate methyl to methylene ratio relative to linear alkanes. Increasing chain length parallels longer elution time, as expected. This is readily apparent as the ratio of methylene to methyl clearly increases in files 3-11. The total separation occurred in 5 minutes. The advantage of SFC/^{1}H NMR is apparent when compared to the total lack of information in Figure 3.5 using normal LC/^{1}H NMR. Direct identification of the components present eliminates the need for additional runs using standards. Through NMR detection, characterization of unknown mixtures by SFC/^{1}H NMR is clearly realizable.

Conclusions

Nuclear magnetic resonance is well-known as a powerful analytical tool directly providing chemical and structural information. An effective interface of superconducting NMR to supercritical fluids has been described which

incorporates the necessary elevated temperatures and pressures. Through modification and adaptation, normal liquid and gas chromatography components have been effectively implemented into a useful SFC system. The higher flow rates were achieved using a modified reciprocating piston pump without adverse effects due to pulsing.

In contrast to reversed phase HPLC/^{1}H NMR (12,20,22,26) the use of supercritical CO_2 requires no background signal suppression; no portion of the spectra has been adulterated. The ability to separate and identify alkanes at milligram levels has been demonstrated which illustrates the potential of on-line SFC/^{1}H NMR. The direct coupling of NMR spectroscopy to SFC further expands the potential of NMR as an analytical tool and permits the investigator to explore and evaluate the emerging importance of supercritical fluids.

Preliminary work in the investigation of detection limits, etc., for on-line SFC/^{1}H NMR suggested a number of potential problems and concerns. Temperature stability, as has already been noted, is more critical than with normal fluids. Pulsing, inherent to reciprocating piston pumps, is

also a concern. In order to achieve sufficient pre-magnetization a pre-equilibrium coil of 1 mL internal volume precedes the detection region. A residence time, prior to observation, of 3 spin-lattice relaxation times (T_1) is required to achieve a 95% Boltzmann distribution. A flow rate of 2 mL/min. results in a residence time of 30 sec., or sufficient time for proton spins having a $T_1 \leq 10$ sec. Under normal LC/^{1}H NMR conditions, dissolved oxygen acts as a relaxation agent to give T_1's of ≈1-2 sec., while supercritical CO_2 offers no means for relaxation reduction. Proton T_1's in the absence of relaxation agents can approach 1 min. requiring residence times, prior to detection, of 3 min. or more to achieve maximum Boltzmann distribution. Early studies suggested that species dissolved in supercritical CO_2 had long T_1's. Minimum detectable quantity tests failed to approach the detection limits anticipated. Chromatographic separation and detection was possible though at the expense of chromatographic efficiency when larger injected quantities were required. In order to determine the nature of relaxation in supercritical CO_2, a study was conducted of the proton relaxation of dilute solutions of benzene and acetonitrile in sub- and supercritical CO_2. (Subcritical being below the supercritical temperature)

CHAPTER FOUR

INVESTIGATION OF RELAXATION AND MOLECULAR MOTION OF DILUTE SOLUTIONS IN CO_2

Introduction

Investigation of nuclear spin-lattice relaxation times (T_1) using nuclear magnetic resonance spectroscopy leads to valuable information concerning molecular motion in liquids and gases. Similarly, studies in supercritical fluids would prove important in understanding the intermediate nature of supercritical fluids with respect to liquids and gases. Despite the importance of such studies, limited work has been done concerning NMR relaxation of supercritical fluids or dense gases.

Proton nuclear magnetic relaxation has been measured for ethylene in the critical region as a function of density (45). The T_1 was found to increase with increasing density to a maximum value ≈45 sec. at 2 times the critical density before decreasing at higher pressures. No deviation in behavior was observed for isotherms above and below the critical temperature. Examination of the effect of temperature on T_1 supports spin-rotation as the dominant relaxation mechanism at low density with intramolecular dipolar interactions being more important with increasing

density. The maximum in T_1 results from competitive inter- and intramolecular dipolar contributions as well as spin-rotation. While only qualitatively discussed due to the competitive processes, spin-rotation is shown to be an important factor in the relaxation of ethylene under sub- and supercritical conditions.

The effect of pressure on spin-lattice relaxation has been investigated by Jonas and coworkers for a number of chemical systems (46-48). While not above the critical temperatures the effect of pressure has allowed evaluation of the rotational and translational motions and the degree of coupling between them. Through examination of deuterated and protonated mixtures the relative intermolecular and intramolecular contributions to proton dipolar relaxation have been separated. The spin-lattice relaxation time (T_1) was found to decrease with increasing pressures for benzene, chlorobenzene (46), bromobenzene and toluene-d_3 (47,48). Through deuterium substitution, separation of intra- and intermolecular contributions to dipolar relaxation allowed determination of molecular translational and rotational correlation times. Experimental values were compared to theoretical values using the microviscosity approach of Hubbard (49).

The effect of pressure on T_1 relaxation of toluene-d_8 was measured at temperatures approaching the critical temperature (200°C or $T/T_c = 0.6$) (50). The observation of deuterium having a spin I = 1 is advantageous since relaxation is dominated by quadrupolar interactions and separation of inter- and intramolecular contributions is unnecessary. Experimental molecular correlation times, determined from T_1, were compared to theoretical values and discussed in terms of various theoretical models of molecular motion. The rotational diffusion model and Enskog theory are applied to overall motion while the Langevin model is also considered for internal methyl rotational motion.

Molecular motion in compressed water has been evaluated by Jonas, DeFries and Wilbur (51). Spin-lattice relaxation rates are discussed as combinations of dipolar and spin-rotation interactions and compared to predicted values. Deviation from the Debye equation results from decreased coupling of the rotational and translational motions.

Proton relaxation in supercritical water has been investigated by Jonas et al. (52,53). The spin-lattice (T_1)

relaxation time increased with increasing density. This is consistent with relaxation dominated by spin-rotation. Consistent with other investigations by Jonas, the experimental relaxation rates ($1/T_{sr}$) are compared to theoretical Enskog hard sphere approaches (52). This work is particularly significant as it emphasizes the importance of spin-rotation in the relaxation of dense gases. It is also noteworthy to mention the extreme conditions under which these measurements were made (150-700°C; 150-9000 bar).

With the increased interest in supercritical fluids in extraction processes, fundamental understanding of transport properties is desirable. Self-diffusion using NMR has been studied by Jonas et al. in compressed supercritical water (54), ethylene (55) and toluene-d_8 (56). Experimental results were consistent with the complementary spin-lattice relaxation measurements (52-53).

NMR has been used in the evaluation of naphthalene solubilities in supercritical CO_2 near the upper critical end point (57). The upper critical end point reflects the optimum condition for sample extractions. Naphthalene was equilibrated with CO_2 at different conditions. The signal

from undissolved solid naphthalene was removed through spin-spin relaxation rate differences. Nuclear magnetic resonance is shown to be effective in the evaluation of solid solubilities in supercritical fluids.

Supercritical fluids, while having densities near those of normal liquids, have viscosities more like those of gases. Reduced viscosity results in increased molecular motion such that nuclear relaxation mechanisms typical of liquids do not necessarily prevail in supercritical fluids. While dipolar interactions typically dominate proton relaxation in liquids, spin-rotation plays an important role under supercritical conditions (47,51-53). For nuclei having spins $I \geq 1$ under extreme narrowing conditions, quadrupolar interactions dominate nuclear relaxation. Efficient relaxation like that in quadrupolar nuclei results in broad observed lines. Observation of ^{14}N ($I = 1$) and ^{17}O ($I = 5/2$) in NO and CO_2 under supercritical conditions as well as NO and NH_3 dissolved in supercritical ethylene results in narrow observed lines (58). The reduction in linewidth is consistent with other relaxation mechanisms competing with quadrupolar relaxation under conditions of high molecular motion. In contrast to the supercritical fluids or dissolved gases studied by Robert and Evilia (58),

Jonas has investigated line-narrowing of dissolved solids containing quadrupolar nuclei in supercritical ethylene (59). Line-narrowing factors on the order of 2-6 were observed in contrast to that predicted (up to 200) from known supercritical fluid viscosities. The high fluid densities necessary for solute solubility are not optimal for low viscosity line-narrowing. Reductions in viscosity improve the line-narrowing at the expense of solute solubility. Despite these limitations the use of supercritical fluids remains an important advantage in the observation of quadrupolar nuclei.

The proton relaxation behavior of liquid benzene has been well studied. Using increased pressure, nuclear relaxation was found to be dipolar dominant (46). Through deuterium substitution intra- and intermolecular interactions were separated. Molecular translational and rotational correlation times were determined. Powles and Figgins have investigated nuclear relaxation in benzene, in a similar manner, using increased temperature (60). The observed dipolar interactions are consistent with Jonas (46) however at high temperatures (≈200°C) measured T_1's approach a maximum discussed in terms of competition of spin-rotation with dipolar relaxation processes.

The molecular motion of acetonitrile has been investigated through the observation of ^{14}N linewidths. Reduction in quadrupolar efficiency through increased molecular motion results in reduced observed linewidths. Tiffon and Ancian have determined molecular correlation times through measurement of ^{14}N linewidths of acetonitrile in CCl_4 at different concentrations (i.e., reduced viscosities) (61). Unusual behavior was reported at low concentrations (0.17 mole fraction) where the observed linewidth decreased dramatically. This was interpreted as the break-up of molecular clusters (62) resulting in a dramatic reduction in intrinsic microviscosity. Molecular rotation of acetonitrile in various n-alkanes has been studied by Ancian and Tiffon (63) through observation of ^{14}N linewidths at various temperatures. The determined molecular correlation times in the different n-alkane solvents are compared to a slip-boundary theoretical model.

Investigations of molecular motion at or near the critical state to date have addressed neat liquids. The behavior of dissolved species has not been addressed. The molecular motion cannot be assumed to be the same as the dense gas, therefore investigations of motion of dilute

species best describes the conditions associated with supercritical extraction and separation transport properties.

Theory

Nuclear magnetic relaxation can be described using the classical Bloch approach (64). The return of the perturbed magnetization (M_z) to thermal equilibrium (M_o) predicted using Boltzmann's distribution law is described as an exponential decay process and can be broken up into parallel and perpendicular components of M:

$$dM_z/dt = -(M_z-M_o)/T_1 \qquad [6]$$

$$dM_x/dt = -M_x/T_2 \qquad dM_y/dt = -M_y/T_2 \qquad [7]$$

Integration of [6] and [7] yields:

$$M_z(t)-M_o = [M_z(0)-M_o]\ \exp(-t/T_1) \qquad [8]$$

$$M_x(t) = M_x(0)\ \exp(-t/T_2) \qquad [9]$$

$$M_y(t) = M_y(0)\ \exp(-t/T_2)$$

The longitudinal relaxation time (T_1) or the relaxation rate ($1/T_1$) is denoted spin-lattice as it describes relaxation

through interactions of the nuclear spin with the lattice. The transverse relaxation time (T_2) is denoted spin-spin as it describes relaxation through interactions between spins of different nuclei.

The relaxation rates can be broken up into sums of contributing mechanisms:

$$1/T_1 = 1/T_{1dd} + 1/T_{1sr} + 1/T_{1sa} + 1/T_{1sc} + 1/T_{1ue} + 1/T_{1q} \quad [10]$$

and similarly:

$$1/T_2 = 1/T_{2dd} + 1/T_{2sr} + 1/T_{2sa} + 1/T_{2sc} + 1/T_{2ue} + 1/T_{2q} \quad [11]$$

The dipolar contribution ($1/T_{1dd}$) can be further broken down into inter- and intramolecular interactions:

$$1/T_{1dd} = 1/T_{1dd}(\text{inter}) + 1/T_{1dd}(\text{intra}) \quad [12]$$

Utilizing dilution in deuterium analogs and under conditions where dipolar interactions are the assumed dominant mechanism of relaxation:

$$1/T_1(\text{exp}) = 1/T_{1dd}(\text{intra}) + [(1+23x)/24]\ 1/T_{1dd}(\text{inter}) \quad [13]$$

where x is the mole fraction of hydrogen containing compound (46,60). The second term takes into account the deuterium intermolecular contribution to relaxation. Hubbard (49) provides the following expression for intermolecular dipolar contributions to $1/T_1$:

$$1/T_{1dd}(\text{inter}) = \frac{12\pi}{5}\hbar^2\gamma^4\frac{N}{dD}[1+0.233(b/a)^2+0.15(b/a)^4+...] \quad [14]$$

where:
- γ - the magnetogyric ratio of proton
- N - the number of molecules/cm^3
- d - the distance of closest approach
- D - the self-diffusion constant
- b - the distance of each proton from the center of the molecule
- a - the molecular radius

Expressing D in terms of viscosity using the Einstein-Stokes relation $D = kT/3\pi\eta d$ yields:

$$1/T_{1dd}(\text{inter}) = \frac{36\pi^2}{5}\hbar^2\gamma^4\frac{\eta N}{kT}[.....] \quad [15]$$

Intramolecular dipolar interactions can be described by (49):

$$1/T_{1dd}(\text{intra}) = \frac{3}{2}\gamma^4\hbar^2\tau_c/r^6 \quad [16]$$

Coherent molecular motion generates a magnetic field

which can couple to the nuclear spin resulting in relaxation. These interactions are referred to as spin-rotation and for cylindrical molecules can described as (65):

$$1/T_1(sr) = \frac{2}{3} I_o \frac{kT}{h^2} \tau_{sr} (2C_{\perp}^2 + C_{||}^2) \qquad [17]$$

where: I_o - the moment of inertia
C - the perpendicular ($\perp$) and parallel ($||$) components of the spin-rotation interaction constant
τ_{sr} - the spin rotation correlation time

The correlation time (τ_{sr}) is related to the time between molecular collisions and is inversely related to the molecular correlation time (τ_c), and under diffusion control, can be described using the Hubbard equation:

$$\tau_c \tau_{sr} = I_o/6kT \qquad [18]$$

where $\tau_{sr} << \tau_c$.

The molecular correlation time τ_c has often been considered related to viscosity through the Debye equation (46,48,50-53,60,63).

$$\tau_c = KV_m\eta/kT \qquad [19]$$

where: V_m - the molecular volume

η - the macroscopic viscosity
K - a parameter introduced by a number of investigators to describe deviation from the ideal condition of Debye.

By substituting [19] into [18] and substituting [18], solved for τ_{sr}, into [17], we note the predicted inverse dependence of $1/T_1(sr)$ on η/T:

$$1/T_1(sr) = [(2I_o^2kC^2)/(18\hbar^2KV_m)](T/\eta) \qquad [20]$$

For quadrupolar nuclei in solution, molecular motion modulates the electric field gradient resulting in efficient relaxation. Under extreme narrowing:

$$1/T_{1q} = 1/T_{2q} = \frac{3\pi^2}{10}\frac{(2I+3)\chi^2\tau_c}{I^2(2I-1)} \qquad [21]$$

where: I - the nuclear spin
χ - the quadrupolar coupling constant (e^2Qq/h)
τ_c - the molecular correlation time

The observed NMR linewidth ($\Delta\nu_{1/2}$) results, for nuclei having spin I = 1/2, from contributions of spin-spin relaxation and B_o inhomogeneity.

$$\pi\Delta\nu_{1/2} = 1/T_2^* = 1/T_2 + 1/T_2(B_o) \qquad [22]$$

For nuclei having spin $I \geq 1$, where quadrupolar relaxation dominates, the electric field gradient modulations result in observed linewidths substantially more than that due to B_o inhomogeneity such that:

$$\pi \Delta\nu_{1/2} = 1/T_{2q} = \frac{3\pi^2}{10} \frac{(2I+3)}{I^2(2I-1)} \chi^2 \tau_c \qquad [23]$$

where $\Delta\nu_{1/2}$, the observed linewidth, is a direct measure of nuclear relaxation and molecular correlation times, under quadrupolar dominated relaxation.

The review of Boere and Kidd discussed rotational correlation times and the equations and models used to describe them (66). Using classical arguments the time required for a freely rotating molecule to rotate any angle is:

$$\tau = \theta(I/3kT)^{1/2} \qquad [24]$$

This constitutes rotation in the absence of any viscous drag, or the inertial region.

Liquid phase rotation experiences viscous drag causing the τ_{rot} to be longer than that in the inertial region. It is however instructive to define a condition approaching the

inertial region as:

$$\tau_{FR} = (I/kT)^{1/2} \qquad [25]$$

where τ_{FR} describes the rotational correlation time in the absence of viscous drag.

In the rotational diffusion region, a τ_C is used to describe the time it takes a molecule to rotate 1 radian. Each rotation is treated as occurring in discreet increments or steps; the number of steps is associated with a collision. The collision frequency is therefore the collision number $(Z)/\tau_C$. There exists then a time $\tau_C/(Z)$ which reflects the time in between collisions. The time (τ_C/Z) is described by τ_{sr}, the spin-rotation correlation time.

The Hubbard relation noted in Equation [18] describes the inverse relationship of these two correlation times. It applies however, only in the diffusion control region of molecular motion. It is important then to recognize when this is the case.

Wallach and Huntress have devised a test for the

diffusion control condition (67). Considering $\tau_{FR} = 3/5(I/kT)^{1/2}$, a constant X can be determined where:

$$X = \tau_C/\tau_{FR} = 5\tau_C/3(kT/I)^{1/2} \quad [26]$$

The factor (3/5) results from equipartitioning of energy approaches. Boltzmann r.m.s. angular velocity results in a factor of 1.0 (68) and a Maxwellian distribution of energies results in a factor of 4/5 (69).

Gillen and Noggle (70) have applied the X test of Wallace and Huntress and have established the arbitrary boundaries of:

$X < 3$	:	inertial
$3 < X < 5$	:	intermediate
$X > 5$	:	diffusion

Various models have been developed to describe molecular motion. Motion in a gas is treated as relatively unhindered and in a liquid, the motion is dependant on viscosity and temperature:

$$\tau_C = \tau_O + \eta\tau_{red} \quad [27]$$

where τ_O represents the condition approaching no viscous

drag, at a constant temperature. For temperature effects:

$$\tau_C = \tau_O + (\eta/T)\tau_{red} \qquad [28]$$

where τ_O is now ambiguous and can represent either $T \approx \infty$ at a given viscosity or viscosity ≈ 0 at a given temperature.

The classical Stokes-Einstein-Debye model describes molecular motion as:

$$\tau_C(SED) = V_m\eta/kT$$

where K=1 of Equation [19]. This approach has been found to overestimate the influence of viscosity therefore Gierer and Wirtz have introduced a constant that reflects the "microviscosity" as a function of solvent/solute dimensions (71):

$$K = f = [6(a_S/a) + (1 + a_S/a)^{-3}]^{-1}$$

where (a_S) and (a) are the solvent and solute radii, respectively. The ratio limits correspond to boundary conditions often referred to as "slip" ($a_S/a>>1$) and "stick" ($a_S/a<<1$). Hu and Zwanzig have extended this approach beyond spherical molecular conditions to that of oblate and prolate spheroids through introduction of a shape factor

(72).

The models however predict τ_{red} of Equation [27] and not τ_c for conditions in the diffusion region. Measurements of τ_c can be related to τ_{red} through plots of τ_c versus η providing a slope of τ_{red}, or through division by η for a single τ_c value. Most investigations have been the latter.

Experimental

A JEOL FX-200 nuclear magnetic resonance spectrometer was used to obtain ^1H and ^{14}N spectra at 199.5 and 14.4 MHz, respectively. The high pressure, elevated temperature conditions were maintained using the flow probe and delivery system described in Appendix I (Figure 3.1). Proton spin-lattice relaxation times were measured using the inversion recovery method discussed in more detail in Appendix II. Stopped flow was used for these measurements, both ^1H and ^{14}N; the chromatographic portion of the experimental set-up was eliminated. Equilibration at a given temperature was determined through signal observation over 10 min. with a relative standard deviation $\sigma_n/\bar{M}_{xy} \leq 0.04$. Despite temperature control $\pm 1°C$, multiple scanning was necessary due to the high sensitivity of supercritical fluid densities to small temperature changes. Typical acquisition parameters

for ^{1}H and ^{14}N are found in Table 4.1.

The proton relaxation rates determined are evaluated relative to macroscopic viscosities determined using tabulated values of pure CO_2 (73,74). The solvent densities used were obtained from the compiled data of Vargaftik (75) and have not been corrected for the presence of solute.

Benzene and acetonitrile solutions were prepared in the following manner. Individual samples were dried over molecular sieves then filtered. Samples were then degassed using dry N_2 for ≈1.5 hr. to remove any O_2 which could act as a paramagnetic relaxation agent. Measured T_1's of these degassed samples were consistent with known values of pure liquid samples (benzene T_1 = 11.6 sec.; acetonitrile T_1 = 8.2 sec.) Known quantities of each were introduced into the sample cylinder under positive N_2; SFC grade CO_2 was then transferred to the cylinder and the increase in cylinder weight was monitored.

Results and Discussion

Proton relaxation rates ($1/T_1$) were measured for benzene in CO_2 at 1.0 and 0.8% (w/w) under different

TABLE 4.1

TYPICAL NMR ACQUISITION PARAMETERS

	T_1 and T_2 Determination	
	^{1}H	^{14}N
Observation Frequency	199.50 MHz	14.38 MHz
Pulse type	180°-τ-90°-Aqu	90°-Aqu
90° Pulse Width	6.3 μsec	43 μsec
Spectral Width	2000 Hz	4000 Hz
Number Points	4096	4096
Number Sample Points	4096	1024*
Acquisition Times	1.024 sec	128 msec
Number of Scans	4	4000

* By zero filling after the FID decay, spectral resolution is retained without sacrificing S/N.

temperatures and pressures. Measurements were made at subcritical ($<T_c$) and under expected critical conditions. A plot of relaxation rate ($1/T_1$) for 1.0% benzene versus viscosity/temperature (η/T) shows inverse behavior indicative of spin rotation dominated relaxation (Equation [20]) (Figure 4.1). Possible minimization of the T_1^{-1} value suggests other mechanisms such as dipolar interactions becoming more important. A similar plot of ($1/T_1$) versus (η/T) for the 0.8% solution shows a more prevalent inverse relationship with possible levelling of T_1^{-1} occurring only at high η/T ($\eta/T \approx 0.32$) (Figure 4.2). Deviation in the behavior in the range of η/T (0.14 - 0.26) is a result of other mechanisms of relaxation influencing the former more so than the latter. The 1% solution was not degassed as described and therefore trace paramagnetic O_2 could have influenced the overall relaxation. The 0.8% solution will therefore be considered representative of the relaxation under no external relaxation influences.

The minimization of T_1^{-1} results from competitive relaxation mechanisms. Assuming dipolar relaxation being the other primary mechanism, at the minimum (60):

$$1/T_1(\text{exp}) = 1/T_1(\text{sr}) + 1/T_1(\text{dd}) \qquad [29]$$

$$\text{and } 1/T_1(\text{sr}) = 1/T_1(\text{dd})$$

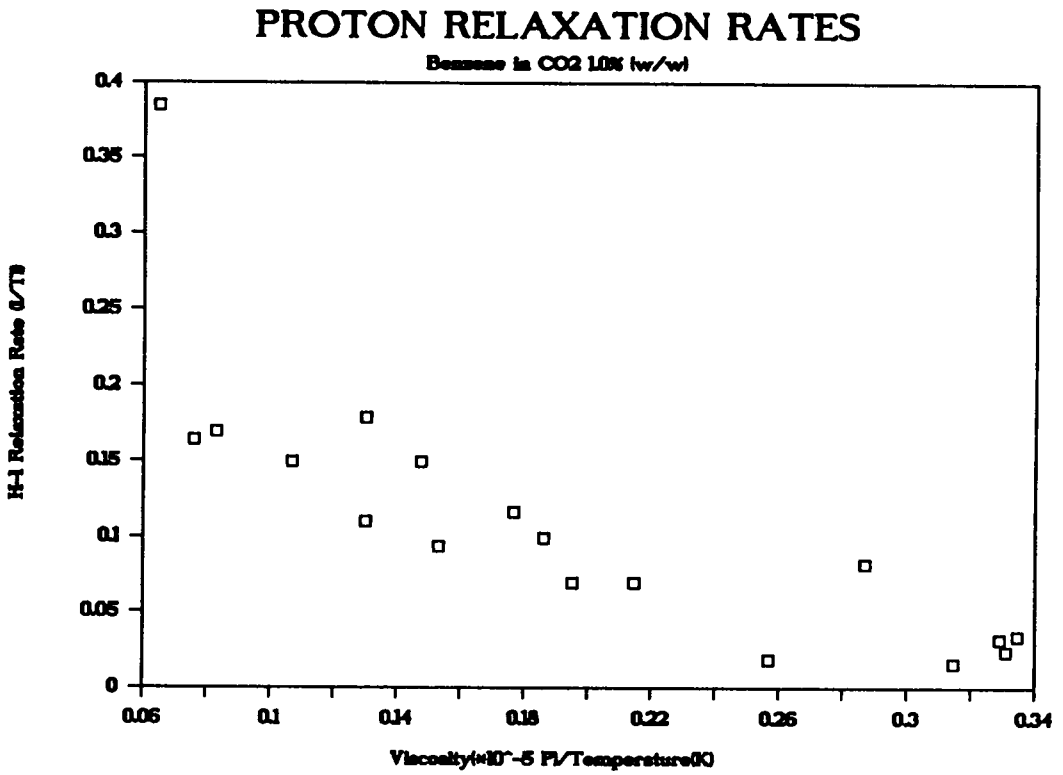

Figure 4.1 Benzene ^{1}H relaxation rates ($1/T_1$) versus viscosity/temperature for 1.0% (w/w) in CO_2.

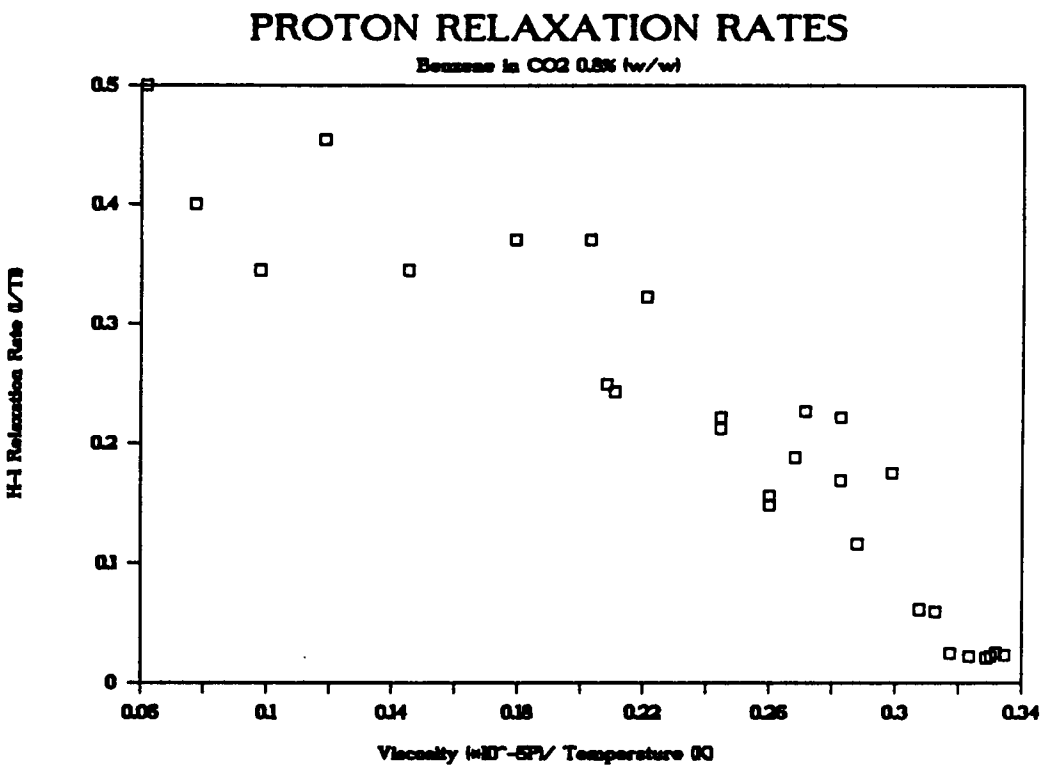

Figure 4.2 Benzene ^1H relaxation rates ($1/T_1$) versus viscosity/temperature for 0.8% (w/w) in CO_2.

Using Equation [16] where $1/T_1(dd) = 1/2[1/T_1(exp)]$ Powles and Figgins established that the transition from dipolar to spin-rotation interactions occurred at $T_1 \approx 140$ sec. and $\tau_c = 0.42 * 10^{-12}$ sec. for liquid benzene. Questionable use of the Hubbard relation ($\tau_{sr} \approx \tau_c$) yielded a $\tau_{sr} = 0.19 * 10^{-12}$ sec. at this condition (59). Examination of the magnitude of T_1 (3-45 sec.) over the η/T range shown (Figure 4.2) suggests that relaxation in supercritical CO_2 is dominated by spin-rotation with only small contributions of dipolar interactions.

Evaluation of molecular motion where $1/T_1(dd) = 1/T_1(sr)$ is difficult since the extent of contribution of dipolar interactions, though small, to the overall relaxation process was not established. If, however, it is assumed that spin-rotation is dominant and neglecting any dipolar contribution, Equation [17] can be used to evaluate τ_{sr}. Using $C^2 = 5.70 * 10^8$ sec.$^{-1}$ from Powles and Figgins (59), τ_{sr} ranges from 1.00 psec. at low η/T to a value of 0.05 psec. at highest η/T. Table 4.2 summarizes all molecular correlation time values obtained. Applying the Hubbard relationship yields τ_c values which, when tested using the X test of Wallach and Huntress, have X values $\approx$0.4. Conditions therefore are not under diffusion control

TABLE 4.2

MOLECULAR MOTION OF BENZENE IN CO_2

[τ_{sr}=0.19 psec for benzene at 443K (57)]
[τ_{sr}=0.04 psec for neat benzene at 300K (77)]

Solvent conditions		Benzene 0.8% (w/w)		Acetonitrile 0.8% (w/w)
temperature (K)	pressure (psi)	^1H T_1 (sec)	τ_{sr} (psec)	τ_c by ^{14}N LW (psec)
295	1500	8.6	0.29	0.62
295	1750	16.2	0.15	
295	2100	45.0	0.05	0.52
295	2300	47.5	0.05	
295	2550	44.9	0.05	0.52
295	2900	39.7	0.06	0.55
295	3300	42.3	0.06	0.60
300	1500	6.7	0.36	
300	2000	5.7	0.42	
300	2500	16.6	0.15	
300	3000	40.5	0.06	
307	1500	4.0	0.59	0.43
307	2000	4.5	0.52	
307	2300	6.4	0.37	
307	2600	4.4	0.54	0.48
307	3000	5.9	0.40	
307	1550	4.1	0.58	
307	2000	4.7	0.50	
307	2500	5.3	0.45	
307	3000	4.5	0.52	
327	2000	2.9	0.76	0.33
327	2500	2.7	0.82	
327	3000	2.7	0.82	0.36
327	3500	3.1	0.71	0.40
361	1500	2.0	1.00	
361	2000	2.5	0.80	0.21
361	2500	2.9	0.69	
361	3000	2.2	0.91	

and the Hubbard relationship cannot be used. While τ_c values cannot be calculated, the τ_{sr} values in Table 4.2 are representative of spin-rotational motion in supercritical CO_2.

Spin-lattice relaxation times for acetonitrile solutions (1% and 0.8% (w/w)) in CO_2 were obtained and can be treated in a similar manner. Examination of $1/T_1$ dependence on η/T of 1% acetonitrile showed the inverse relationship reflective of spin-rotation. The same plot for the 0.8% (w/w) solution confirms spin-rotation dominated relaxation under critical conditions (Figure 4.3). Applying the same reasoning developed earlier, τ_{sr} values can be determined using the spin-rotation coupling constant of Lyerla, Grant and Wang (76). These are similarly summarized in Table 4.3. As seen with benzene, the τ_c values calculated using the Hubbard relation yield X values ($\approx$0.03) indicative of inertial control and not diffusion control.

From Equation [27], molecular correlation times can be determined directly from the observed linewidth of quadrupolar nuclei. It is then fortuitous that ^{14}N (I = 1) was monitored under the same conditions. Observation of ^{14}N of acetonitrile (0.8% (w/w)) yielded the observed linewidths

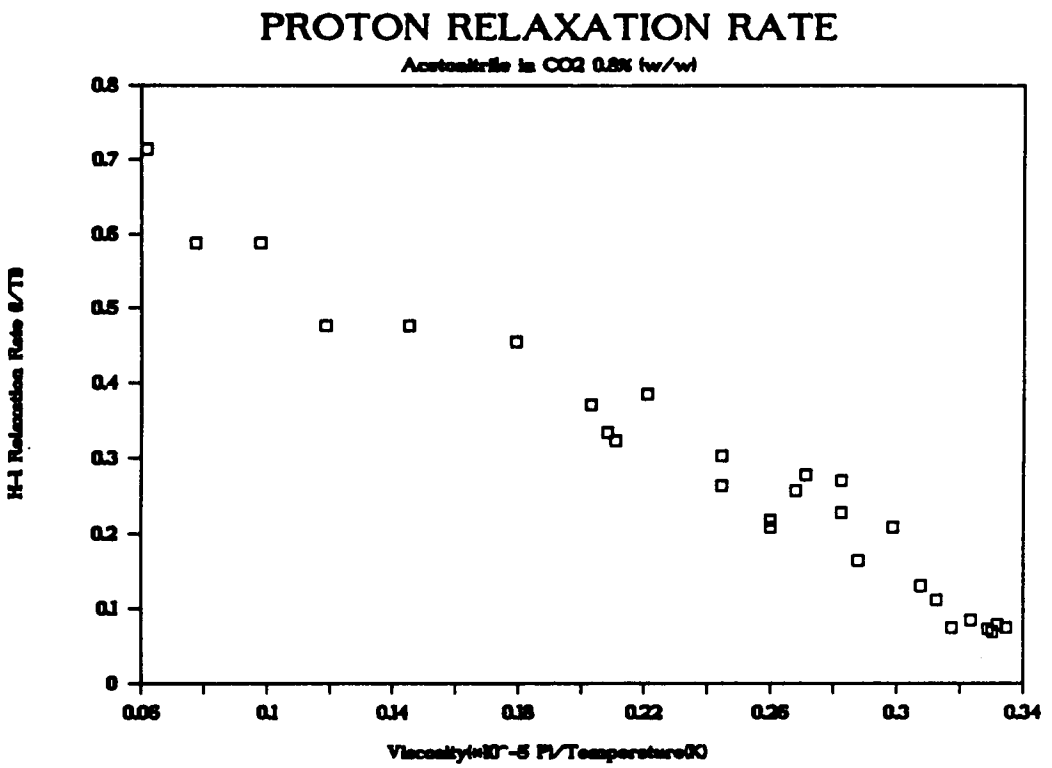

Figure 4.3 Acetonitrile ^{1}H relaxation rates ($1/T_1$) versus viscosity/temperature for 0.8% (w/w) in CO_2.

TABLE 4.3

MOLECULAR MOTION OF ACETONITRILE IN CO_2

[τ_c=1.1 psec for neat acetonitrile at 298K (70)]

Solvent conditions		Acetonitrile 0.8% (w/w)				by Hubbard
temperature (K)	pressure (psi)	^1H T_1 (sec)	τ_{sr} (psec)	^{14}N LW (Hz)	τ_c (psec)	τ_{sr} (psec)
295	1500	6.1	0.27	52	0.62	0.0036
295	1750	7.7	0.21			
295	2100	11.9	0.14	44	0.52	0.0043
295	2300	13.7	0.12			
295	2550	14.5	0.11	44	0.52	0.0043
295	2900	12.7	0.13	46	0.55	0.0041
295	3300	13.5	0.12	50	0.60	0.0038
300	1500	4.6	0.35			
300	2000	4.8	0.33			
300	2500	9.0	0.18			
300	3000	13.4	0.12			
307	1500	3.0	0.52	36	0.43	0.0050
307	2000	3.3	0.47			
307	2300	4.8	0.33			
307	2600	3.6	0.43	40	0.48	0.0045
307	3000	4.4	0.36			
307	1550	3.1	0.50			
307	2000	3.8	0.41			
307	2500	3.9	0.40			
307	3000	3.7	0.42			
327	2000	2.1	0.70	28	0.33	0.0061
327	2500	2.2	0.67			
327	3000	2.7	0.54	30	0.36	0.0057
327	3500	2.6	0.56	34	0.40	0.0050
361	1500	1.4	0.95			
361	2000	1.7	0.78	18	0.21	0.0086
361	2500	1.7	0.78			
361	3000	2.1	0.63			

in Table 4.3. Applying Equation [23] and using the gas phase QCC = 4.22 MHz (59,61) yields τ_c for acetonitrile under the conditions noted (Table 4.3). For comparison, the molecular correlation time (τ_c) of neat acetonitrile at 298K is 1.1 psec. (68). Through the use of CO_2, a reduction in τ_c by a factor of 2 occurs at subcritical conditions and a factor of 5 at lowest η/T. Also shown in Table 4.3 are τ_{sr} values calculated from Equation [18], the Hubbard relation, using the τ_c values obtained directly from ^{14}N linewidth. Lack of correlation with τ_{sr} obtained directly from ^1H T_1 of acetonitrile further emphasizes inertial controlled and not diffusion controlled conditions under which the Hubbard relation is not applicable.

The τ_c values obtained for acetonitrile are plotted versus η/T in Figure 4.4. Equation [28] predicts the linear dependence seen. From Equation [28], the intercept value of 0.16 psec. is related to τ_o and can be compared to τ_{FR} of Equation [25] (66). At 300K, τ_{FR} = 0.11 psec., consistent with the observed intercept value of 0.16 psec. The slope obtained from Equation [28], τ_{red} = 1186 (psec*K/cP) can be compared to theoretical reduced τ_c values for 300K conditions after division by 300 (Table 4.4). The obtained value is consistent with the experimental value of Gillen and Noggle (70) and correlates with the Gierer and Wirtz

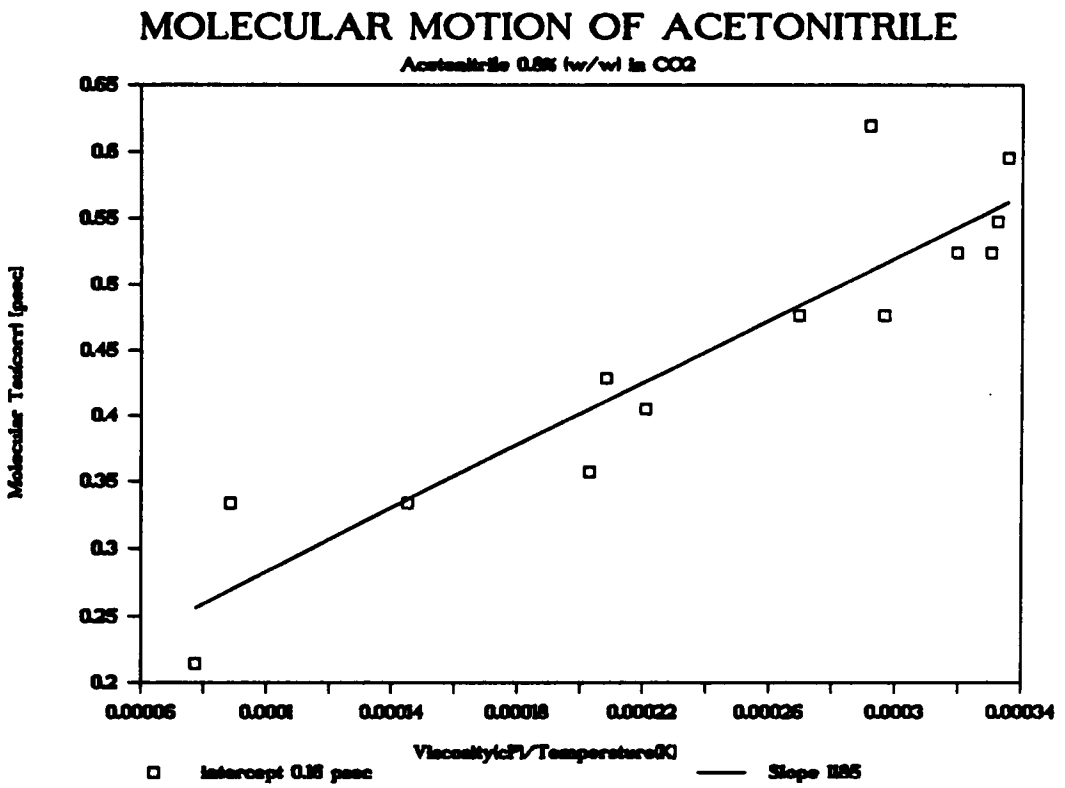

Figure 4.4 Acetonitrile τ_C versus η/T for the determination of τ_C (reduced)

Table 4.4

REDUCED τ_c FOR ACETONITRILE IN CO_2

[All τ_{red} values have the units (psec/cP) for 300K]

τ_{red} [a]	$\tau_{red}(exp)$ [b]	$\tau_{red}(SED)$	$\tau_{red}(GW)$ [c]	$\tau_{red}(HZ)$ [b]
4.0	3.1	11.6	3.1	1.4

Where:

$\tau_{red}(SED)$ = Stokes - Einstein - Debye model

$\tau_{red}(GW)$ = Gierer - Wirtz model

$\tau_{red}(HZ)$ = Hu - Zwanzig model

a - Value experimentally obtained converted to value at 300K to be consistent

b - Values of Gillen and Noggle (70)

c - Obtained using $a_s/a \approx 0.55$

Table 4.5

REDUCED τ_c FOR BENZENE IN CO_2

[All τ_{red} values have the units (psec/cP) for 300K]

τ_{red} [a]	$\tau_{red}(exp)$ [b]	$\tau_{red}(SED)$	$\tau_{red}(GW)$ [c]	$\tau_{red}(HZ)$ [b]
4.0	3.5	19.4	5.9	5.5

Where:

$\tau_{red}(SED)$ = Stokes - Einstein - Debye model

$\tau_{red}(GW)$ = Gierer - Wirtz model

$\tau_{red}(HZ)$ = Hu - Zwanzig model

a - Value experimentally obtained for acetonitrile and converted to value at 300K to be consistent

b - Values of Alm, et al (77)

c - Obtained using $a_s/a \approx 0.5$

model value. The same reduced τ_c value can be applied to benzene for comparison to predicted model values (Table 4.5). The value is consistent with the experimental value of Alm et al. (70), and shows best correlation with the Hu and Zwanzig model value. For comparison τ_{FR} = 0.84 psec. for benzene at 300K.

Applying the τ_c values determined directly through ^{14}N linewidth measurements to Equation [16] for intramolecular dipolar relaxation yields T_1 values of 202-595 sec. over the η/T range studied. The magnitude of T_1 predicted for dipolar interactions, when compared to observed T_1 for acetonitrile (2-15 sec. over the same range) supports the assumption of negligible dipolar contribution to the overall relaxation.

The τ_c(red) values of benzene and acetonitrile are similar (68,69) therefore the τ_c values determined for acetonitrile can be applied to that of benzene. Using Equation [16] for intramolecular dipolar relaxation yields large T_1 values (190-560 sec.). The contribution of dipolar relaxation at low η/T is therefore negligible based on the magnitude of these values.

The line-narrowing of quadrupolar nuclei has been examined in more detail with respect to η/T and concentration. Three solutions of acetonitrile in CO_2 have been investigated using ^{14}N NMR at sub- and supercritical conditions. Solutions of 3.3, 1.5 and 0.8% (w/w) were made in the manner already described.

The solubility of acetonitrile in CO_2 is, however, considered low [≈2.5% (w/w) at 2400 psi and 40-50°C (78)], with solubility under the conditions of the sample cylinder even less. This would result in attenuation of the concentrations expected and possible equivalence of the observed signal of each mixture under the same conditions. The observed S/N of the three mixtures measured was significantly different for the three concentrations. This suggests little or no attenuation of the predicted concentrations. More detailed studies of absolute solubility can be done using NMR (57) however for these cases only relative spectral differences will be noted.

Shown in Table 4.6 are the measured linewidths for the three concentrations and the resulting τ_c from Equation [22]. A concentration dependance on τ_c is evident for equivalent conditions. A linewidth of 27 Hz for 3.3% can be

TABLE 4.6

ACETONITRILE ^{14}N LINEWIDTHS IN CO_2 WITH τ_c

Solvent condition		Concentration					
		3.3% (w/w)		1.5% (w/w)		0.8% (w/w)	
temperature (K)	pressure (psi)	^{14}N LW (Hz)	τ_c (psec)	^{14}N LW (Hz)	τ_c (psec)	^{14}N LW (Hz)	τ_c (psec)
295	1500	57	0.68	34	0.40	52	0.62
295	2000	53	0.63	62	0.74	44	0.52
295	2500	55	0.66	42	0.42	44	0.52
295	3000	57	0.68	50	0.60	46	0.55
295	3500	69	0.82	54	0.64	50	0.60
307	1550					36	0.43
307	2550					40	0.48
307	3500					40	0.48
311	1550	51	0.61	42	0.50		
311	2000	49	0.58	42	0.50		
311	2500	51	0.61	48	0.57		
311	3000	47	0.56	38	0.45		
311	3500	55	0.66	38	0.45		
327	1500					28	0.33
327	2000					28	0.30
327	3100					30	0.36
327	3500					34	0.40

TABLE 4.6 (cont.)

ACETONITRILE ^{14}N LINEWIDTHS IN CO_2 WITH τ_c

Solvent condition temperature (K)	pressure (psi)	Concentration 3.3% (w/w) ^{14}N LW (Hz)	τ_c (psec)	1.5% (w/w) ^{14}N LW (Hz)	τ_c (psec)	0.8% (w/w) ^{14}N LW (Hz)	τ_c (psec)
332	1500			25	0.30		
332	2000			33	0.39		
332	2500			33	0.39		
332	3000			39	0.46		
332	3500			33	0.39		
333	1500			24	0.29		
333	2000			30	0.36		
333	2500			34	0.40		
333	3000			35	0.42		
333	3500			35	0.42		
361	1500	33	0.39	25	0.22		
361	2000	27	0.32	25	0.22	18	0.21
361	2500	27	0.32	23	0.27		
361	3000	31	0.37	29	0.35		
361	3500	29	0.35	23	0.27		

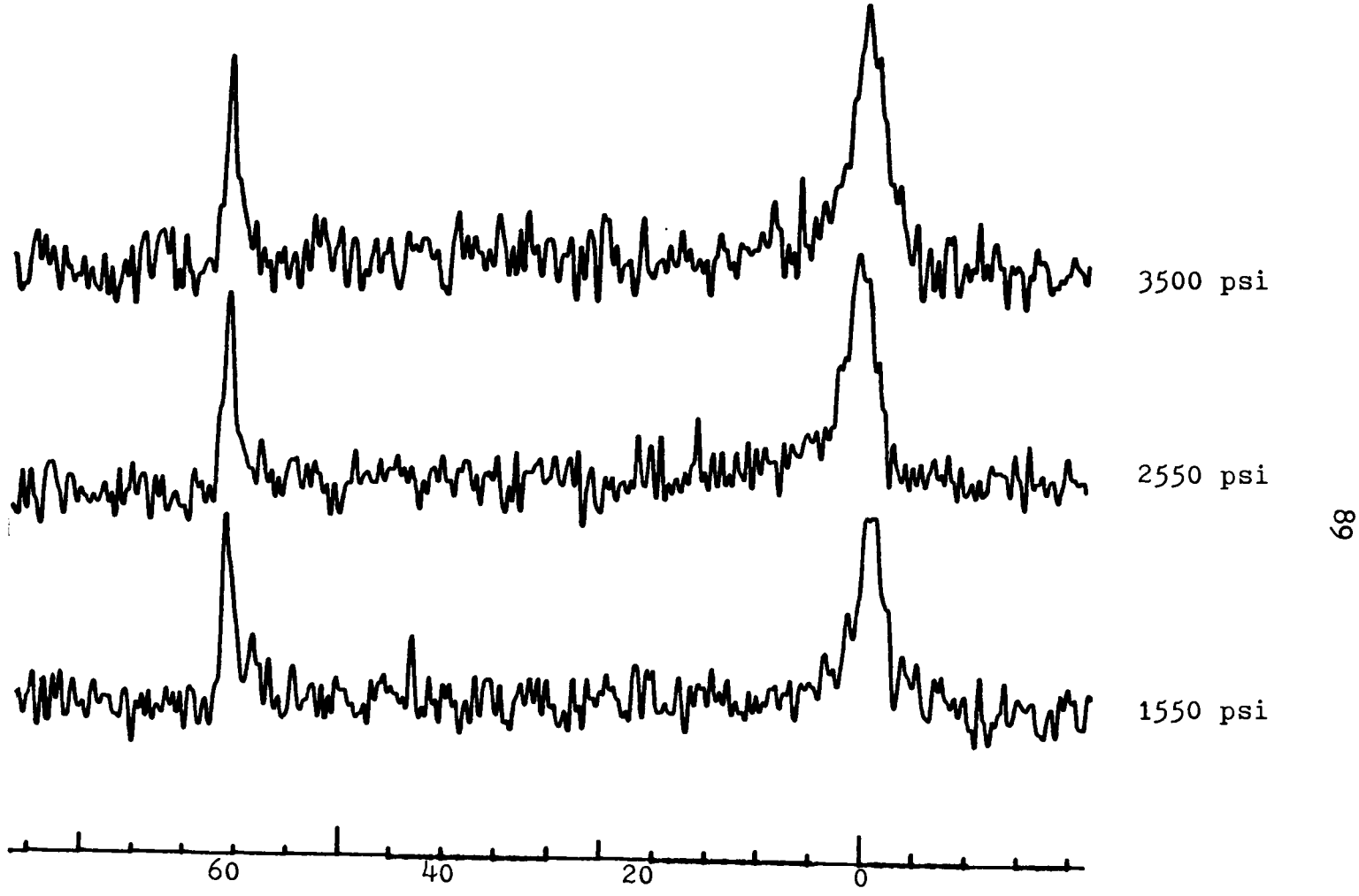

Figure 4.5 ^{14}N spectra of acetonitrile in CO_2 (0.8% w/w) at 34°C and different pressures.

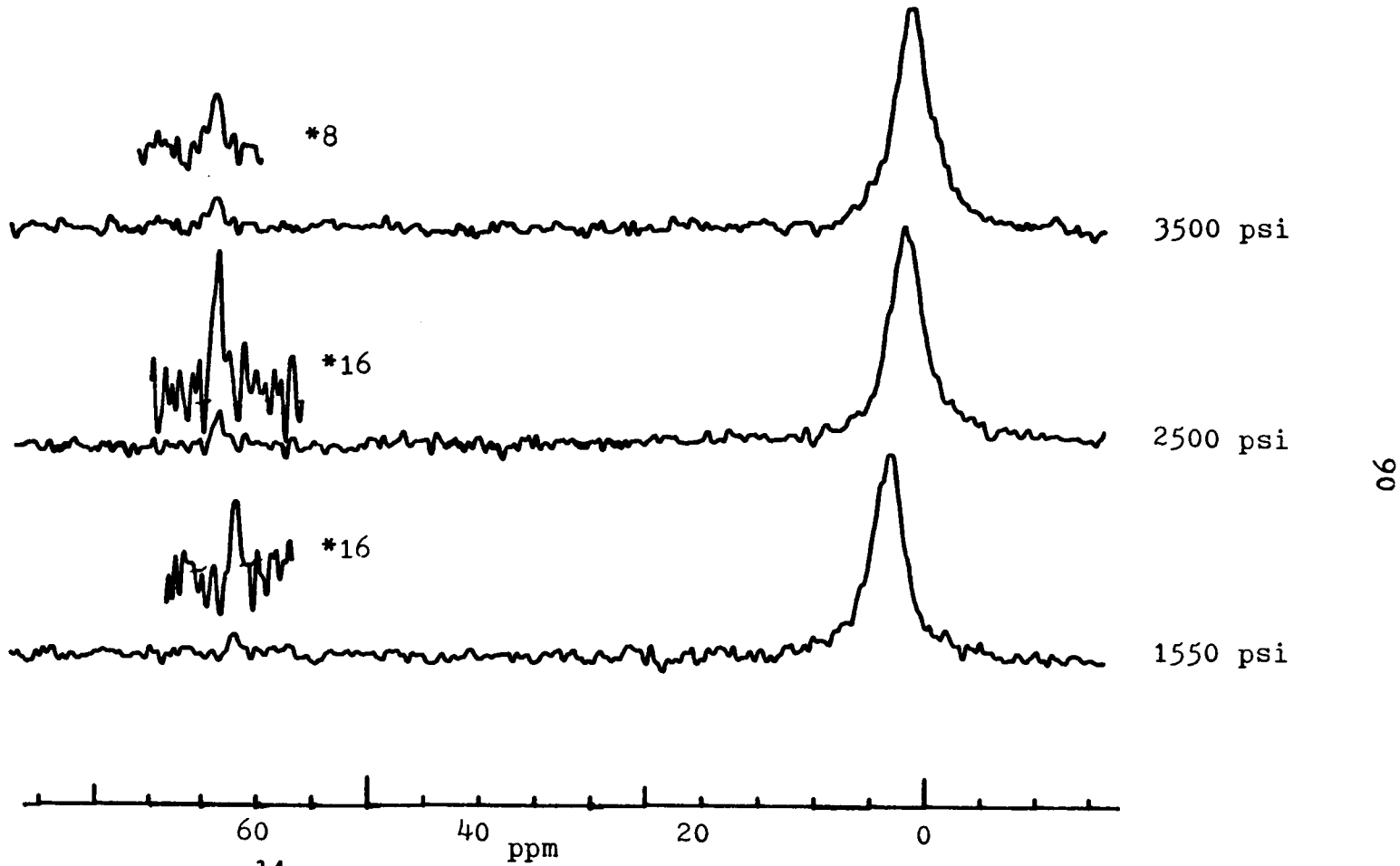

Figure 4.6 ^{14}N spectra of acetonitrile in CO_2 (3.6% w/w) at 38°C and different pressures.

compared to 18 Hz at 0.8%. Similarly, linewidths range from 57 to 46 in going from 3.3% to 0.8% under subcritical conditions. Due to the low sensitivity of ^{14}N and the low concentrations being measured, S/N was only marginally adequate for these comparisons however the trend is evident at a number of conditions. Shown in Figure 4.5 are the series of ^{14}N spectra obtained at different pressures for 0.8% (w/w) acetonitrile in CO_2 at 34°C. The downfield peak at 61.1 ppm relative to acetonitrile is N_2 gas present as a result of degassing. Figure 4.6 shows the series of ^{14}N spectra for the 3.6% (w/w) solution at 38°C with the S/N improvement quite evident. These spectra were obtained using 2000 accumulations in contrast to the former using 5000 accumulations. Since this sample was not degassed, only trace amounts of N_2 are evident.

The magnitude of line-narrowing can be appreciated by considering the observed signal under different η/T conditions when compared to neat acetonitrile (Figure 4.7). An improvement of ≈3 is observed, consistent with those reported by Jonas (59). Line-narrowing ranged from (1.2-4.5) for the conditions and concentrations measured (Table 4.7).

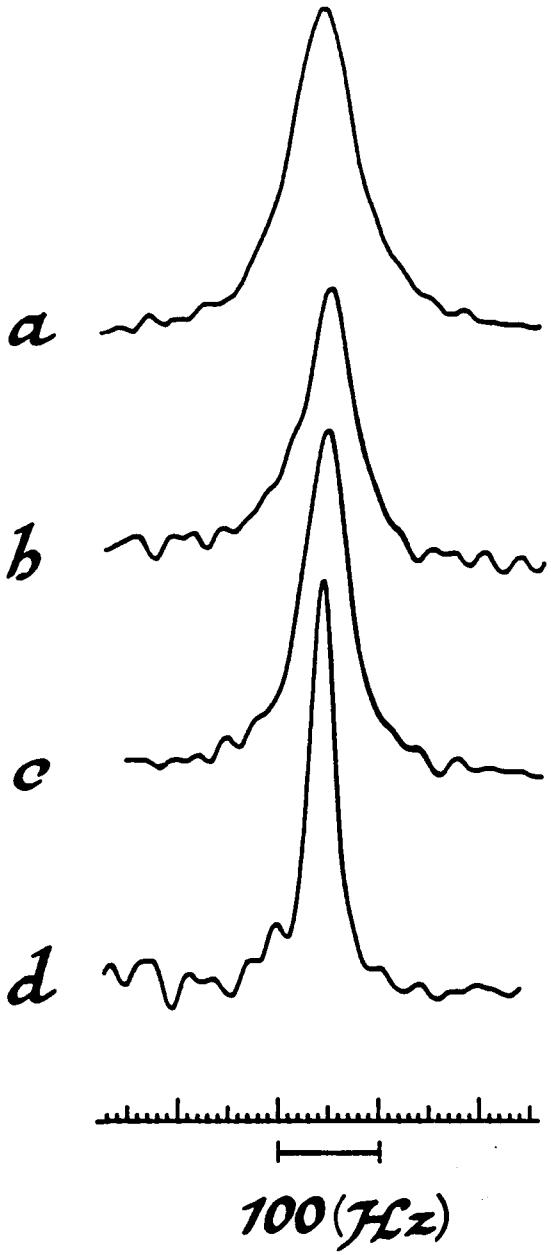

Figure 4.7 Changes in ^{14}N linewidth due to different viscocity/temperature conditions:
(a) Neat acetonitrile at room temperature
(b) 3.3% w/w acetonitrile in CO_2 @ 23°C 2500 psi
(c) 3.3% w/w acetonitrile in CO_2 @ 38°C 2500 psi
(d) 3.3% w/w acetonitrile in CO_2 @ 88°C 2500 psi

TABLE 4.7

ACETONITRILE ^{14}N LINEWIDTHS IN CO_2 WITH IMPROVEMENT OVER NEAT LIQUID

[neat acetonitrile 295K linewidth = 82 Hz (61)]

Solvent condition		Concentration					
		3.3% (w/w)		1.5% (w/w)		0.8% (w/w)	
temperature (K)	pressure (psi)	^{14}N LW (Hz)	LW imprvmt	^{14}N LW (Hz)	LW imprvmt	^{14}N LW (Hz)	LW imprvmt
295	1500	57	1.4	34	2.4	52	1.6
295	2000	53	1.5	62	1.3	44	1.9
295	2500	55	1.5	42	2.0	44	1.9
295	3000	57	1.4	50	1.6	46	1.8
295	3500	69	1.2	54	1.5	50	1.6
307	1550					36	2.3
307	2550					40	2.1
307	3500					40	2.1
311	1550	51	1.6	42	2.0		
311	2000	49	1.7	42	2.0		
311	2500	51	1.6	48	1.7		
311	3000	47	1.7	38	2.2		
311	3500	55	1.5	38	2.2		
327	1500					28	2.9
327	2000					28	2.9
327	3100					30	2.7
327	3500					34	2.4

TABLE 4.7 (cont.)

ACETONITRILE ^{14}N LINEWIDTHS IN CO_2 WITH IMPROVEMENT OVER NEAT LIQUID

[neat acetonitrile 295K linewidth = 82 Hz (61)]

Solvent condition		Concentration					
		3.3% (w/w)		1.5% (w/w)		0.8% (w/w)	
temperature (K)	pressure (psi)	^{14}N LW (Hz)	LW imprvmt	^{14}N LW (Hz)	LW imprvmt	^{14}N LW (Hz)	LW imprvmt
332	1500			25	3.3		
332	2000			33	2.5		
332	2500			33	2.5		
332	3000			39	2.1		
332	3500			33	2.5		
333	1500			24	3.4		
333	2000			30	2.7		
333	2500			34	2.4		
333	3000			35	2.3		
333	3500			35	2.3		
361	1500	33	2.5	25	3.3		
361	2000	27	3.0	25	3.3	18	4.6
361	2500	27	3.0	23	3.6		
361	3000	31	2.6	29	2.8		
361	3500	29	2.8	23	3.6		

The concentration dependence can be attributed to a number of possibilities. The macroscopic viscosity could vary enough for the different concentrations to make the conditions nonequivalent. Clustering of acetonitrile molecules, as noted in (61,62) could contribute to a reduced intrinsic viscosity upon dilution. The linewidths expected based on CO_2 viscosities (58,59) are not observed and as suggested by Jonas (59) are prevented by limited solubility at the optimum conditions.

The proton relaxation rates of benzene and acetonitrile can also be plotted as functions of density (Figures 4.8 and 4.9). Similar trends are seen with $1/T_1$ being inversely related to density. This is expected since density varies as η/T (Figure 4.10).

Also informative is the plot of T_1 versus η/T (or density) where the magnitude of T_1 changes can be best appreciated. Benzene T_1 changes from minimum values of 2-5 sec. at low to moderate η/T with a rapid increase in T_1 approaching the critical temperature (Figure 4.11). Maximum T_1 values of $\approx$45 sec. are achieved where $T < T_c$. Acetonitrile T_1 remains relatively constant at low to moderate η/T with values of 1.5 - 3.0 sec. (Figure 4.12).

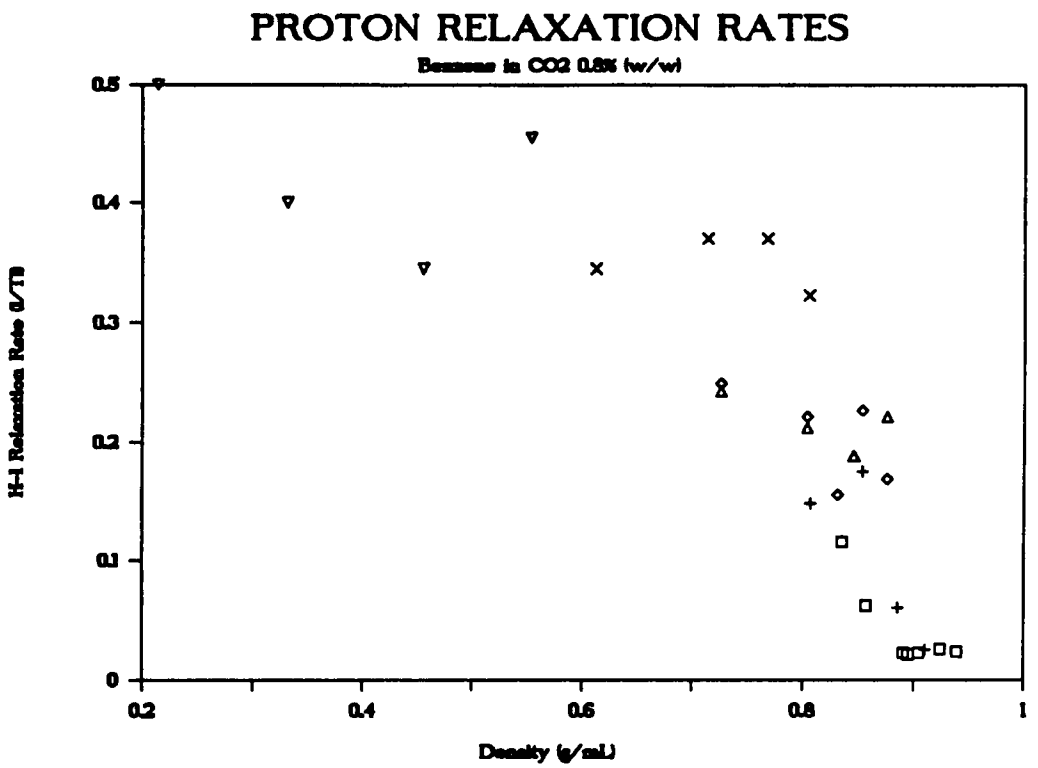

Figure 4.8 Benzene ^{1}H relaxation rates ($1/T_1$) versus density for different temperatures.

□ 295K
\+ 300K
◇△ 307K
× 327K
▽ 362K

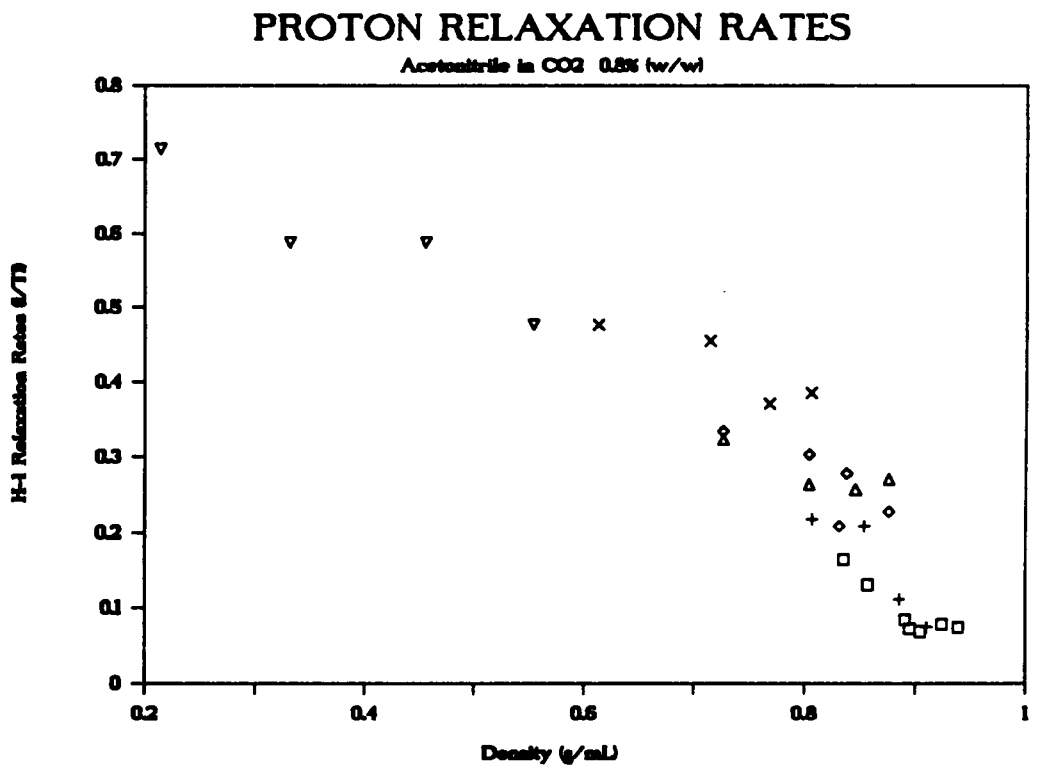

Figure 4.9 Acetonitrile ^1H relaxation rates ($1/T_1$) versus density for different temperatures.

□ 295K
\+ 300K
◇ △ 307K
× 327K
▽ 362K

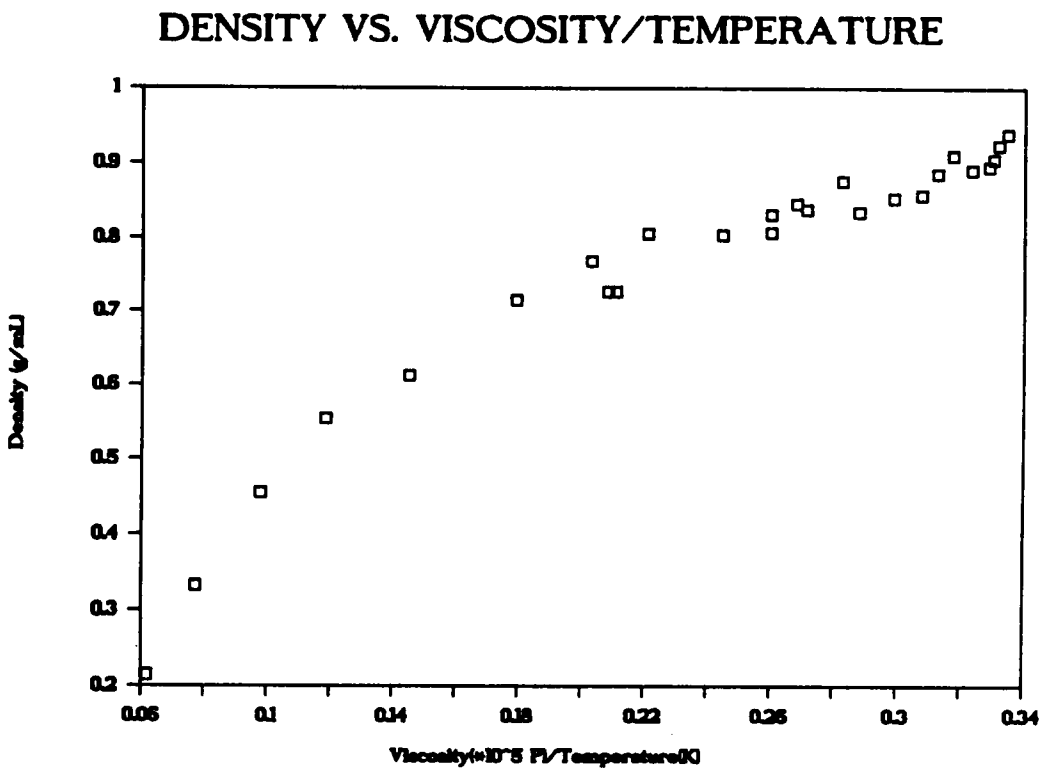

Figure 4.10 The relationship between density and viscosity/temperature.

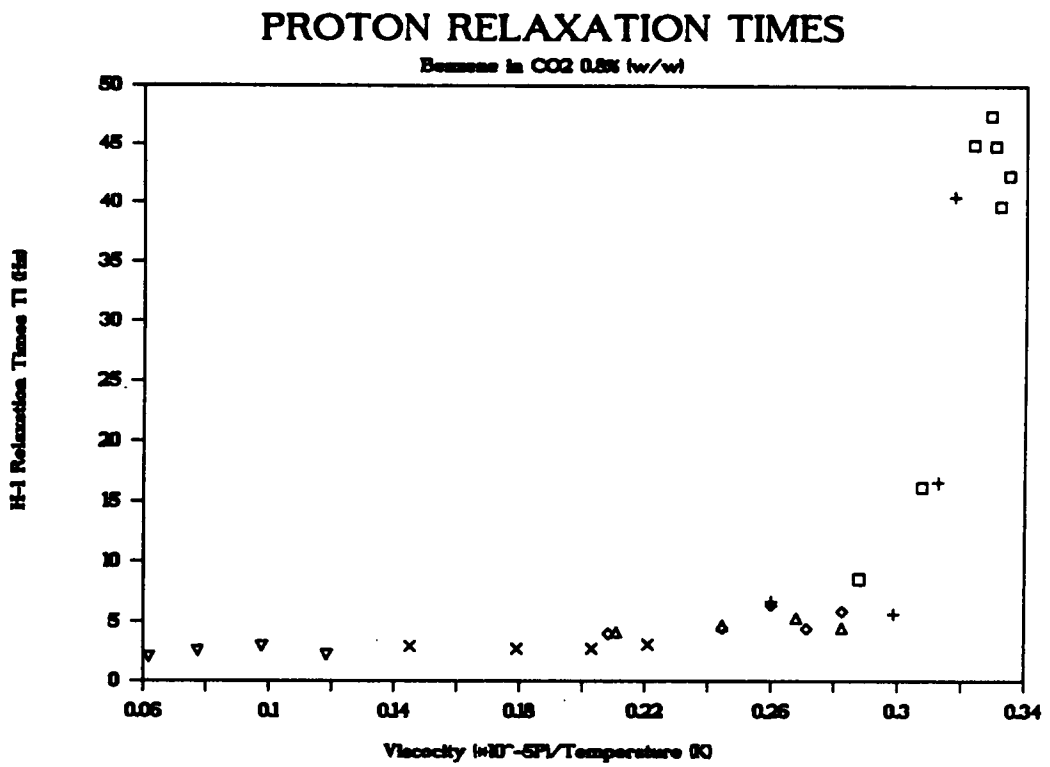

Figure 4.11 Benzene ^{1}H relaxation times (T_1) versus viscosity/temperature for different temperatures.

□ 295K
\+ 300K
◇ △ 307K
× 327K
▽ 362K

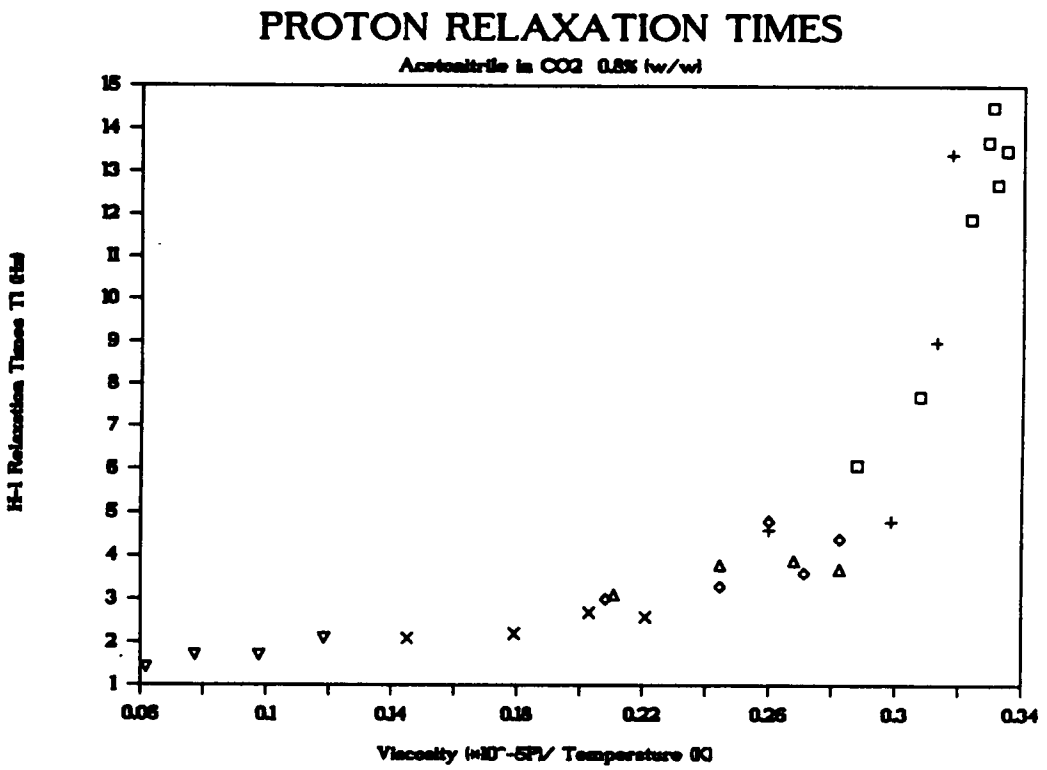

Figure 4.12 Acetonitrile ^{1}H relaxation times (T_1) versus viscosity/temperature for different temperatures.

□ 295K
✚ 300K
◇ △ 307K
× 327K
▽ 362K

Approaching $T = T_c$ at high η/T, a rapid increase in T_1 results with maximum T_1's of ≈13.5 sec. These transitions are possibly due to the increasing importance of dipolar relaxation interactions. As already noted, the magnitude of T_1 as a result of dipolar relaxation is very large, which would result in large changes in T_1 for even small contributions of dipolar interactions.

Conclusions

The understanding of molecular motion and relaxation is important when one considers the use of NMR in the observation of dissolved molecules in a flowing supercritical fluid (SFC/NMR). As has already been discussed, premagnetization is an important factor in the optimization of observed signals. Large changes in T_1 can cause strong attenuation of the observed signal when premagnetization is not sufficiently achieved. For the conditions typically encountered in SFC, the magnitude of T_1's observed for benzene and acetonitrile reflect the need for added paramagnetic relaxation agents prior to detection by NMR. Suppression of the spin-lattice relaxation times allows premagnetization to occur over a reasonable time frame under flowing conditions. The reduction in quadrupolar linewidth as a result of increased molecular

motion makes the use of supercritical fluids important in the observation of dilute quadrupolar species since reduced linewidth improves spectral dispersion and corresponds to increased S/N for the same number of accumulations.

CHAPTER FIVE

USE OF SUPERCRITICAL CO_2 IN FLOW DYNAMIC NUCLEAR POLARIZATION (DNP-NMR)

Introduction

Nuclear magnetic resonance (NMR) spectroscopy, while an important tool in chemical analysis, suffers from poor sensitivity. A potentially powerful method of signal enhancement is dynamic nuclear polarization (DNP), sometimes referred to as nuclear electron double resonance. DNP involves the transfer of polarization from a saturated electron spin system to that of a nuclear spin system. The technique has been widely studied in solutions and solids and several excellent reviews exist (79-82). Dramatic improvement of observed NMR signals is predicted since the enhancement is proportional to the ratio of the magnetogyric ratios, however, a number of experimental difficulties prevent observation of the predicted enhancements.

The majority of DNP NMR studies have been static samples and require placement of the NMR rf coil within the microwave cavity. The NMR coil shields the microwave field reducing the microwave efficiency, thus requiring increased microwave power for equivalent saturations (Figure 5.1 a,b). Increased power results in potential heating of the sample.

In this configuration, NMR detection is also not optimized with respect to the rf coil.

Dorn et al. have shown that, through flow, the microwave cavity and NMR coil can be separately optimized thus allowing significantly reduced microwave power to achieve similar saturations (Figure 5.1 c) (83). Utilizing the observation of DNP enhancements of a sealed sample, a measure of the microwave magnetic field, (B_{1s}) has been made for typical static and flow configurations. These are then compared to an unperturbed microwave cavity (Appendix III).

Gitti has applied normal liquid flow DNP-NMR to immobilized free radical systems (84). The immobilized radical is isolated in the microwave region where dynamic nuclear polarization transfer occurs. The flowing liquid, in the absence of radical, returns to its normal liquid T_1 ≈1-2 sec. for efficient transfer to the NMR detection region. Overall enhancements were reduced as a result of the decreased molecular motion during polarization transfer.

An important requirement for optimum DNP enhancement is $(\omega_e \tau_c)^2 << 1$, the extreme narrowing condition. The electron resonance frequency (ω_e) is dictated by the

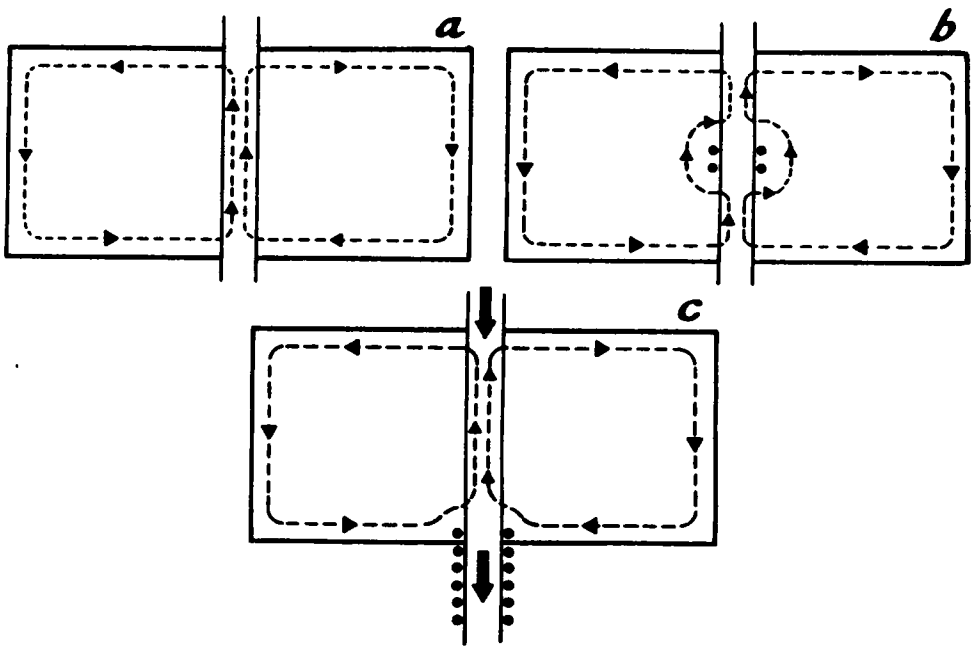

Figure 5.1 Microwave magnetic fields for:

(a) Unperturbed microwave cavity
(b) Typical static configuration for DNP-NMR
(c) Flow configuration for DNP-NMR

magnitude of the magnetic field used and τ_c, the molecular correlation time, reflects the mobility of the molecule. Through the use of supercritical fluids the molecular motion can be increased thereby reducing τ_c. This offers the possibility of extending the extreme narrowing condition to higher useful fields for optimum DNP.

The extreme narrowing condition $[(\omega_o\tau_c)^2<<1]$ reflects the maximum in spectral density for the range of molecular motion possible. Figure 5.2 shows spectral density as a function of frequency. Regions A, B and C describe conditions of different degrees of available motion. Region A is like that in solids where motion is limited, $\tau_c \approx 10^{-7}$ sec., while region C is like that of liquids, $\tau_c \approx 10^{-12}$ sec. Region B is intermediate with molecular motion on the order of polymers or viscous liquids. Efficient relaxation occurs when the spectral density has a significant value at the resonance frequency, $\omega = \omega_o$. For the case of liquids, the extreme narrowing condition is that plateau of maximum spectral density for a large range of ω, hence efficient relaxation occurring for a large range of resonance frequencies.

For ^1H observation at 4.7 T in liquids the resonance

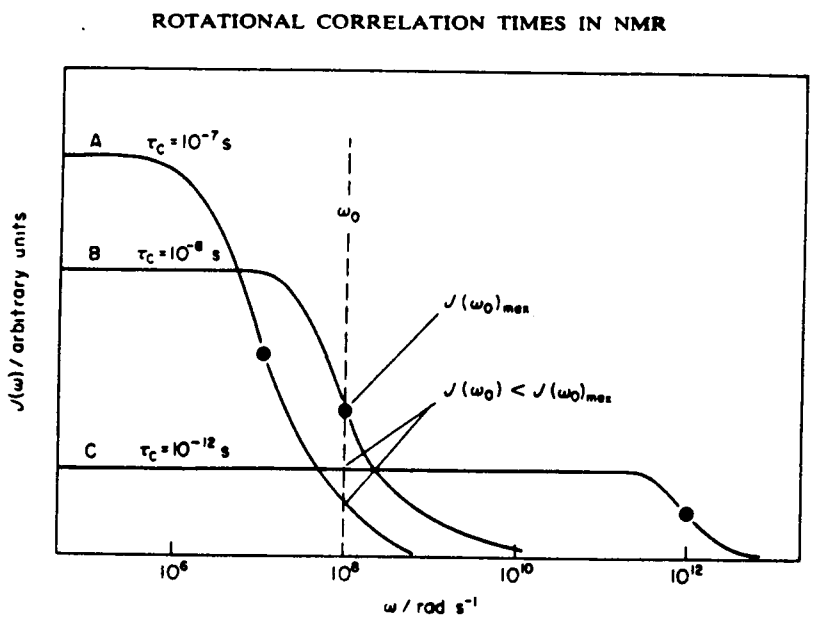

Figure 5.2 Spectral density as a function of molecular motion for three conditions (66).

Region A: Solids
Region B: Viscous liquids
Region C: Normal liquids

frequency (ν) is 200 MHz corresponding to $\omega_o = 1.26 * 10^9$ radian*sec^{-1}. Using $\tau_c = 5 * 10^{-12}$ sec., a typical value for liquids, $(\omega_o\tau_c)^2 \approx 4.0 * 10^{-5} << 1$. For viscous liquids, having $\tau_c \approx 10^{-8}$ sec., observation at 200 MHz results in $(\omega_o\tau_c)^2 \approx 1.6 * 10^4$ which does not satisfy the extreme narrowing requirement. The spectral density is reduced resulting in inefficient relaxation.

Electron resonance frequencies are on the order of Gigahertz and at 3.3 kG, ν_e = 9.3 GHz. In normal liquids using $\tau_c = 5 * 10^{-12}$ sec., $(\omega_e\tau_c)^2 \approx 8.5 * 10^{-3} < 1$, still approaching the extreme narrowing condition. At higher magnetic fields, e.g. 14 kG or 60 MHz ^{1}H, ν_e = 39.5 GHz resulting in $(\omega_e\tau_c)^2 = 1.2$, not satisfying the extreme narrowing requirement. If, however, the molecular motion available to the molecule could be increased, e.g. through the use of supercritical fluids, the extreme narrowing condition could be extended to higher effective magnetic fields. Using CO_2 under moderate supercritical conditions $\tau_c \approx 5 * 10^{-13}$ sec. yielding $(\omega_e\tau_c)^2 \approx 1.5 * 10^{-2} < 1$; thereby extending the extreme narrowing condition to higher magnetic fields.

The technique of flow DNP ^{1}H NMR is presented using

benzene and TTBP solutions in sub- and supercritical CO_2. The use of flow allows optimization of both electron spin saturation and NMR signal detection. Supercritical fluids offer optimum enhancement under the extreme narrowing condition.

Theory

Dynamic nuclear polarization occurs with saturation of an electron spin transition at or near ω_e. As the electron spins attempt to reestablish Boltzmann the distribution, relaxation occurs. Polarization transfer is a relaxation mechanism that occurs through coupled electron-nuclear transitions. Figure 5.3 shows the electron-nuclear spin levels and the accompanying transition probabilities. While all transitions are allowed, the radiationless zero quantum (W_0) and double quantum (W_2) transitions are responsible for DNP as they involve simultaneous flips of both electron and nuclear spins. The intensity of the NMR signal (I_z) is proportional to $(N_{\alpha\alpha} + N_{\beta\alpha}) - (N_{\alpha\beta} + N_{\beta\beta})$ and under thermal equilibrium is denoted (I_o). When the electron spin transition is saturated $N_{\alpha\beta} = N_{\beta\beta}$ and $N_{\alpha\alpha} = N_{\beta\alpha}$ with relaxation to thermal equilibrium involving interactions through W_1, W_2 and W_o. A rigorous treatment of all transitions leads to the observed NMR enhancement

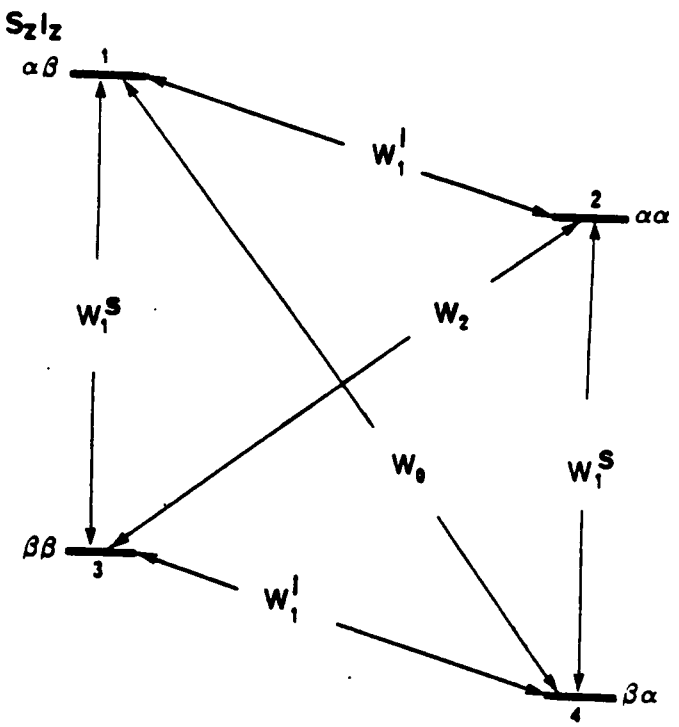

Figure 5.3 Spin level diagram for a coupled electron-nuclear spin system (84).

described as (81):

$$A = (I_z - I_o)/I_o = -\rho f\ s\ [\gamma_s]/\gamma_I \qquad [30]$$

with each term to be discussed in further detail.

The coupling factor (ρ) reflects the mechanism being involved and can be described in terms of the transition probabilities as:

$$\rho = (W_2^d - W_0^d - W_0^{sc}) \ / \ (W_2^d + W_0^d + W_0^{sc} + 2W_1^d) \qquad [31]$$

for the dipolar and scalar mechanisms of interaction. For most ^1H DNP studies dipolar interactions are thought to dominate therefore Equation [31] reduces to:

$$\rho = (W_2^d + W_0^d) \ / \ (W_2^d + W_0^d + 2W_1^d) \qquad [32]$$

Under the extreme narrowing condition the ratios of $W_0^d:W_1^d:W_2^d = 2:3:12$ resulting in $\rho = 0.5$ for dipolar dominated polarization transfer. For scalar dominated interactions $\rho = -1.0$ under the extreme narrowing condition.

The leakage factor (f) reflects the degree the electron and nucleus are coupled. Described in terms of transition probabilities:

$$f = (W_0^d + W_0^{sc} + 2W_1^d + W_2^d) / (W_0^d + W_0^{sc} + 2W_1^d + W_2^d + W_I) \quad [33]$$

and, under dipolar dominated interaction reduces to:

$$f = (W_0^d + 2W_1^d + W_2^d) / (W_0^d + 2W_1^d + W_2^d + W_I) \quad [34]$$

where W_I is used for transitions other than those described. The nuclear spin-lattice relaxation rates ($1/T_1$) in the absence and presence of a free radical can also be expressed in terms of transition probabilities:

$$1/T_{1no} = W_{I0}$$
$$1/T_{1n} = W_0^d + 2W_1^d + W_2^d \quad [35]$$

and substitution into [34] yields:

$$f \approx 1 - (T_{1n} / T_{1no}) \quad [36]$$

The leakage factor can be estimated by measurement of

nuclear T_1 in the absence of radical (T_{1no}) and in the presence of radical (T_{1n}).

The electron saturation factor (s) reflects the degree the electron transitions are saturated. (For complete saturation s = 1.)

$$S = (S_o - S_z)/S_o$$

$$S_z = S_o/(1 + \alpha B_{1s}^2 T_{1s} T_{2s}) \qquad [37]$$

where: T_{1s} - the electron spin-lattice relaxation time

T_{2s} - the electron spin-spin relaxation time

B_{1s} - the microwave magnetic field

α - a constant

Since B_{1s}^2 is proportional to P where P is the applied microwave power, after substitution, Equation [30] can be rearranged to yield:

$$[(I_z - I_o)/I_o]^{-1} = [f \rho [\gamma_s]/\gamma_I]^{-1} [1 + 1/(\alpha P T_{1s} T_{2s})] \qquad [38]$$

Plotting the inverse enhancement $[(I_z - I_o)/I_o]^{-1}$ versus applied power (P) yields a straight line whose intercept (A_∞^{-1}) is the enhancement value where s = 1.

Typically A_{∞} values are cited since observed enhancements are often much less due to the high power typically required for static DNP.

The potential enhancement using DNP is illustrated when one considers the ideal case where f = 1; s = 1. For dipolar dominated interactions $\rho = 0.5$ yielding $A_{\infty} = -0.5\ [\gamma_S]/\gamma_I = -330$ for ^1H observation. For scalar interactions $\rho = -1$ yielding $A_{\infty} = 1\ [\gamma_S]/\gamma_I = 660$ for ^1H observation.

Experimental

The flow DNP experiment was performed using a modified Varian E-3 ESR spectrometer operating at B_o = 3.3 kG. The klystron microwave source had a maximum output of 250 mW which was, for some experiments, increased to a maximum of 4.4 W using an external Hughes TWT model 8010 amplifier in order to insure complete saturation of the electron transition. A diagram of the flow DNP apparatus is shown in Figure 5.4. In this configuration the microwave quality factor (Q) was not visibly degraded by the presence of the NMR coil.

The ^1H signal was detected at 14.1 MHz using an rf coil

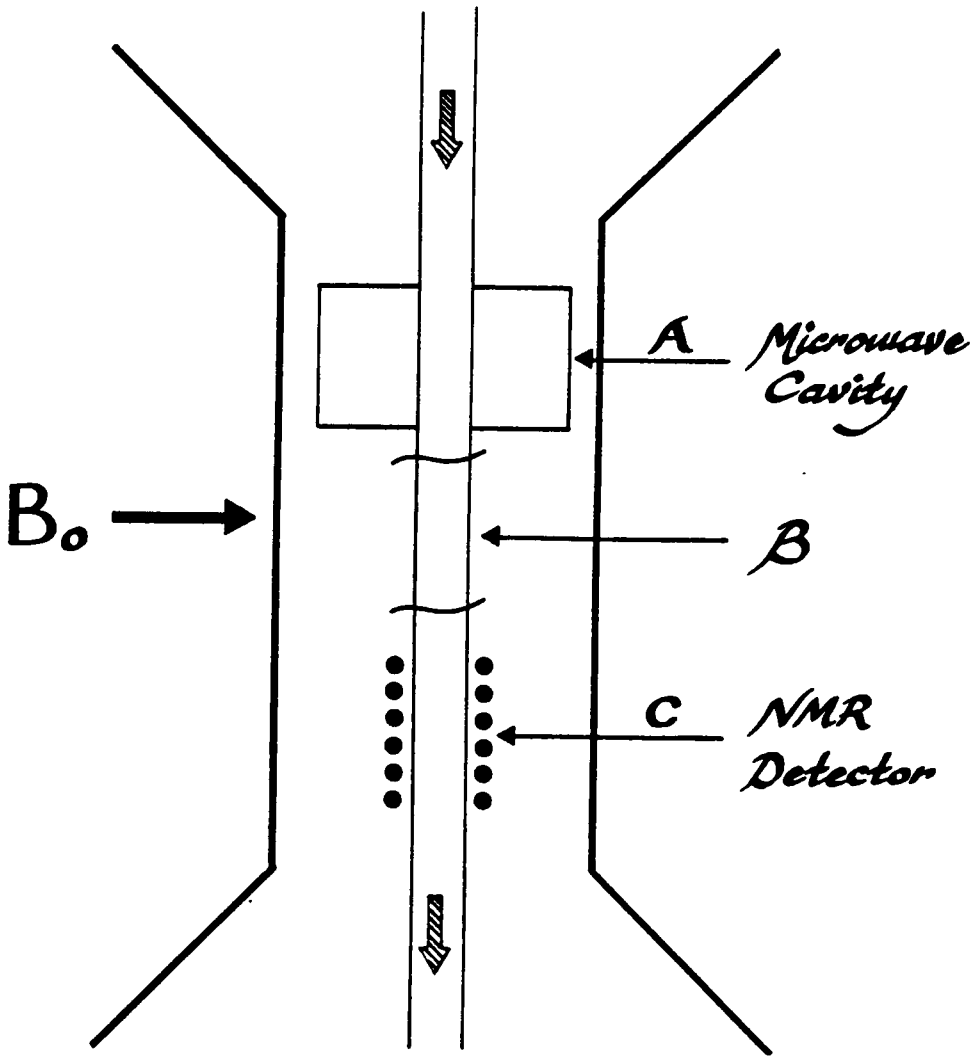

Figure 5.4 Flow DNP-NMR apparatus.

Region A: Microwave cavity, saturation volume
Region B: Transfer volume
Region C: NMR observation volume

and the broadband capability of a JEOL FX-200 NMR spectrometer. Due to lack of homogeneity using the Varian magnet ^1H NMR linewidths of 600 Hz are observed. A ceramic flow cell, like that described in Appendix I, was used. An 18 turn solenoid coil was wound directly onto the ceramic cell providing an NMR observation volume of ≈20 μL. As emphasized in Chapter Three, operation under supercritical conditions requires elevated pressures and temperatures. Flow under increased pressure was obtained using the solvent delivery system of Figure 3.1. Increased temperature was accomplished by passing blast tube heated air directly into the Varian cavity. The temperature was monitored using a Cu/constantan thermocouple adjacent to the observation cell and controlled using a JEOL JNM-VT unit ($\pm$1°C). The supercritical state was insured by preheating in a water bath prior to detection.

The flow rate was kept at 1.4 mL/min. which was found optimal based on transfer and residence times for the flow DNP ^1H NMR apparatus described. The free radical 2,4,6-tri-t-butylphenoxide (TTBP) was generated from the corresponding phenol by activation with PbO_2 (81) after being added to benzene. The sample was transferred under positive N_2 to the CO_2 cylinder (as described in Appendix I) prior to

charging with CO_2. The total weight of the CO_2 cylinder was monitored to give sample concentrations of 1.5-5.6% (w/w) and radical concentrations of $5*10^{-2}$ M. Decompression of the CO_2 at the restrictor orifice resulted in precipitation of the radical; clogging was avoided through the use of a hot water bath as previously described.

Results and Discussion

Explicit determination of the enhancement factor (A) requires detection of both the enhanced (I_z) and the unenhanced (I_o) NMR signals. For the case of liquid flow DNP-NMR, this presents no problem since the solvent and solute are the same. The radical present (TTBP) has been found to experience no observed enhancement and its low concentration offers negligible contribution to the observed unenhanced signal. This is not the case under supercritical flow DNP-NMR conditions. The observed solute is kept at low concentrations in order to preserve the integrity of the supercritical fluid (<5% (w/w)). For efficient enhancements, the minimum [TTBP] is $\approx 10^{-2}$ M making the signal due to the radical significant with respect to the overall unenhanced NMR signal. Methods must therefore be adopted which explicitly determine this contribution or implicitly allow its determination. Due to the

inhomogeneity of the system used, chemical shift differences could not be used.

One method used utilizes the extrapolated value of the unenhanced signal, I_o, based on liquid flow DNP-NMR values using the same configuration. The I_o was observed for 100% benzene at 50°C. The observed I_o for a 5.6% (w/w) solution of benzene in CO_2 under SFC conditions was consistent with that expected for the reduced quantity. In subsequent mixtures, where the I_o could not be observed, an extrapolated I_o value was used based on that of the 5.6% solution. The intensity values obtained were based on a measure of S/N of the Fourier transformed free induction decay. The enhancement factor can thus be expressed as:

$$A = (I_z - I_o)/I_o = [(S/N)_z - (S/N)_o]/(S/N)_o$$

Since high microwave power was used, complete saturation was obtained and the A values obtained represent A_∞. Table 5.1 summarizes the enhancements obtained using this method. As can be seen, the variation in A_∞ is significant however the A_∞(ave) clearly exceeds that of the normal liquid DNP-NMR determination. All were determined at 50°C since both the cavity and rf quality factors are affected by temperature

TABLE 5.1

FLOW DNP-NMR ENHANCEMENTS
FOR BENZENE SOLUTIONS IN CO_2

SFC/NMR

50°C 2000 psi
[TTBP] = $5*10^{-2}$ M

BENZENE	A_∞
5.6% (w/w)	-170
4.5% (w/w)	-245
3.7% (w/w)	-398
1.6% (w/w)	-154

A_∞(ave) = -242 $\pm$ 96

LC/NMR

50°C
[TTBP] = $5*10^{-2}$ M

BENZENE	A_∞
100%	-131

and play important roles in the overall enhancement.

The intrinsic viscosity of the solution affects the molecular motion, therefore should be kept constant for a series of measurements to be comparable. It is for this reason that deuterium analog dilution is used in the evaluation of relaxation mechanisms. A series of benzene and benzene-d_6 (<0.05% C_6H_6) mixtures were used in supercritical fluid flow DNP-NMR in order to effectively measure I_o without changing the solvent conditions. The benzene/benzene-d_6 ratio varied from 100-0% with an overall 2% (w/w) solution in CO_2. The [TTBP] was kept at $5*10^{-2}$ M.

An unenhanced I_z was obtained based on the observed S/N of the free induction decay (FID) prior to Fourier transform. For these measurements, 64 co-added scans were required to observe the I_o. The I_o values were corrected for S/N improvement through multiple scanning and compared to the I_z (enhanced) values obtained after a single scan. The measured I_o for benzene-d_6 at 100% was used as the background I_o(bkg) contribution from radical or other impurities. The observed I_o's for the other mixtures were then corrected to give the unenhanced I_o used.

$$I_o(obs) - I_o(bkg) = I_o(corr)$$

or specifically:

$$\frac{(S/N)obs}{8} - \frac{(S/N)bkg}{8} = (S/N)corr$$

Since complete saturation was not obtained, all NMR observed signals were determined as functions of applied power. As noted in Equation [33], A^{-1} versus P^{-1} yields a slope of (s), the saturation factor. The A(obs) is corrected for (s) by $A(obs)/s = A_\infty$ where:

$$A(obs) = \frac{(S/N)_Z - (S/N)corr}{(S/N)corr} = \frac{I_Z - I_o}{I_o}$$

Recall that the enhancements determined were based on S/N measurements of the FID. It has been found that a S/N increase of 3 fold results following Fourier transform for the present conditions, therefore, in order to compare measurements, $A_\infty(FID)*3 = A_\infty(FT)$. Table 5.2 summarizes these results.

The average A_∞ determined using deuterium dilution agrees remarkably well with the previous SFC value (Table 5.1). The error has been reduced by a factor of 2 through better determination of the unenhanced signal. The value of

TABLE 5.2

FLOW DNP-NMR ENHANCEMENTS
FOR BENZENE/BENZENE-d_6 SOLUTIONS IN CO_2

2% (w/w) overall in CO_2 50°C 2000 psi [TTBP] = $5*10^{-2}$ M

C_6H_6/C_6D_6	Unenhanced $(S/N)_{FID}$ 64 scans	1 scan	Enhanced $(S/N)_{FID}$ 1 scan	Saturation Factor (s)	ENHANCEMENT $\frac{(S/N)-(S/N)_{corr}}{(S/N)_{corr}}$	A_∞(FID)	A_∞(FT)
0:100	11.5	1.4=I_o(bkg)	-4.58				
50:50	16.7	2.1	-24.5	0.44	-38.2	-86.7	-260
75:25	14.3	1.8	-18.8	0.77	-47.8	-62.1	-186
100:0	20.9	2.5	-27.0	0.48	-32.6	-68.0	-204
100:0	23.3	2. 9	-55.0	0.39	-38.6	-99.0	-297

A_∞(ave) = -237 $\pm$ 44

$A_{\infty} \approx -240$ approaches the theoretical maximum of -330 for proton systems under dipolar controlled DNP ($\rho = -0.5$). A value of $f \approx 1$ was determined by measurement of spin-lattice T_1's in the presence and absence of radical. Relating the value of A_{∞}(obs) with A_{∞}(theoretical) assumes that dipolar interactions in polarization transfer were dominant. Contributions through scalar interactions will significantly reduce the A_{∞}(theoretical) due to the opposite sign of ρ ($\rho = -1$ in the scalar dominated extreme). The error in the determination of the unenhanced signal can also contribute to a reduced A_{∞}(obs) value.

Future efforts in supercritical flow DNP-NMR will address the problem of unenhanced signal through the use of a different radical for which the A_{∞}(theoretical) has been determined at low magnetic field, where the extreme narrowing condition clearly prevails. The use of SFC in extending the extreme narrowing condition will be investigated further at 3.3 kG and at higher fields.

APPENDIX I

SUPERCRITICAL FLUID CHROMATOGRAPHIC SYSTEM AND SCF FLOW PROBE

For completeness, the supercritical fluid chromatographic system and NMR flow probe are discussed in further detail. The modifications required are described and diagnostics performed are presented. Each component of Figure 3.1 will be discussed sequentially.

Sample/Solvent Delivery Carbon dioxide (Scott SFC Grade) was supplied to the pump directly from a gas cylinder equipped with an eductor tube or from an inverted cylinder previously charged with CO_2. Custom compositions were delivered by first introducing a known weight of solute (e.g. polar modifier), followed by charging the cylinder with CO_2 and monitoring the appropriate increase in cylinder weight. Efficient transfer of CO_2 was aided by cooling the cylinder in a dry ice bath at ≈-20°C however care must be taken to avoid overfilling which leads to excessive pressures at ambient temperature. Continuous flow samples have also been introduced by a second pump downstream, to be discussed later.

Modified LC Pump A single piston reciprocating pump

(Scientific Systems Incorporated (SSI) Model 200) was adapted for SFC. A single piston pump was chosen to avoid the additional seals of dual piston pumps. Cooling of the exposed pump head to -10°C using a dry ice/ethanol/water bath facilitates efficient delivery of liquid CO_2. Operation at temperatures <10°C failed to give reproducible, efficient solvent delivery. Linearity of solvent delivery was achieved over a wide range of flow rates (Figure I.1). In the absence of cooling, the SSI pump can be used, as expected, as a normal LC pump. In making the transition from LC to SFC one must purge the pump and pulse dampener with CO_2 gas prior to cooling to avoid freezing of the piston.

Pulse Dampener Pulsing, inherent to reciprocating piston pumps, was reduced through a diaphragm type SSI Model 210 pulse dampener which also required an important modification. The fluorocarbon polymer diaphragm failed to isolate the pumped liquid CO_2 from the compressible fluid. Increasing back-pressure resulting from the permeating CO_2 caused premature diaphragm failure. Replacement with a convoluted stainless steel diaphragm with a necessary increase in internal volume eliminated seal failure with no loss in pulse dampening ability. Flow rates up to 8.0

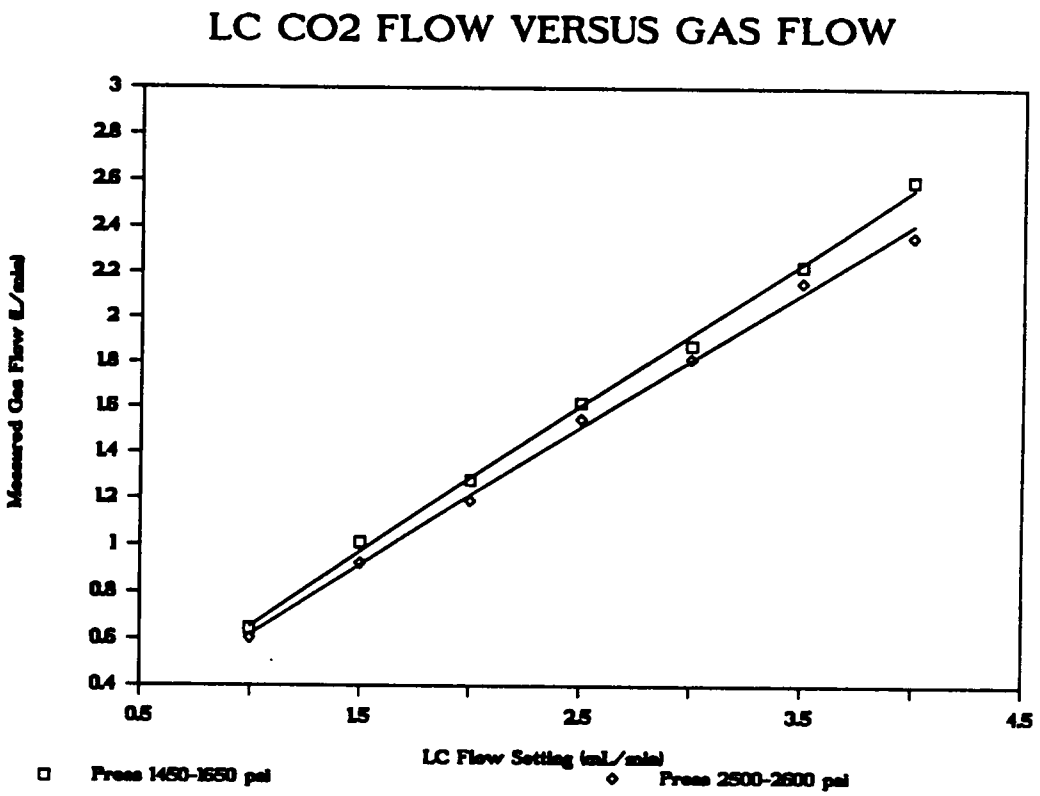

Figure I.1 Linearity of solvent delivery using the reciprocating piston pump. Non-coincidence of the two lines results from different compressibility at the different pressures.

mL/min. (2500 psi) and pressures up to 4500 psi (2 mL/min) have been used with no seal or pump failure. Flow modulation remained at <2% with pressure stabilities of ≤1% over 5 min. (Tables I.1,I.2)

Sample Delivery Pump A second LC pump (Waters M45) has been used to introduce a constant flow sample at concentrations limited by the pump minimum flow rate. An SSI three-way valve allowed introduction or elimination of the side stream without interrupting normal SFC flow. In order to avoid vapor lock by CO_2 of the second pump, the side stream pump required pressurization at or above the SFC stream pressure before introduction into the SFC stream. Continuous flow samples up to 10% (v/v) were routinely analyzed.

Supercritical Region Supercritical conditions for the chromatographic separations were established using a Varian Series 1200 GC oven prior to detection by NMR. The solvent was preheated to the preset operating temperature using a coil of 1/16" x 0.05" stainless steel tubing having an internal volume of 2 mL placed inside the oven. Separation within the oven followed injection using a standard Valco valve. Oven dimensions allow for packed columns (analytical or semi-preparative) up to 25 cm long; two 25 cm long

TABLE I.1

Pressure Stability at 2 mL/min

Pressure (psi)	Deviation (psi) [maximum-minimum]	Stability [deviation/pressure]
1438	12.6	0.008
1859	23.0	0.012
1948	13.5	0.007
3099	28.5	0.009
	Average Stability	0.9 %

TABLE I.2

Pressure Modulation

Flow Rate (mL/min)	Pressure (psi)	Pulse Duration (psi)	% Relative
2	2920	52	1.8
4	2373	29	1.2
8	2684	36	1.3
		Average Modulation	1.4 %

columns placed in tandem is also possible. An Econosphere C_{18} 250 x 4.6 mm analytical column with 5 μm packing was used for the SFC separation presented. A precolumn of pellicular packing preceeded the analytical column to prevent analytical column contamination. The column used generated a 600 psi pressure drop across the column. Chromatographic separation thus occurs under the controlled temperature of the oven ($\pm$1°C) with the pressure controlled by the flow rate and restrictor orifice. An in-line analog pressure gauge monitored post column pressure; precolumn pressure was determined at the pulse dampener.

SFC/NMR Flow Probe In contrast to a typical LC/NMR flow probe, the flow probe developed required increased pressure and variable temperature capability. The probe was designed specifically for flow and is not a modified commercial NMR probe. The probe can be used stop-flow without spinning. A Be/Cu frame insured structural stability without ferromagnetic interference. Figure 3.2 should be used as a guide to the components of interest.

Variable temperature was incorporated using heated forced air. Air at flow rates ≈22 L/min. was passed through a blast tube heater connected to the probe. Heated air

passed through an insulated 1/4" tapered line (a) to the pre-equilibrium region. The air was then channeled into the observation region (b). (Probe dimensions prevented direct passage). The temperature was monitored using a Cu/Constantan thermocouple (c) adjacent to the flow cell. The temperature was controlled using a JEOL JNM-VT-3B unit (±1°C). In-situ monitoring was considered but the thermocouple to be used had insufficient resistance for the VT unit. A glass insert in the observation region directs the heated air flow along the outside of the observation region to avoid thermal gradients. A Teflon probe end cap further insulates the observation region.

Flowing sample achieves premagnetization through a 1/4" x 0.05" SS pre-equilibrium coil (d) having an internal volume of 1 mL. Brass Swagelok fittings (h) (1/4" x 1/8") are used to couple the 1/8" SS line to the flow cell. Brass was chosen to minimize ferromagnetic materials which can degrade magnetic field homogeneity.

Various materials were investigated for use as a flow cell with respect to operation compatibility. Precision bored thick walled quartz cells in conjunction with graphite or Vespel ferrules failed to give sufficient high pressure

capabilities. Machined Teflon was considered however, swelling and limited pressure capability prevented its use. Kel-F, $+CHF-CH_2+$, is a more rigid fluoropolymer and was more easily machined than Teflon. It could also be threaded, however optimum pressure and temperature capability appeared limited. Delrin, $+CH_2-CHO+$, was investigated however hoop stress test values (86) suggest a maximum pressure of 3000 psi at 1/4" x 1/16". The aforementioned polymer materials have been used in solid state NMR as sample rotors; the background signals of the latter two can be eliminated through pulse techniques. High temperature, high speed rotors are manufactured from ceramics such as Macor, zirconia, alumina or sapphire. Alumina was chosen as the flow cell (g) due to its ready availability as an extruded tube (Omegatite thermocouple sleeve). Pretreatment of the ceramic tube with concentrated nitric acid insured that no residual iron was present as a result of the extrusion method of manufacturing which could degrade spectral resolution. Vespel ferrules were retained to allow cell changing, however brass ferrules could be used for enhanced pressure capability. Using Vespel ferrules pressures up to 4000 psi have been used with no seal or cell failure. Tubes of 1/4" OD are available with different ID's (1/8", 1/16") providing observation volumes of 20 μL and 80 μL,

respectively. Tubes of 1/8" x 1/16" were considered too fragile for routine use. Larger observation volumes are possible using 3/16" OD tubes.

A single turn Helmholtz coil (f) (22 gauge) wrapped parallel on the flow cell was tuned to 199.5 MHz for proton observation. A second 5 turn Helmholtz coil (24 gauge) wrapped on a glass form orthogonal to the ^{1}H coil was tuned to 14.4 MHz for ^{14}N observation. Both circuits can be externally tuned. Typical acquisition parameters for ^{1}H and ^{14}N appear in Table 4.1. A brass shield (e) prevents signal detection through the coil leads.

Restrictor Following detection by NMR, the sample flows out of the magnet to the back-pressure restrictor. Pinched SS tubing proved inadequate due to sample deposition at the orifice as a result of desolvation. Due to the higher flow rates, effective back-pressure restriction was possible using a SS microvernier GC valve at its lowest settings. Carbon dioxide deposition due to adiabatic expansion at the orifice and subsequent clogging was eliminated by immersion of the restrictor in a hot water bath. Pressure "programming" can be accomplished using a varying flow rate at a fixed orifice setting (Figure I.2). Following the hot

water bath is a bubble trap to recover any dissolved organics.

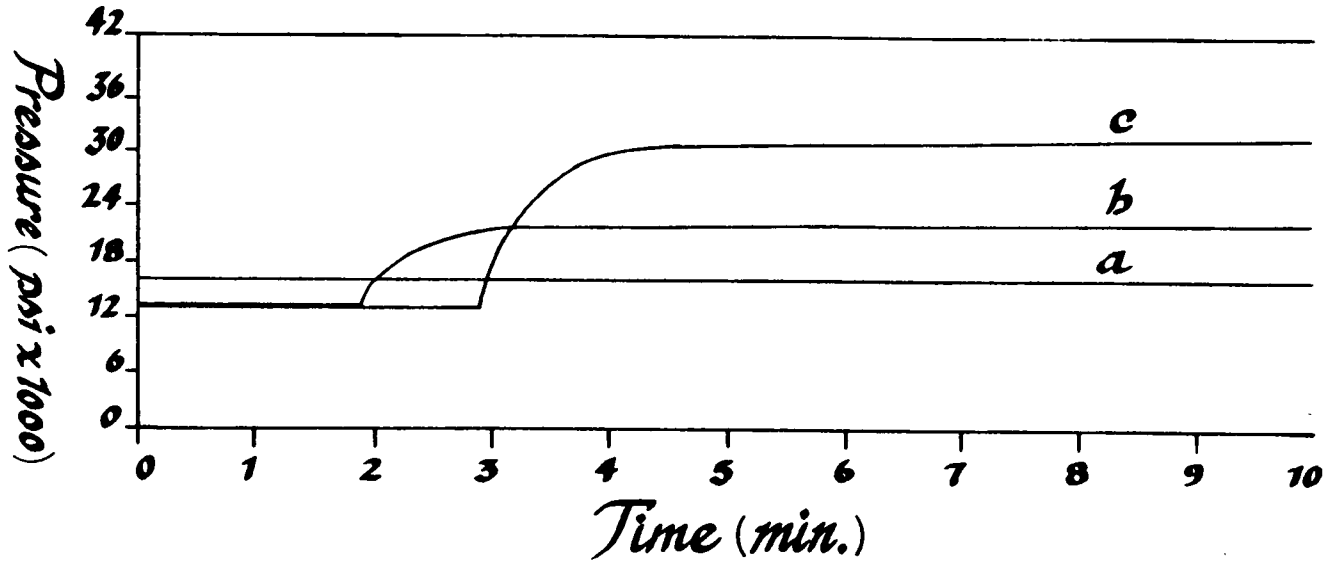

Figure I.2 "Pressure programming" through increased flow rate at a fixed orifice setting.
(a) 2 mL/min
(b) 2 mL/min increased to 4 mL/min at 2 minutes
(c) 2 mL/min increased to 5 mL/min at 3 minutes

APPENDIX II

SPIN LATTICE RELAXATION TIME MEASUREMENTS BY THE INVERSION RECOVERY METHOD

The nuclear spin-lattice relaxation time (T_1) can be measured by different methods. Inversion recovery, saturation recovery and progressive saturation methods can be used depending on the nature of the sample being measured. Of these methods, saturation recovery has been used and will be described. The JEOL software mathematical treatment of the data will also be outlined.

In this method, the observation of the free induction decay is preceeded by inversion of the magnetization and a varying delay period τ.

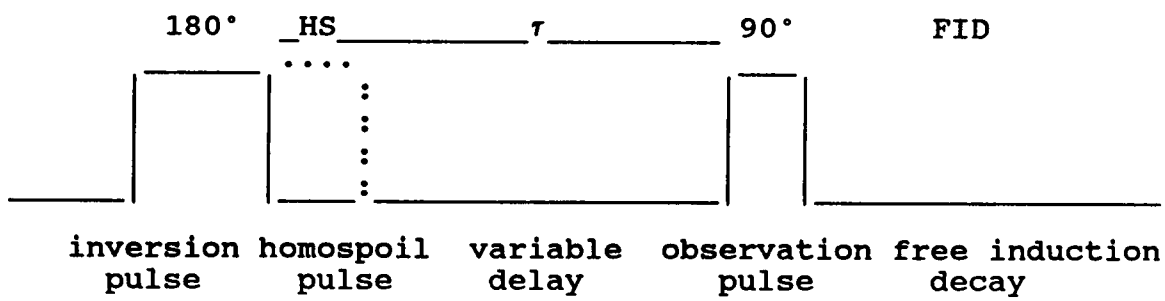

An appreciation of the inversion recovery method is gained if the magnetization vector description is used for

three cases of τ (Figure II.1). The observed magnetization passes from an inverted signal at $\tau \approx 0$ to a positive signal at $\tau \approx 5T_1$ with signal inversion occurring at $\tau \approx T_1$.

In practice the measurement is repeated with τ being varied; the observed magnetization can be described by:

$$M(\tau) = M_o[1-2 \exp (-\tau/T_1)] \qquad [39]$$

The observed $M(\tau)$ as a function of τ follows an exponential curve from a minimum of $-M_o$ ($\tau \approx 0$) to a maximum of M_o ($\tau > 5T_1$) Figure II.2. Rearrangement of Equation [39] yields:

$$(-\tau/T_1) = \ln[(M_o - M(\tau))/2M_o] \qquad [40]$$
$$(-\tau/A) = \ln Z$$

Where $A=T_1$; $Z= [(M_o - M(\tau))/2M_o]$

Introducing a constant B and an exponential weighting factor W, allows experimental error minimization, where E is now minimized through $W = Z = [(M_o - M(\tau))/2M_o]$.

$$\Sigma\{[\ln Z - (-1/A)\tau - B]W\} = E \qquad [41]$$

The reported relaxation time is obtained by the method

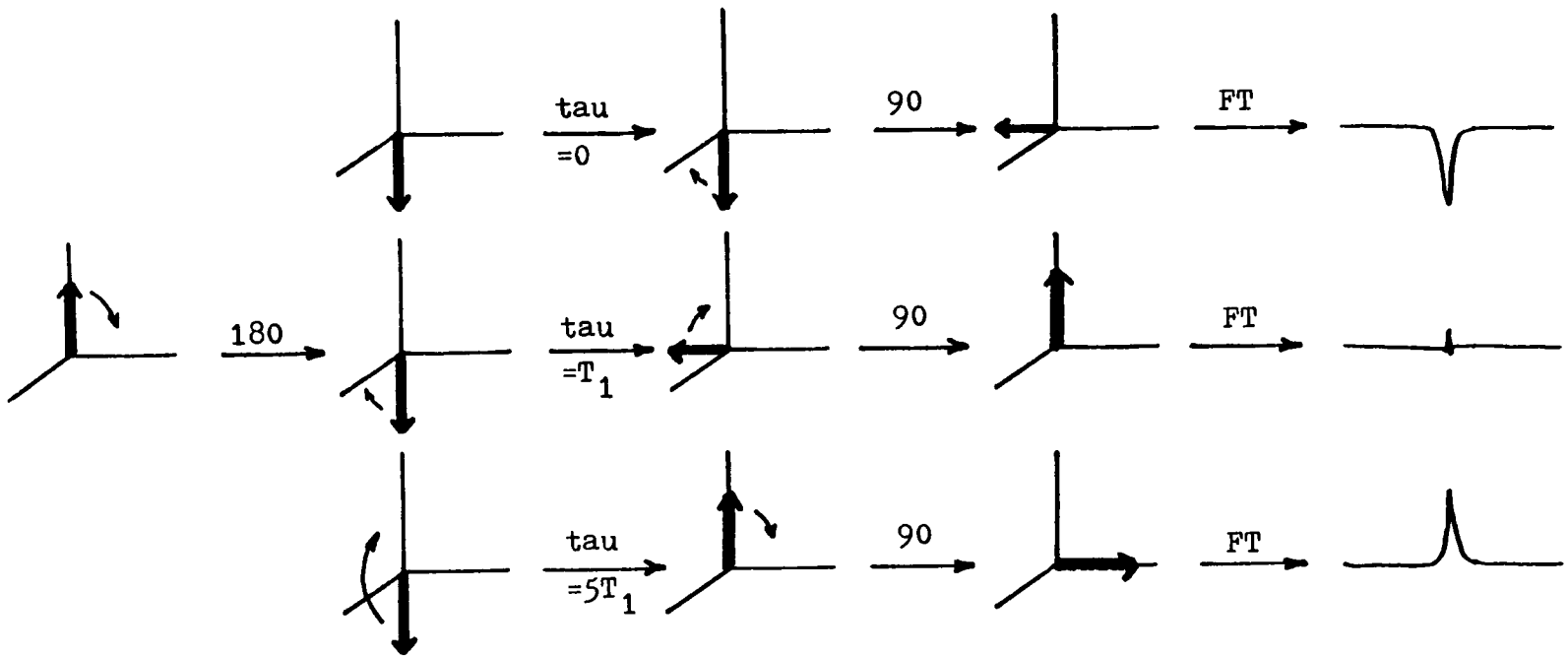

Figure II.1 Magnetization vector description of the inversion recovery method of T_1 determination.

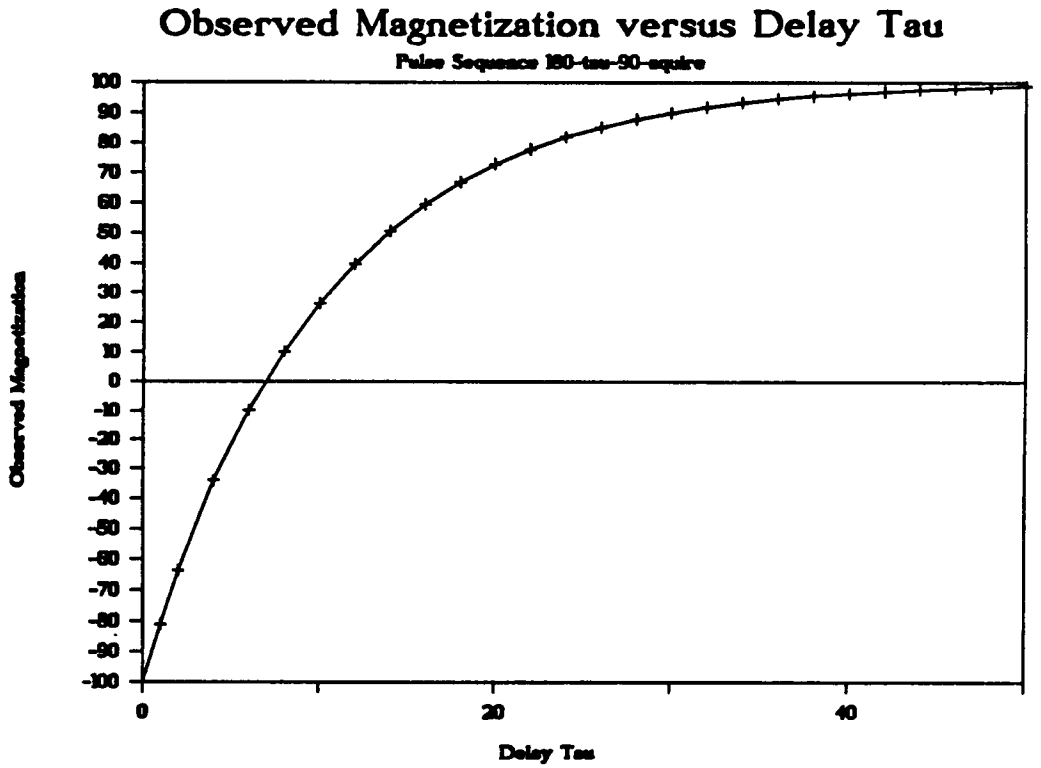

Figure II.2 The observed magnetization as a function of delay period (tau) for the 180°-tau-90° inversion recovery pulse sequence.

of least squares as:

$$T_1 = A = \frac{(\Sigma w^2 \tau)^2 - \Sigma w^2 \Sigma w^2 \tau^2}{\Sigma w^2 \Sigma w^2 T(\ln Z) - \Sigma w^2 (\ln Z) \Sigma \tau w^2} \qquad [42]$$

APPENDIX III

DETERMINATION OF MICROWAVE B_{1S} FIELD BY THE DNP-^{1}H NMR METHOD

Introduction

The microwave magnetic field strength at the sample determines the efficiency of saturation at a given output power. The magnitude of the magnetic field (B_{1S}) varies as the square-root of applied power (P^{-2}), therefore saturation can always be achieved at the expense of high applied power. The cavity quality factor (Q) is effected by any object within the cavity and is significantly degraded by the presence of the rf coil within the cavity in DNP-NMR. The result is increased power levels required to achieve saturation (2-10 watts). In the case of flow DNP-NMR, the cavity Q is effected only by the flow cell and sample, thereby allowing efficient saturation at 250 mW applied power for the TTBP radical at 10^{-2} M (83).

In order to quantify the improvement of flow DNP over static DNP, the magnitude of B_{1S} was measured at a given power and compared to the unperturbed cavity. Microwave magnetic field strengths can be measured in a variety of ways. The perturbing sphere method is the most common however it requires additional equipment (87,88).

Progressive saturation of a well-known radical system can be used since the square of the derivative peak-to-peak ESR linewidth is proportional to B_{1s}^2 which varies as applied power (P). The radical peroxylamine disulfonate dianion (PADS) has been well characterized in solution and has been used effectively to measure B_{1s} through saturation broadening (88-91). Saturation broadening has also been applied to single crystals of N-methylphenazinium tetracyanoquino-dimethan (NMP-TCNQ) by Vistnes and Dalton (92). The use of NMP-TCNQ was compared to that of PADS and the advantages of the former were emphasized. NMP-TCNQ can be used at high temperatures as well as below 0°C and since the NMP-TCNQ is insoluble in most solvents used in ESR, it can be used as an internal standard for B_{1s} determinations for any sample.

For our configuration, the use of NMP-TCNQ saturation broadening was found inconclusive for measurement of B_{1s} due to limited available power. NMP-TCNQ is useful for B_{1s} values of 0.1-0.5 gauss. The DNP-NMR enhancement factor (Equation [30]) is also dependant on B_{1s}^2 or applied microwave power. Using a sealed sample of benzene and radical, the DNP-NMR enhancement factor was determined in the vicinity of the rf coil for typical static and flow

configurations. The values were then normalized and compared to B_{1s}^2/P values of an unperturbed cavity.

Results and Discussion

For the apparatus discussed in Chapter Five, the observed magnetization was measured using DNP-NMR as a function of applied microwave power at different positions within the cavity (Figure III.1). The static configuration consisted of a two turn solenoid coil wound on the form (1/4" OD glass flow cell) placed in the middle of the microwave cavity (81). The flow configuration consisted of the same ceramic cell described in Chapter Five. A sealed sample of benzene ($\approx$2 mm^3) having a [TTBP] concentration of $5*10^{-2}$ M was lowered through each cell.

Observed magnetization (I_Z) was obtained for each configuration as functions of applied microwave power in the vicinity of the rf coil. Since the NMR method was used, only sample near the coil can be measured however, since the objective is to determine the relative advantage of flow over static DNP-NMR, other portions of the cavity were not of interest.

Plots of $1/[(I_Z - I_O)/I_O]$ versus $1/P$ yielded A_∞ values

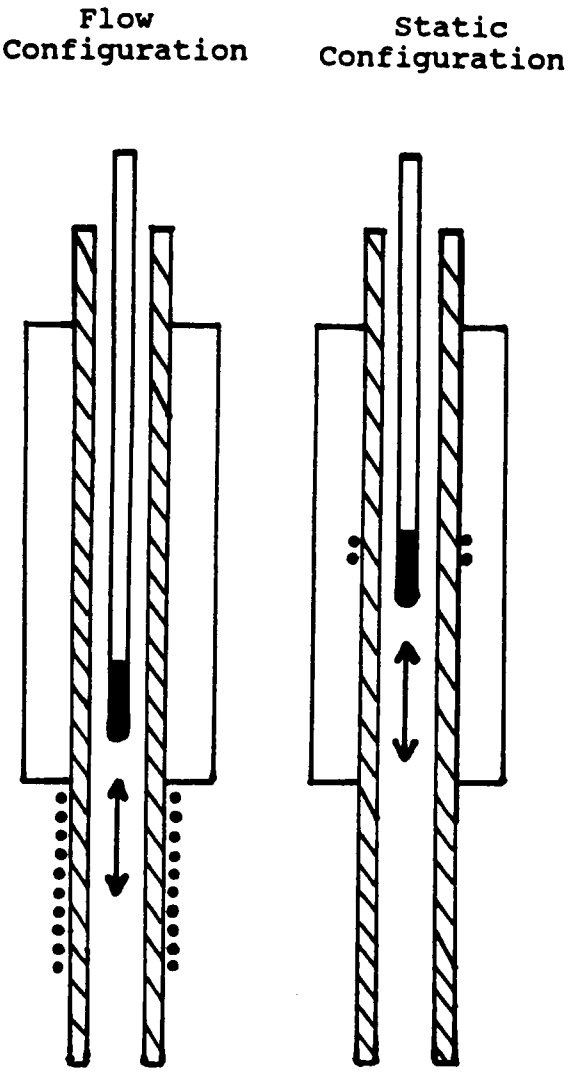

Figure III.1 Method of microwave B_{1S} mapping using DNP-NMR observed enhancements of a sealed sample.

for the various positions. The resulting $A_{\infty}(ave) = -70$ is consistent with the value obtained in the liquid flow DNP-NMR analysis of the same solution (83). The $[(I_z - I_o)/I_o]$ values were normalized with respect to $A_{\infty}(ave)$ and P to yield average enhancement factors at the various positions (A(ave)).

Fajer and Marsh have measured B_{1s}^2/P as a function of distance for the Varian TE_{102} cavity using the PADS saturation broadening method (91). The A(ave) value determined using the flow configuration furthest away from the rf coil is assumed to represent an unperturbed B_{1s} microwave field (8mm below cavity center). Since A(ave) α B_{1s}^2/P the above value was set equal to that B_{1s}^2/P value of Fajer and Marsh at the same position. Figures (III.2-5) show the normalized values of A(ave) for the static and flow configurations compared to the B_{1s}^2/P values of Fajer and Marsh as functions of distance within the cavity.

For the unperturbed case, a maximum in B_{1s}^2/P occurs in the center of the cavity and decays rapidly above and below the cavity center (Figure III.2). For the flow DNP-NMR configuration the normalized B_{1s}^2/P increases steadily inside the cavity at a rate approximately the same as in the

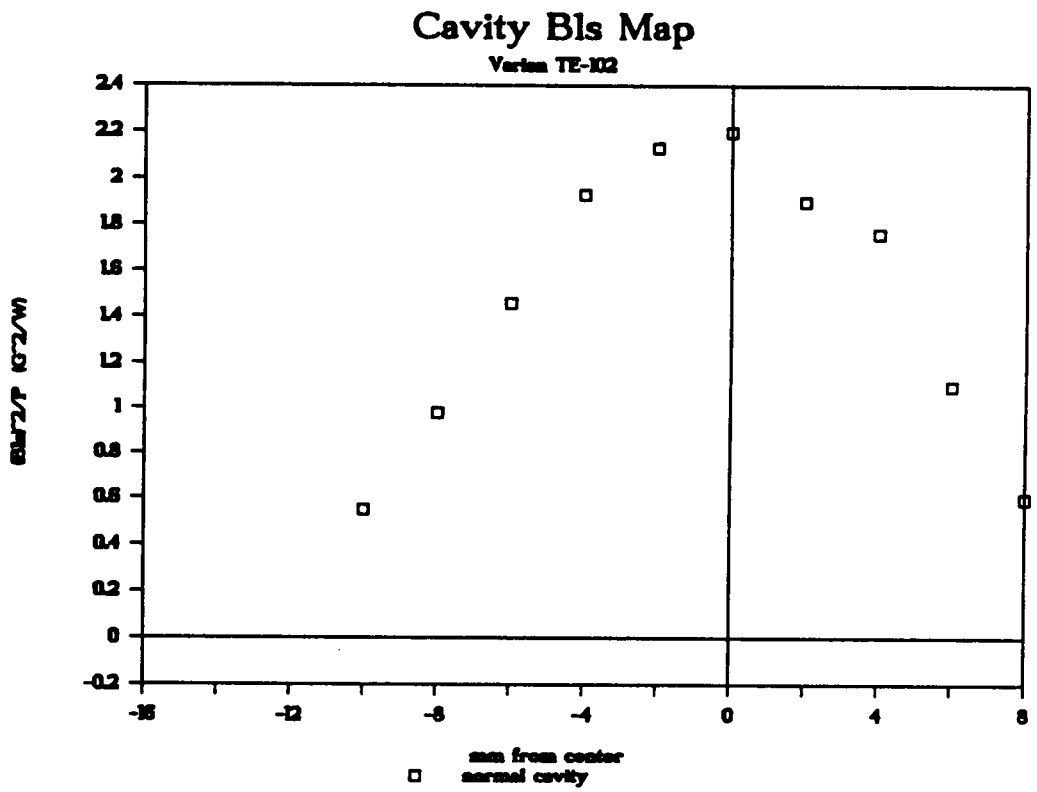

Figure III.2 Microwave magnetic field map of an unperturbed cavity (87).

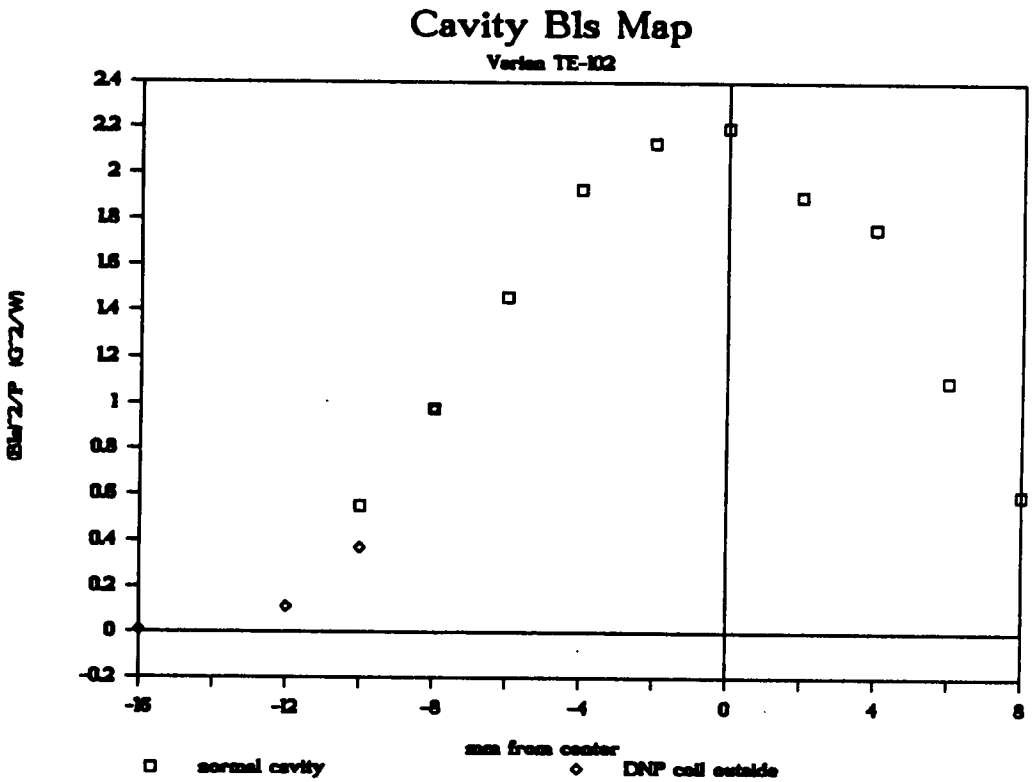

Figure III.3 Microwave magnetic field map using observed DNP-NMR for a typical flow DNP-NMR configuration.

unperturbed case (Figure III.3). (The minimum values of B_{1s}^2/P noted, positions -12 and -16 mm below center, represent positions outside the cavity.) For the static configuration, in which the rf coil is placed in the middle of the cavity, significant shielding occurs and the microwave cavity quality factor (Q) is significantly reduced (Figure III.4). At the position +6 mm from cavity center, $B_{1s}^2/P(\text{center}) \approx B_{1s}^2/P(\text{norm})$. A minimum in B_{1s}^2/P occurs at the center of the cavity, not surprising considering the presence of the rf coil in the center of the cavity. The B_{1s}^2/P value increases moving away from the center in contrast to the behavior of the unperturbed cavity. (The asymmetry is presumably a result of the NMR rf coil leads.)

Using flow DNP-NMR, electron saturation occurs in the center of the microwave cavity before transfer to the NMR observation region. As evident in Figure III.5, the expected B_{1s}^2/P value for flow DNP is significantly different from that of static DNP. This large difference is supported by the large power levels required to achieve saturation, i.e. equivalent B_{1s} values, in static DNP-NMR measurements. Flow DNP-NMR is thus able to optimize both saturation and observation for more efficient, improved enhancements.

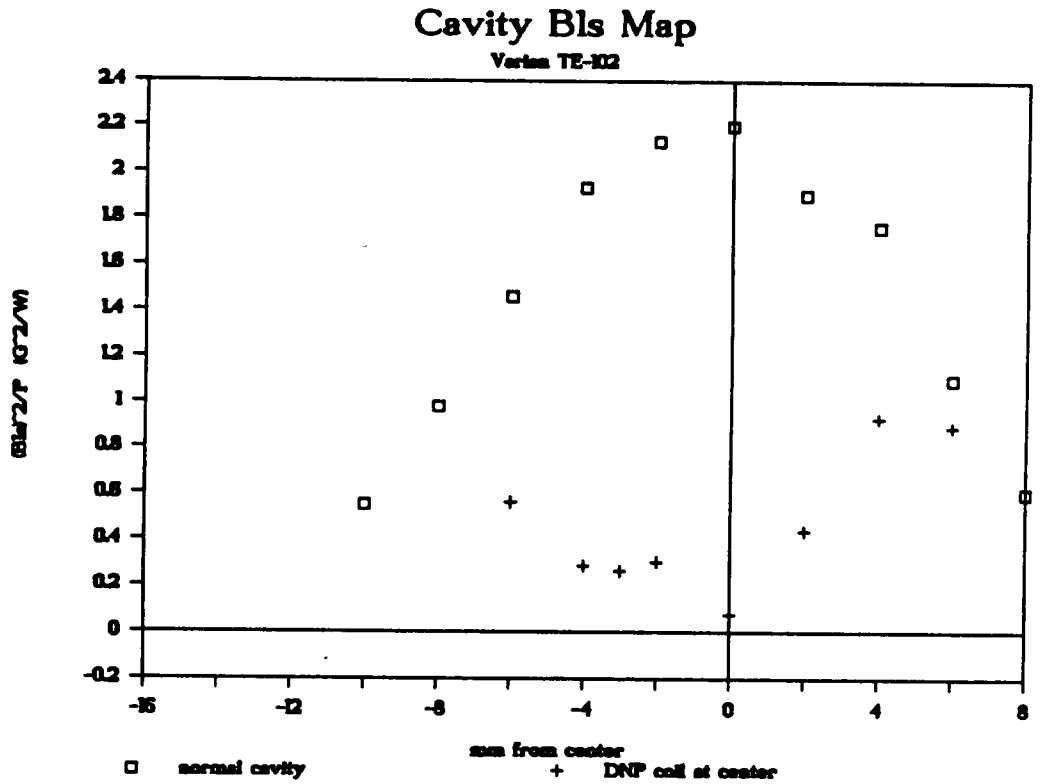

Figure III.4 Microwave magnetic field map using observed DNP-NMR for a typical static DNP-NMR configuration.

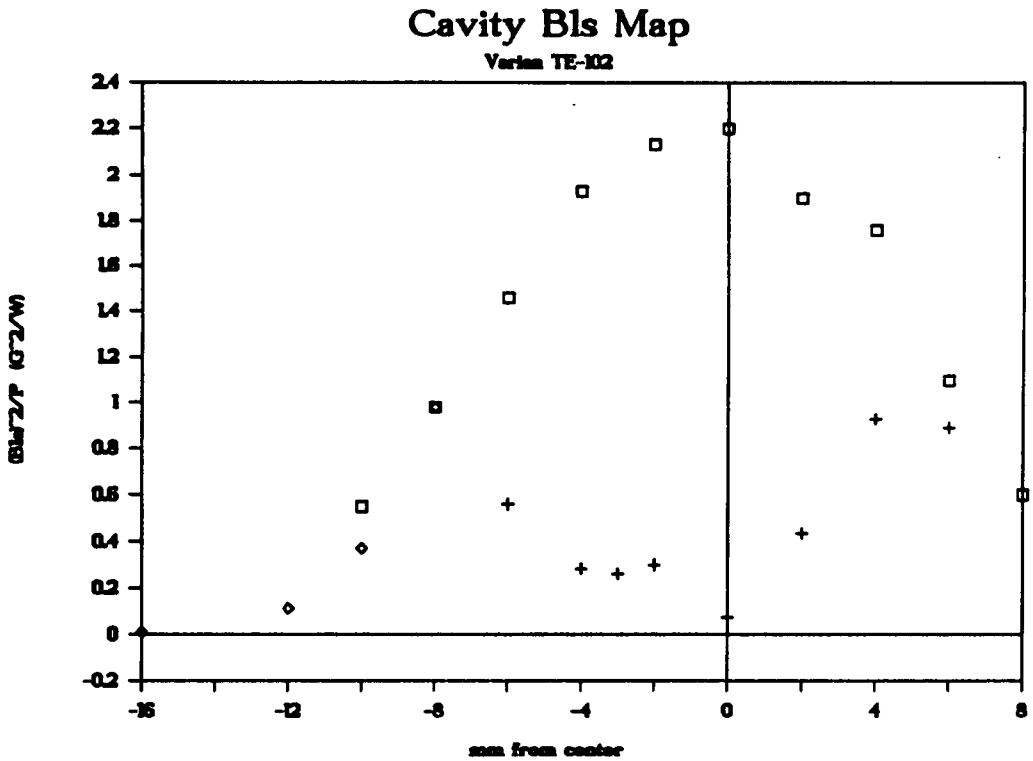

Figure III.5 Superposition of all three microwave magnetic fields maps.

- □ Normal cavity
- ✚ DNP coil at cavity center
- ◇ DNP coil outside of cavity

APPENDIX IV

FLOW DYNAMICS BY NMR

Introduction

The application of pulsed NMR in the analysis of flow dynamics has been addressed in detail by Haw (42). Using the Radda sequence (41) [90°(HS)-τ-90°-T] (Chapter 3), the initial 90°(HS) portion destroys all magnetization present in the cell. During the following delay period, τ, premagnetized "new" spins enter the cell displacing the earlier "old" spins. The "new" spins are detected using the second 90° pulse. The "old" spins are not detected so long as $T_1 >> \tau$, i.e. they have not had sufficient time to reestablish a premagnetization Boltzmann distribution. The quantity of spins detected is reflective of the flow type, e.g. laminar or plug.

The observed magnetization can be described using equations [2] and [3]:

$$M_{xy}(2) = f(1)M_o + [1 + e^{-(\tau/T_1)}]M_o[1 - f(1)] \qquad [2]$$

$$M_{xy}(2) = f(1)M_o \text{ where } \tau << T_1 \qquad [3]$$

where M_o is the equilibrium magnetization and f(1) is the fraction of "new" spins which enter the detection volume

during the time τ. The fraction f(1) has been described by Haw for three dynamic flow models: plug, exponential and laminar (42).

Under idealized plug flow the sample volume (V_p) entering the flow cell corresponds to $V_p=F\tau$ where F is the flow rate. It follows then that:

$$f(1)=\frac{V_p(1)}{V_c}$$

with V(1) equaling V_c at times $\tau \geq V_c/F$. Exponential flow results when one considers the fraction:

$$f(t)=V_p(t)/V_c$$

and the rate of change of f(t) as:

$$df(t)/dt=F-f(t)F$$

which yields, upon integration:

$$f(1)=1-e^{(-FT/V_c)}$$

Laminar flow is more complex and reduces to two cases:

$$f(1)=1-V_c/4FT \quad \text{for} \quad f(1) > 0.5$$

$$\text{and } f(1)=FT/V_c \quad \text{for} \quad f(1) < 0.5$$

For $f(1) \leq 0.5$, the quantity of "new" spins observed is identical for laminar and plug flow. At $f(1)>0.5$, residual "old" spins remain at the walls under laminar flow as a result of viscous interactions thereby attenuating the observed signals (42).

Examining magnetization as a function of delay (τ), for laminar flow (Figure IV.1), the observed signal slowly increases to a maximum value when $T_1 >> \tau$ and reaches the maximum more rapidly as T_1 approaches τ. The latter is due to the ability of "old" spins to reestablish premagnetization during the delay, prior to detection.

Examining magnetization for plug flow (Figure IV.2) when $T_1 >> \tau$, the magnetization increases linearly to the maximum at $\tau = V_c/F$, the flush period. As T_1 approaches τ, the maximum is reached more quickly as before.

Flow profiles in supercritical fluids are likely to have turbulent character as a result of liquid-like densities and gas-like viscosities (93). The extent of turbulence is often described using the dimensionless Reynold's number (R_e) (94):

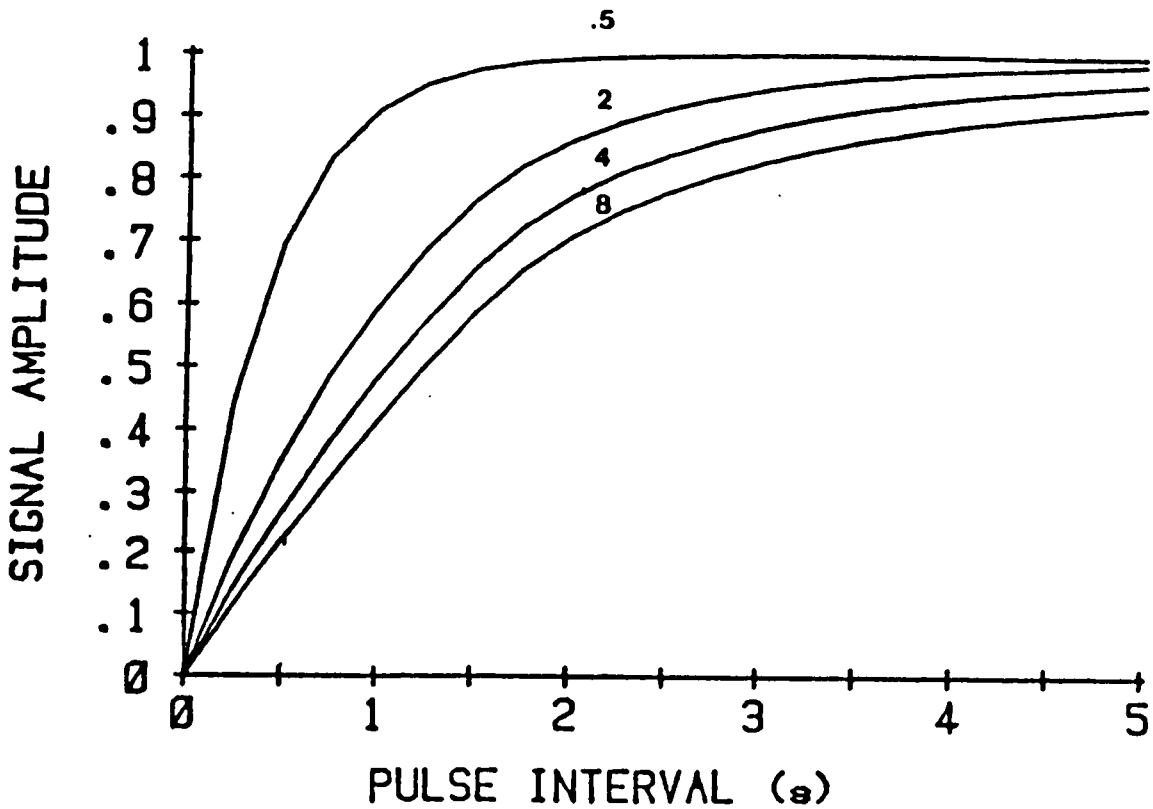

Figure IV.1 Steady state laminar flow NMR response for various T_1's (sec) versus pulse delay (τ). F= 1 mL/min Vc= 50 μL (42)

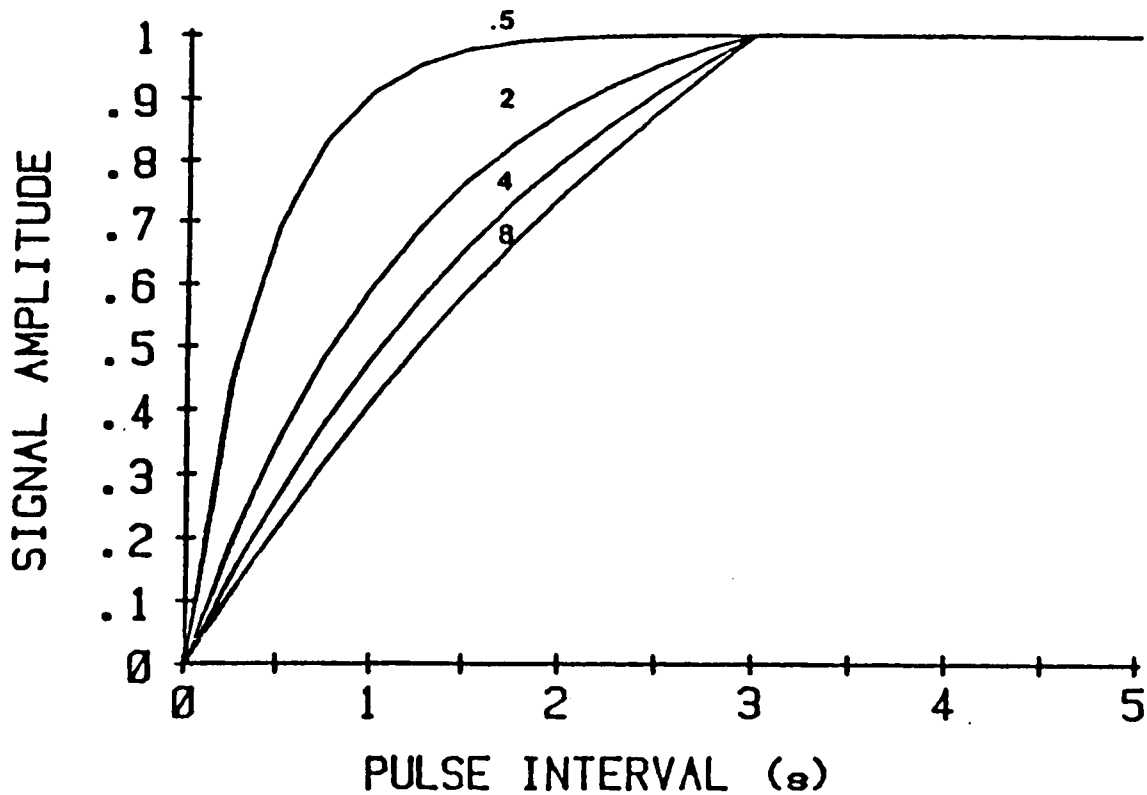

Figure IV.2 Steady state plug flow NMR response for various T_1's (sec) versus pulse delay (τ).
F= 1 mL/min Vc= 50 μL (42)

$$R_e = \frac{\text{Inertial Forces}}{\text{Viscous forces}} = \frac{d_p v D}{\eta}$$

where: d_p - the diameter of the tube or particle
v - linear velocity
D - density
η - viscosity

Turbulence occurs in open tubes at $R_e \approx 2100$ and in packed tubes for $R_e \approx 1\text{-}100$. The latter is significantly less due to the number of pathways available. Turbulent flow in supercritical fluids is more readily achieved over other mobile phases, low pressure gases and liquids, due to favorable D/η values (95).

The important implications of turbulence in chromatography are described by Giddings (94). The turbulent flow profile is intermediate to laminar and plug with reduced tailing at the walls as a result of reduced viscous interactions (Figure IV.3). One would then expect the observed magnetization using the Radda sequence to achieve the maximum value for $T_1 >> \tau$ more quickly than under laminar flow but not quite linearly as in plug flow.

Results and Discussion

Flow dynamics were investigated under different conditions using the flow probe described in Appendix I (Figure 3.2). For supercritical investigations the oven of

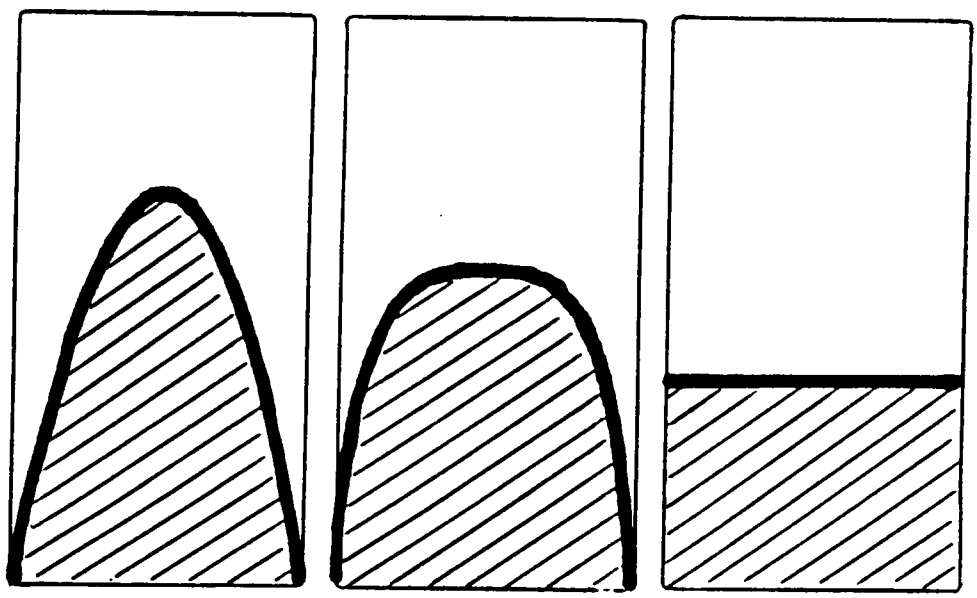

Figure IV.3 Laminar, turbulent and plug flow profiles.

Figure 3.1 was retained to insure supercritical conditions. Preliminary results comparing liquid laminar flow and dilute benzene solutions in CO_2 are shown in Figures IV.4-6. The Reynold's numbers achieved for this limited study fail to reach the value of 2100 required for turbulent flow in open tubes however evidence suggests reduced tailing and more rapid growth of M_{xy}/M_o as a result of favorable D/η. Under the supercritical conditions used, $T_1 \approx 3$ sec. therefore $T_1 >> \tau$ only for the flow rates of 4 mL/min and 8 mL/min (Figures IV.5-6).

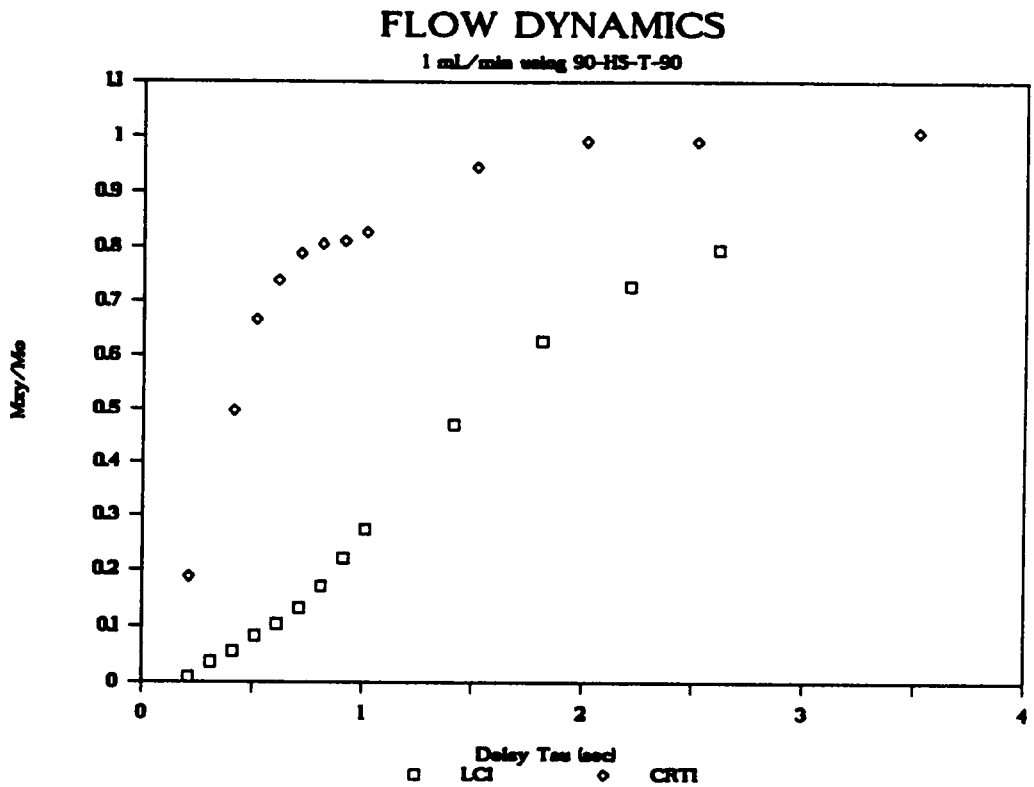

Figure IV.4 Observed NMR response versus delay under different flow dynamic conditions at 1 mL/min.
$V_c \approx 20\ \mu L$
LC1 : 3.3% (v/v) benzene in CCl_4 $R_e \approx 16$
CRT1 : 1% (w/w) benzene in CO_2 at 54°C 1500 psi
$R_e \approx 386$

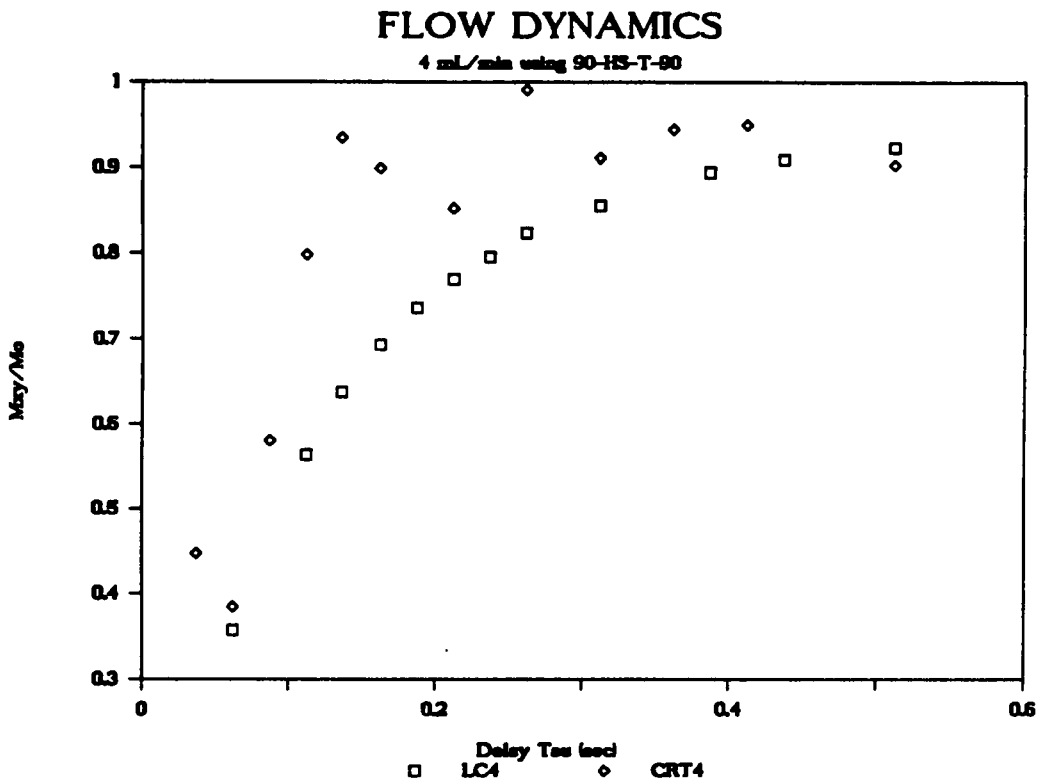

Figure IV.5 Observed NMR response versus delay under different flow dynamic conditions at 4 mL/min.
$V_c \approx 20\ \mu L$
LC1 : 3.3% (v/v) benzene in CCl_4 $R_e \approx 67$
CRT1 : 1% (w/w) benzene in CO_2 at 62°C 1500 psi
$R_e \approx 664$

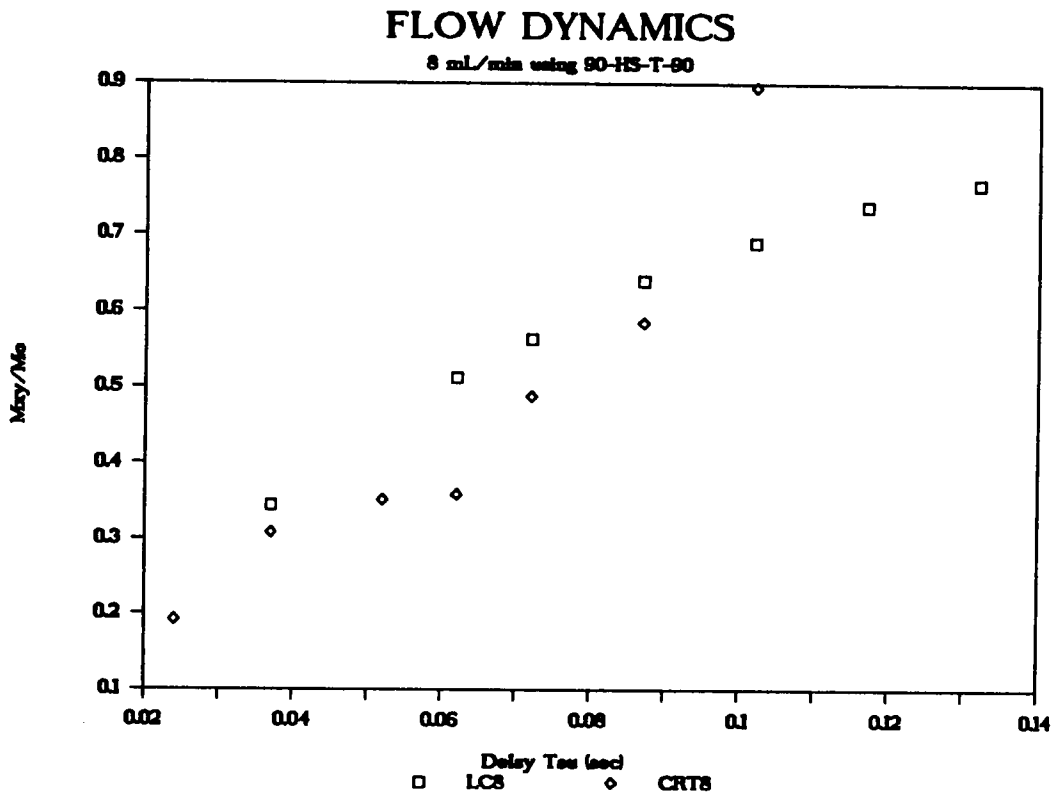

Figure IV.6 Observed NMR response versus delay under different flow dynamic conditions at 8 mL/min.
$V_c \approx 20\ \mu L$
LC1 : 3.3% (v/v) benzene in CCl_4 $R_e \approx 134$
CRT1 : 1% (w/w) benzene in CO_2 at 54°C 1500 psi
$R_e \approx 1382$

SUMMARY

The direct coupling of liquid chromatography and ^{1}H NMR has been used in the identification of eluting compounds. Normal phase applications are possible through the use of non-protonated solvents such as CCl_4 and Freon-113. Reverse phase applications have been pursued using deuterated solvent systems or solvent signal suppression techniques. The exclusive use of deuterated solvents is prohibitively expensive making solvent signal suppression the most viable approach. Suppression methods reduce or eliminate the solvent signal and those immediately adjacent; nearby signals are often distorted making quantification difficult. Alternatives, however, exist which avoid the problems associated with solvent background signals.

Observation of ^{19}F NMR instead of ^{1}H offers comparable sensitivity and selectivity without solvent signal interferences. After p-fluorobenzoate derivatization, mixed alkyl and aryl alcohols have been analyzed using the LC/^{1}H and LC/^{19}F {^{1}H} NMR approaches. The presence of J_{HF} couplings was eliminated through effective implementation of phase-cycled MLEV-16 decoupling. Efficient decoupling was shown over a large ^{1}H spectral width and for large J_{HF} couplings. The complementary nature of ^{19}F detection was

demonstrated and shown advantageous where ^{1}H spectral differences are minor. In the absence of chromatographic resolution, the sensitivity of the ^{19}F nucleus to its electronic environment permitted coeluting compound identification.

The observation of ^{19}F NMR is amenable when ^{19}F nuclides are present or using fluorine-tagging. A more universal alternative to LC is the use of supercritical fluid chromatography which, using CO_2, offers no ^{1}H solvent background signal. A chromatographic system and NMR flow probe were developed which allow the direct coupling of supercritical fluid chromatography and ^{1}H NMR (SFC/^{1}H NMR). The system utilized both LC and GC elements and the modifications required were described in detail. The flow probe incorporated the required variable temperature and elevated pressure capability necessary to insure supercritical conditions. The direct observation of eluting hydrocarbons of a model fuel mixture demonstrated the utility of SFC/^{1}H NMR when compared to the normal phase LC/^{1}H NMR analysis of the same mixture. Investigations required higher injected quantities for detection than expected requiring investigation into the nature of dilute solutions in CO_2 with respect to NMR detection before the

SFC/^{1}H NMR approach could be optimized.

The relaxation behavior of dilute solutions of benzene and acetonitrile in CO_2 under sub- and supercritical conditions was studied using stop-flow ^{1}H and ^{14}N NMR. Measurement of ^{1}H T_1's established that spin-rotation interactions were responsible for ^{1}H relaxation in benzene and acetonitrile in contrast to the dipolar interactions typical of normal liquids. Molecular spin-rotation correlation times (τ_{sr}) were calculated directly from the ^{1}H T_1 values over the large range of viscosities and temperatures studied. Through ^{14}N linewidth measurements, molecular correlation times (τ_c) were determined directly for acetonitrile. Molecular motion was found to be 2 to 5 times faster in sub- and supercritical CO_2 than the neat liquid. Molecular motion was found to be under inertial control making application of the Hubbard relation inappropriate. A reduced τ_c was obtained for acetonitrile (τ_{red}), normalized to 300K, and compared to experimental and theoretical predicted values. The value obtained compared favorably with the other experimental value and similarly showed that the applied theory fails to consistently describe molecular motion.

The values of ^1H T_1's measured over the viscosity and temperature range investigated were large compared to that required for efficient application of SFC/^1H NMR. The time required for premagnetization prior to detection would be prohibitively long unless a paramagnetic relaxation agent was included in the CO_2, (e.g. O_2) prior to detection.

The increased molecular motion through the use of supercritical CO_2 was shown advantageous in dynamic nuclear polarization. The use of flow has been shown effective in improving the efficiency of DNP-NMR signal enhancement. An improvement in the signal enhancement by a factor of two resulted with supercritical CO_2/benzene over normal liquid benzene under the same conditions. This was due to improved spectral density at the frequency observed. Large errors were present in the measurements due to problems associated with detection of the unenhanced NMR signal. Signal enhancement through DNP offers improved applicability of directly coupled chromatography NMR.

Through observation of DNP-^1H NMR enhancements of a sealed sample, typical static and flow configurations were compared. Normalization to previously determined microwave magnetic field values (91) allowed direct comparisons of the

two configurations to the unperturbed cavity and the improved efficiency of the flow configuration over the static is evident.

The flow dynamics of normal liquids can be measured using pulsed NMR; the differences expected between idealized plug flow and laminar flow have been discussed in detail by Haw (42). The liquid-like densities and gas-like viscosities of supercritical fluids offer favorable conditions for turbulent flow. Observation of turbulent flow by NMR is expected to be intermediate to plug and laminar flow. Results obtained under less than ideal conditions support non-laminar flow characteristics of supercritical fluids.

REFERENCES

(1) Suryan, G. Proc. Indian Acad. Sci. Sect. A **1951** 33,107.

(2) Zhernovoi, A.; Latyshev, G. "Nuclear Magnetic Resonance in Flowing Liquids", Consultants Bureau, New York **1965**.

(3) Jones, D.; Child, T. Adv. Magn. Reson. **1976** 8, 123.

(4) Watanabe, N.; Niki, E. Proc. Jpn. Acad. Su. B. **1978** 54, 194.

(5) Bayer, E.; Albert, K.; Nieder, M.; Grom, E. J. Chromatogr. **1979** 186, 497.

(6) Buddrus, J.; Herzog, H. Org. Magn. Res. **1980** 13, 153.

(7) Haw, J.; Glass, T. E.; Motell, E.; Dorn, H. C. Anal. Chem. **1980** 52, 1135.

(8) Bayer, E.; Albert, K.; Nieder, M.; Grom, E.; Zhu, An Fresenius' Z. Anal. Chem. **1980** 304, 111.

(9) Buddrus, J.; Herzog, H. J. Magn. Reson. **1981** 42, 453.

(10) Haw, J.; Glass, T.E.; Dorn, H.C. Anal. Chem. **1981** 53 2327.

(11) Haw, J.; Glass, T. E.; Dorn, H. C. Anal. Chem. **1981** 53, 2332.

(12) Bayer, E.; Albert, K.; Neider, M.; Grom, E.; Wolff, G.; Rindlisbacher, M. Anal. Chem. **1982** 54, 1747.

(13) Haw, J.; Glass, T. E.; Dorn, H. C. J. Magn. Reson. **1982** 49, 22.

(14) Haw, J.; Glass, T. E.; Dorn, H. C. Anal. Chem. **1983** 55, 22.

(15) Buddrus, J.; Herzog, H. Anal. Chem. **1983** 55, 1611.

(16) Bayer, E.; Albert, K. J. Chromatogr. **1984** 312, 91.

(17) Dorn, H. C. Anal. Chem. **1984** 56, 747A.

(18) Laude, D., Jr.; Wilkins, C. L. Anal. Chem. **1984** 56, 2471.

(19) Laude, D., Jr.; Lee, R.; Wilkins, C. L. J. Magn. Reson. **1984** 60, 453.

(20) Laude, D., Jr.; Lee, R.; Wilkins, C. L. Anal. Chem. **1985** 57, 1464.

(21) Clore, G. M.; Kimber, B. J.; Gronenborn, A. M. J. Magn. Reson. **1983** 54, 170.

(22) Albert, K.; Nieder, M.; Bayer, E.; Spraul, M. J. Chromatogr. **1985** 346, 17.

(23) Hore, P. J. J. Magn. Reson. **1983** 54, 539.

(24) Doddrell, D. M.; Pegg, O. T. J. Am. Chem. Soc. **1980** 102, 6388.

(25) Bendall, M. J.; Pegg, D. T.; Doddrell, D. M.; Jonas, S. R.; Willing, R. I. J. Chem. Soc. Chem. Comm. **1982** 1138.

(26) Laude, D. Jr.; Wilkins, C. L. Anal. Chem. **1987** 59, 546.

(27) Allen, L. A.; Glass, T. E.; Dorn, H. C. Anal. Chem. **1988** 60, 390.

(28) Allen, L. A.; Spratt, M. P.; Glass, T. E.; Dorn, H. C. Anal. Chem. **1988** 60, 675.

(29) Buddrus, J.; Herzog, H. Org. Magn. Reson. **1981** 15, 211.

(30) Buddrus, J.; Herzog, H. Chromatographia **1984** 18, 31.

(31) Manatt, S. L., et al. Tetrehedron Lett. **1980** 21, 1397.

(32) Spratt, M. P.; Dorn, H. C. Anal. Chem. **1984** 56, 2038.

(33) Spratt, M. P.; Meng, Yi; Dorn, H. C. Anal. Chem. **1985** 57, 76.

(34) Taft, R. W.; Prosser, F.; Goodman, L.; Davis, G. T. J. Chem. Phys. **1963** 38, 380.

(35) Freeman, R.; Frenkiel, T.; Levitt, M. H. J. Magn. Reson. **1982** 50, 345.

(36) Shaka, A. J.; Keeler, J.; Freeman, R. J. Magn. Reson. **1983** 53, 313.

(37) Fung, B. M. J. Magn. Reson. **1984** 59, 275.

(38) Waugh, J. S. J. Magn. Reson. **1982** 50, 30.

(39) Randall, L. G. Sep. Sci. and Tech. **1982** 17, 1.

(40) Greibrokk, T.; Billie, A. L.; Johansen, E. J.; Landames, E. Anal. Chem. **1984** 56, 2681.

(41) Radda, G. K.; Styles, P.; Thulborn, K. R.; Waterton, J. C. J. Magn. Reson. **1981** 42, 488.

(42) Haw, J. F. Ph.D. Thesis **1982** Virginia Polytechnic Institute and State University.

(43) Denis, P. M.; Bene, G. J.; Exterman, R. C. Arch. Sci. **1952** 5, 32.

(44) Peter, S.; Brunner, G. Angew. Chem. Int. Ed. Engl. **1978** 17, 746.

(45) Trappeniers, N. J.; Prins, K. O. Physica **1967** 33, 435.

(46) Bull, T. E.; Jonas, J. J. Chem. Phys. **1970** 52, 4553.

(47) Wilbur, D. J.; Jonas, J. J. Chem. Phys. **1971** 55, 5840.

(48) Parkhurst, H. J.; Lu, Y.; Jonas, J. J. Chem. Phys. **1971** 55, 1368.

(49) Hubbard, P. S. Phys. Rev. **1963** 131, 275.

(50) Wilbur, D. J.; Jonas, J. J. Chem. Phys. **1975** 62, 2800.

(51) Jonas, J.; DeFries, T.; Wilbur, D. J. J. Chem. Phys. **1976** 64, 582.

(52) Jonas, J.; DeFries, T.; Lamb, W. J. J. Chem. Phys. **1978** 68, 2988.

(53) Lamb, W. J.; Jonas, J. J. Chem. Phys. **1981** 74, 913.

(54) Baker, E. S.; Brown, D. R.; Lamb, D. M.; Jonas, J. J. Chem. Eng. Data **1985** 30, 141.

(55) Baker, E. S.; Brown, D. R.; Jonas, J. J. Chem. Phys. **1984** 88, 5425.

(56) Lamb, W. J.; Hoffman, G. A.; Jonas, J. J. Chem. Phys. **1981** 74, 6875.

(57) Lamb, D. M.; Barbara, T. M.; Jonas, J. J. Phys. Chem. **1986** 90, 4210.

(58) Robert, J. M.; Evilia, R. F. J. Am. Chem. Soc. **1985** 107, 3733.

(59) Lamb, D. M.; Vander Velde, D. G.; Jonas, J. J. Magn. Reson. **1987** 73, 345.

(60) Powles, J. G.; Figgins, R. J. Chem. Phys. **1967** 19, 155.

(61) Tiffon, B.; Ancian, B.; Dubois, J. J. Chem. Phys. **1981** 74, 6981.

(62) Knoezinger, E.; Lentloff, D.; Wittenbeck, R. J. Mol. Struct. **1980** 60, 115.

(63) Tiffon, B.; Ancian, B. J. Chem. Phys. **1982** 76, 1212.

(64) Harris, R. K. "Nuclear Magnetic Resonance Spectroscopy", Chapter 3, Pittman, London **1983** 66.

(65) Hubbard, P. S. Phys. Rev. **1963** 131, 1155.

(66) Boere, R. T.; Kidd, R. G. "Annual Reports on NMR Spectroscopy", Vol. 13, ed. G. A. Webb, Academic Press, New York **1982** 319.

(67) Wallach, D.L; Huntress, W. T. J. Chem. Phys. **1969** 50, 1219.

(68) Maryott, A. A.; Farrar, T. C.; Malmberg, M. S. J. Chem. Phys. **1971** 54, 64.

(69) Wasylishen, R. E.; Pettitt, B. A. Canad. J. Chem. **1977** 55, 2564.

(70) Gillen, K. T.; Noggle, J. H. J. Chem. Phys. **1970** 53, 801.

(71) Gierer, A.; Wirtz, K. Zeit. Naturforsch. **1953** A8, 532.

(72) Hu, C. M.; Zwanzig, R. J. Chem. Phys. **1974** 60, 4354.

(73) Stephan, K.; Lucas, K. "Viscosity of Dense Fluids" Plenum Press, New York **1979** 75.

(74) Herreman, W.; Grevendonk, W.; DeBock, K. J. Chem. Phys. **1970** 53, 185.

(75) Vargaftik, N. B. "Handbook of Physical Properties of Liquids and Gases", 2nd. Ed., Hemisphere Publishing, New York **1983** 178.

(76) Lyerla, J. R. Jr.; Grant, D. M.; Wang, C. H. J. Chem. Phys. **1971** 55, 4676.

(77) Alms, G. R.; Bauer, D. R.; Brauman, J. I.; Pecora, R. J. Chem. Phys. **1973** 58, 5570.

(78) Scott Specialty Gas, personal communication.

(79) Hauser, K. H.; Stehlik, D. "Advances in Magnetic Resonance" Vol. 3, ed. J. S. Waugh, Academic Press, New York **1968** 79.

(80) Dwek, R. A.; Richards, R. E.; Taylor, D. "Annual Reports on NMR Spectroscopy", Vol. 2, ed. G. A. Webb, Academic Press, New York, **1969** 293.

(81) Mueller-Warmuth, W.; Meise-Gresch, K. "Advances in Magnetic Resonance", Vol. 11, ed. J. S. Waugh, Academic Press, New York **1983** 1.

(82) Wind, R. A.; Duijveshijn, M. J.; van der Lugt, C.; Mannshijn, A.; Vriend, J. "Progress in NMR Spectroscopy" Vol. 17, Pergamon Press, Great Britain **1985** 33.

(83) Dorn, H. C.; Wang, J.; Allen, L.; Glass, T. E. J. Magn. Reson. accepted **1988**.

(84) Gitti, R. K. Masters Thesis **1988** Virginia Polytechnic Institute and State University.

(85) Trommel, J. Thesis Delft **1978**.

(86) Guide to Plastics - Property and Specification Charts **1975** 239.

(87) Ginzton, E. L., "Microwave Measurements" McGraw -Hill, New York, Chapter 10, **1957** 435.

(88) Thomas, D. P.; Dalton, L. R.; Hyde, J. S. J. Chem. Phys. **1976** 65, 3006.

(89) Kooser, R. G.; Volland, W. V.; Freed, J. H. J. Chem. Phys. **1969** 50, 5243.

(90) Beth, A. H.; Balasubramanian, K.; Robinson, B. H.; Dalton, L. R.; Venkataramu, S. D.; Park, J. H. J. Phys. Chem. **1983** 87, 361.

(91) Fajer, P.; Marsh, D. J. Magn. Reson. **1982** 49, 212.

(92) Vistnes, A. I.; Dalton, L. R. J. Magn. Reson. **1983** 54, 78.

(93) Peadon, P. A.; Lee, M. L. J. Liquid Chrom. **1982** 5, 179.

(94) Giddings, J. C. "Dynamics of Chromatography" Marcel Dekker, New York, **1965** 217.

(95) Sie, S. T.; Rijnders, G, W. A. Sep. Sci. **1967** 2, 699.

The vita has been removed from the scanned document

FLOW AND STATIC ^{1}H, ^{19}F AND ^{14}N NMR STUDIES IN DENSE FLUIDS

by

Lee Allen

(ABSTRACT)

The use of ^{19}F observation using MLEV ^{1}H decoupling in LC/^{19}F (^{1}H) NMR was investigated as an alternative to LC/^{1}H NMR for fluorine containing mixtures and in order to avoid the solvent background problems associated with LC/^{1}H NMR. P-fluorobenzoate derivatives of various alcohols were analyzed by both LC/^{19}F (^{1}H) and LC/^{1}H NMR.

Another alternative exists in supercritical fluid chromatography. A delivery system was assembled and an NMR flow probe was developed and demonstrated practical for directly coupled SFC/^{1}H NMR. The alkane substituents of a model fuel mixture were identified using SFC/^{1}H NMR in contrast to using the normal phase LC/^{1}H NMR approach.

The relaxation behavior and molecular motion of dilute solutions of benzene and acetonitrile in sub- and supercritical CO_2 were determined using stopped flow ^{1}H and ^{14}N NMR. The nuclear spin-lattice relaxation times (T_1) for ^{1}H and ^{14}N were measured through inversion recovery and

linewidth, respectively. Relaxation was found to be dominated by spin-rotation interactions with molecular correlation times (τ_{sr} and τ_c) being determined directly from the ^1H and ^{14}N T_1 over a wide range of viscosities and temperatures. Line-narrowing improvements of ^{14}N averaged 3-fold as a result of the increased molecular motion.

The increased molecular motion as a result of supercritical CO_2 resulted in improved signal enhancement using flow dynamic nuclear polarization. The observed enhancements were two times greater than that typically achieved for the same system and configuration using normal liquid solutions. Through observed NMR enhancements, relative microwave magnetic field values in the vicinity of the NMR coils were measured for typical flow and static DNP-NMR configurations. The advantages of the former were noted.